

ПРИМЉЕНО: 28-09-2016			
Рад.јед.	б р о ј	Арх.шифра	Прилог
0001	1615/11		

Научном већу Института за физику
Београд, 22. септембар 2016.

Предмет: Молба за покретање поступка за реизбор у звање истраживач сарадник

С обзиром да испуњавам критеријуме прописане од стране Министарства просвете, науке и технолошког развоја за реизбор у звање истраживач сарадник, молим Научно веће Института за физику да покрене поступак за мој реизбор у наведено звање.

У прилогу достављам:

1. Мишљење руководиоца пројекта
2. Кратку биографију
3. Списак објављених радова и њихове копије
4. Потврду о упису на докторске студије
5. Потврде о завршеним основним и мастер студијама
6. Преглед научне активности
7. Решење о претходном избору у звање истраживач сарадник

С поштовањем,
Војислав Милошевић



Научном већу Института за физику Београд

Београд, 26. септембар 2016.

Предмет: Мишљење руководиоца пројекта за реизбор Војислава Милошевића у звање истраживач сарадник

Војислав Милошевић је запослен у Лабораторији за метаматеријале Центра за фотонику, Института за физику Београд од 1. јануара 2010. године. Он је ангажован на два пројекта која финансира Министарство просвете, наука и технолошког развоја ТР-32024 "Реконфигурабилне, мултибанд и скениране антене на бази метаматеријала за бежичне комуникационе системе и сензоре" и ИИИ-045016 "Генерисање и карактеризација нанофотонских функционалних структура у биомедицини и информатици".

С обзиром да испуњава критеријуме прописане од стране Министарства просвете, науке и технолошког развоја, сагласни смо са покретањем поступка за реизбор Војислава Милошевића у звање истраживач сарадник.

Предлог Комисије за избор Војислава Милошевића у звање истраживач сарадник је следећи:

1. др Бранка Јокановић, научни саветник, Институт за физику Београд,
2. Проф. др Слободан Вуковић, научни саветник у пензији, Институт за хемију, технологију и металургију, Београд,
3. др Горан Исић, научни сарадник, Институт за физику Београд.

Руководилац пројекта ИИИ 45016,

ЗК Бранислав Јеленковић
ЗК др Бранислав Јеленковић,
научни саветник, Институт за
физику Београд

Руководилац пројекта ТР 32024,

Бранка Јокановић
др Бранка Јокановић,
научни саветник, Институт за
физику Београд

БИОГРАФИЈА КАНДИДАТА

Војислав Милошевић је рођен 5.4.1986. у Београду, где је завршио основну школу и Математичку гимназију, где је током школовања освојио више награда на националним такмичењима из математике и физике. Године 2005. уписао је Електротехнички факултет у Београду на коме је дипломирао 2009. године на смеру за Микроталасну технику одсека за Телекомуникације, са просечном оценом 9,09. Исте године уписао је дипломске-мастер студије на модулу за Микроталасну технику, које је завршио у априлу 2012. године, са просечном оценом 9,57. У новембру 2012. године уписао је докторске студије на Физичком факултету у Београду, на смеру Квантна оптика и ласери.

На Институту за физику запослен је од 01.01.2010. године. Био је ангажован на пројекту технолошког развоја ТР-11009 «Дуал-банд и три-банд микроталасна кола и антене базирани на метаматеријалима за комуникационе системе нове генерације», а тренутно ради на пројектима Министарства просвете, науке и технолошког развоја ТР-32024 «Реконфигурабилне, мултибанд и скениране антене на бази метаматеријала за бежичне комуникационе системе и сензоре» и ИИИИ-045016 «Генерисање и карактеризација нанофотонских функционалних структура у биомедицини и информатици».

Као аутор или коаутор има три рада у међународним часописима (од тога два категорије М21), преко двадесет учешћа на домаћим и међународним конференцијама, и четири техничка решења категорије М85. Такође је први аутор поглавља прихваћеног за међународну монографију, која још није објављена.

Војислав Милошевић

Поглавља у међународним монографијама

1. Vojislav Milosevic, Branka Jokanovic, Olga Boric-Lubecke, Victor M. Lubecke, "Key Microwave and Millimeter Wave Technologies for 5G Radio," прихваћено за објављивање у монографији "Powering the Internet of Things with 5G Networks," IGI Global – **M14**.

Часописи

1. Р. Бојанић, Б. Јокановић, В. Милошевић, F. Medina, F. Mesa, "Enhanced Modelling of Split-Ring Resonators Couplings in Printed Circuits", *IEEE Trans. Microw. Theor. Tech.*, vol. 62, br. 8, pp. 1605 - 1615, doi: 10.1109/TMTT.2014.2332302, 2014 – **M21**.
2. В. Милошевић, Б. Јокановић, Р. Бојанић, "Retrieval and validation of the effective constitutive parameters of bianisotropic metamaterials", *Phys. Scr.*, vol. T162, br. , pp. 014046, doi: 10.1088/0031-8949/2014/T162/014046, 2014 – **M22**.
3. В. Милошевић, Б. Јокановић, Р. Бојанић, Б. Јеленковић, "Classical Electromagnetically Induced Transparency in Metamaterials", *Microw. Rev.*, vol. 19, br. 2, pp. 76-81, 2013 – **M53**.
4. В. Милошевић, Б. Јокановић, Р. Бојанић, "Effective Electromagnetic Parameters of Metamaterial Transmission Line Loaded with Asymmetric Unit Cells", *IEEE Trans. Microw. Theor. Tech.*, vol. 61, br. 8, pp. 2761-2772, doi: 10.1109/TMTT.2013.2268056, 2013 – **M21**.
5. Р. Бојанић, Б. Јокановић, В. Милошевић, "Reconfigurable Delay Lines with Split-Ring Resonators", *Microw. Rev.*, vol. 17, br. 2, pp. 7-12, 2011 – **M52**.

Конференције

1. V. Milosevic, M. Radovanovic, B. Jokanovic, O. Boric-Lubecke, V.M. Lubecke, "Tx Leakage Cancellation Using Antenna Image Impedance for CW Radar Applications," *European Microwave Conference (EuMC) 2016* – **M33**.
2. В. Милошевић, Р. Бојанић, Б. Јокановић, "Анализа антисиметричних сплит-ринг резонатора спрегнутих са водом помоћу парног и непарног мода," *ЕТРАН 2016* – **M33**.
3. В. Милошевић, Б. Јокановић, Г. Исић, "Coupled-mode Theory Approach for Analysis of Resonant Transmission Line", *Metamaterials 2015* – **M33**.

4. Г. Исић, D. Zografopoulos, R. Veccherelli, В. Милошевић, Б. Јокановић, Р. Гајић, "Liquid crystal reflection modulators based on coupled terahertz resonant cavities", *Photonica 2015* – **М34**.
5. В. Милошевић, М. Радовановић, Б. Јокановић, "Тх/Рх канцелер за FMCW радар на Ку-опсегу", *ЕТРАН 2015* – **М33**.
6. В. Милошевић, Б. Јокановић, Г. Исић, "Анализа дисперзионих ефеката у метаматеријалима помоћу теорије спрегнутих модова", *Радионица из фотонице 2015* – **М64**.
7. В. Милошевић, Б. Јокановић, Р. Бојанић, "Analytical Model of Transmission Line Metamaterial with Asymmetrically Coupled Split-Ring Resonators", *Metamaterials 2014* – **М33**.
8. Р. Бојанић, Б. Јокановић, В. Милошевић, "Enhanced Modelling of Asymmetric Split-Ring-Resonators in Printed Circuits", *Metamaterials 2014* – **М33**.
9. Е. Петронијевић, Б. Јокановић, В. Милошевић, "Електромагнетски индукована транспаренција у асиметричној структури сплит-ринг резонатора у таласоводу", *ЕТРАН 2014* – **М63**.
10. В. Милошевић, Б. Јокановић, Р. Бојанић, "Аналитичко моделовање коефицијента трансмисије на воду спрегнутом са сплит-ринг резонатором", *ЕТРАН 2014* – **М63**.
11. Р. Бојанић, В. Милошевић, Б. Јокановић, F. Medina, F. Mesa, "Моделовање асиметричног сплит-ринг резонатора спрегнутог са микрострип водом помоћу еквивалентне шеме", *ЕТРАН 2014* – **М63**.
12. В. Милошевић, Б. Јокановић, Р. Бојанић, "Класична аналогија електромагнетно индуковане транспаренције (ЕИТ) у метаматеријалима", *Радионица из фотонице 2014* – **М64**.
13. В. Милошевић, Б. Јокановић, Р. Бојанић, "Effective Bianisotropic Parameters of Metamaterial Transmission Line", *Metamaterials 2013* – **М33**.
14. В. Милошевић, Б. Јокановић, Р. Бојанић, "Retrieval and validation of the effective constitutive parameters of bianisotropic metamaterials", *Photonica 2013* – **М33**.
15. В. Милошевић, Б. Јокановић, Р. Бојанић, "Валидација екстрахованих параметара за асиметричне јединичне ћелије метаматеријала", *ЕТРАН 2013* – **М63**.
16. Р. Бојанић, Б. Јокановић, В. Милошевић, F. Medina, F. Mesa, "Еквивалентна шема микрострип вода оптерећеног сплит ринг резонатором са различитим положајем процепа", *ЕТРАН 2013* – **М63**.
17. Р. Бојанић, Б. Јокановић, В. Милошевић, "On the orientation of split-ring resonators excited by guided waves", *Metamaterials 2012* – **М33**.

18. В. Милошевић, Б. Јокановић, Р. Бојанић, Б. Јеленковић, "EIT-like response in asymmetrically coupled split ring resonators", *Metamaterials 2012* – **M33**.
19. В. Милошевић, Б. Колунџија, "Ispitivanje potencijala za frekvencijsku rekonfigurabilnost monopola antene", *ETPAH 2012* – **M63**.
20. В. Милошевић, Б. Јокановић, Р. Бојанић, "Generalizovana metoda za ekstrakciju efektivnih parametara kod nesimetričnih struktura", *ETPAH 2012* – **M63**.
21. В. Милошевић, Б. Јокановић, "Resonant Frequencies of Split Ring Resonator in Respect of Angle Between Slits", *Metamaterials 2011* – **M33**.
22. Б. Јокановић, Р. Бојанић, В. Милошевић, "Multiband Delay Lines with Reconfigurable Split-Ring Resonators", *Telsiks 2011* – **M33**.
23. Р. Бојанић, Б. Јокановић, В. Милошевић, "Investigation of Group Delay in Transmission Lines Consisting of Reconfigurable Split-Ring Resonators", *Photonica 2011* – **M34**.
24. Р. Бојанић, Б. Јокановић, В. Милошевић, "Rekonfigurabilne linije za kasnjenje sa split-ring rezonatorima", *ETPAH 2011* – **M63**.
25. В. Милошевић, "Rezonantne učestanosti usamljenih split-ring rezonatora i spregnutih sa mikrostrip vodom u zavisnosti od ugla između procepa", *ETPAH 2011* – **M63**.
26. В. Милошевић, Б. Јокановић, Р. Бојанић, "Tuning EIT-Like Response in Cross Coupled SRRs", *Telsiks 2013* – **M33**.

Техничка решења

1. В. Милошевић, Б. Јокановић, М. Радовановић, "Балансни циркулатор за примопредајну штампану антену на Ку-опсеги", 2014 – **M85**.
2. В. Милошевић, Б. Јокановић, Р. Бојанић, "Екстракција еквивалентних шема сплит ринг резонатора спрегнутих са микрострип вodom за различите положаје процепа", 2013 – **M85**.
3. В. Милошевић, Б. Јокановић, Р. Бојанић, "Метода екстракције параметара за несиметричне јединичне ћелије", 2012 – **M85**.
4. Р. Бојанић, Б. Јокановић, В. Милошевић, "Линије за каснjenje са спрегнутим split-ring резонаторима за рад на више опсега", 2011 – **M85**.

Effective Electromagnetic Parameters of Metamaterial Transmission Line Loaded With Asymmetric Unit Cells

Vojislav Milosevic, Branka Jokanovic, *Member, IEEE*, and Radovan Bojanic

Abstract—In this paper, we propose the generalized extraction procedure for retrieval of the effective constitutive parameters for a metamaterial transmission line loaded with asymmetric unit cells. The asymmetric unit cell is replaced with a transmission line immersed in equivalent bianisotropic medium described by effective parameters ϵ , μ , and Z_c , and bianisotropic parameters u and η . The proposed retrieval procedure is applied to novel dual-band unit cells and compared with the standard Nicolson–Ross–Weir (NRW) method that is originally developed for the symmetric unit cell and then extended to the asymmetric one using the averaged value of reflection coefficients. It has been shown that, in case of pronounced asymmetry, the NRW method gives only the exact value of refraction, but effective permittivity and permeability are considerably different from the exact values since they are calculated by means of the approximate value of characteristic impedance.

Index Terms—Asymmetric unit cell, split-ring resonator (SRR), effective material parameters, bianisotropic medium, metamaterial transmission line.

I. INTRODUCTION

METAMATERIALS are artificial electromagnetic (EM) composites that can host a number of unusual properties. Among them, the *negative index* or *left-handed* (LH) metamaterials have been a research focus over the past decade. Their distinctive characteristics include the opposite direction of power flow and phase velocity and the inversion of Snell Law, Doppler shift, and Cherenkov radiation [1]. These properties make them suitable candidates for some ground-breaking applications, such as invisibility cloak and sub-wavelength imaging [2].

Alongside with 2-D or 3-D volumetric metamaterials, which interact with free-space radiation, an analogous concept for guided waves has emerged. These structures represent transmission lines or waveguides loaded with sub-wavelength inclusions, and they are termed metamaterial transmission lines or composite right/left-handed (CRLH) transmission lines. They can be used for numerous improvements of practical

microwave devices, such as leaky-wave antennas, couplers, shifters, etc. [3].

The key assumption for understanding the EM behavior of metamaterials is that homogenization theory can be applied to them, in the same fashion as it is applied to natural materials. In other words, we assume that we can average Maxwell's equations over small volumes (with respect to wavelength), to obtain equivalent homogeneous medium described by a set of effective constitutive parameters [4]. In the case of metamaterial transmission lines, we assume that the line's conductors are immersed in equivalent homogeneous medium that substitutes the effect of the inclusions, like in planar transmission lines where homogenous medium with the effective permittivity is introduced to emulate the presence of two dielectrics (substrate and air). Apart from providing a simple physical picture, the importance of effective parameters lies in the fact that they can greatly facilitate the design of optimal metamaterial structures.

To determine the values of these effective parameters, several approaches can be used: for example, analytical solutions exist in some simpler cases [5], [6], and there is also a possibility of numerical averaging of fields. However, by far the most frequently used procedure is based on the inversion of scattering data (S -parameters) of a finite slab, called the NRW procedure. It was developed for the measurements of complex permittivity and permeability of natural materials [7], [8], and more recently applied to metamaterials [9], [10]. Effective parameters of metamaterial transmission lines can be deduced from the equivalent-circuit model, but the latter is sometimes not readily available. In such cases, we can resort to the same procedure of parameter retrieval. Formally, the only difference in the procedure is that the impedances have to be normalized with a factor that depends on transmission-line geometry [11].

One of the problems with the standard Nicolson–Ross–Weir (NRW) procedure arises in the case when the metamaterial sample under study has asymmetric reflection. It is obvious that the isotropic medium model cannot reproduce this property, as it is intrinsically symmetric. Smith *et al.* proposed a modification of the procedure to solve this problem by using averaged value of the reflection coefficients, which we will call NRW_{avg} . It provides the correct value of the index of refraction, but the value of the characteristic impedance remains approximate [12]. Another problem is that the isotropic medium model assumes that the induced electric and magnetic dipoles are mutually independent, but Marques *et al.* reported that the split ring, which is commonly used in metamaterials, has a simultaneous electric and magnetic response, i.e., corresponding

Manuscript received April 30, 2013; accepted May 30, 2013. Date of publication June 25, 2013; date of current version August 02, 2013. This work was supported by the Serbian Ministry of Education, Science and Technological Development under Project TR-32024 and Project III-45016.

The authors are with the Institute of Physics, University of Belgrade, Belgrade 11000, Serbia (e-mail: vojislav@ipb.ac.rs; brankaj@ipb.ac.rs; radovan@ipb.ac.rs).

Color versions of one or more of the figures in this paper are available online at <http://ieeexplore.ieee.org>.

Digital Object Identifier 10.1109/TMTT.2013.2268056

dipoles are coupled [13]. It is not always possible to neglect that coupling, depending on the orientation of the split rings and their excitation.

To account for both asymmetric reflection and magneto-electrical coupling, bianisotropic medium model can be used, which has already been considered by various authors [13]–[16]. We can distinguish several sources of bianisotropy—cross polarizability of constitutive elements (e.g., split ring), asymmetric position of elements within the unit cell (e.g., due to the substrate) [16], and even in the case of symmetric unit cells with center-symmetric inclusions (i.e., without cross-polarizability), spatial dispersion effects [17]. In any case, a significant improvement over the standard retrieval technique is achieved.

In this paper, we consider the bianisotropic homogenization and retrieval of corresponding parameters for metamaterial transmission lines loaded with asymmetric inclusions, which, to our best knowledge, have not been published in the literature thus far. This paper is organized as follows. In Section II, we discuss properties of transmission lines filled with bianisotropic medium. We then develop the circuit matrix of such transmission lines (we use $ABCD$ matrices as they allow most convenient formulation). From this matrix, we show how material parameters, including bianisotropy parameters u and η , can be retrieved, and discuss potential problems that may occur. We will refer to this procedure as the generalized approach (GA).

In Section III, the proposed GA procedure is applied to novel dual-band unit cells, which consist of a microstrip line loaded with broadside coupled (BSC) split-ring resonators (SRRs), with gaps either on parallel or on perpendicular arms of the SRRs. We compared this approach and the NRW retrieval procedure, originally developed for symmetric unit cells, and found that NRW was not able to extract constitutive parameters such as permittivity, permeability, and characteristic impedance for asymmetric unit cells correctly, even if the average value of reflections was used.

Section IV presents validation of the proposed extraction procedure for the asymmetric unit cells. We provide the simulation results of a homogeneous slab with the effective parameters that we extracted using both the GA and NRW_{avg} methods and compare them with the simulated response of the real unit cell. To simulate the bianisotropic medium, we replaced it with two isotropic slabs and recomposed the obtained S -parameters to get the final S -parameters.

Any retrieval technique based on analyzing the scattering data of a finite slab can suffer from some problems, e.g., unphysical antiresonances with a negative imaginary part for some of the parameters. Koschny *et al.* reported that these anomalies could be traced back to the periodicity of the structure [18], and Alù reported that they could be associated with a weak form of spatial dispersion [19]. In our current work, however, we found these anomalies to be negligible, so we did not include them in the scope of our study.

II. GENERALIZED RETRIEVAL PROCEDURE

A. Transmission Line Filled With Bianisotropic Medium

Consider a transmission line (i.e., structure that supports a guided TEM wave), with its axis placed along the z coordi-

nate. Assume that the line is immersed in homogeneous bianisotropic medium described by the following constitutive relations (ε_0 , μ_0 and c are permittivity, permeability and velocity of light in vacuum, respectively):

$$\begin{aligned}\vec{D} &= \varepsilon_0 \varepsilon \vec{E} + \vec{\xi} \vec{H} \\ \vec{B} &= \vec{\zeta} \vec{E} + \mu_0 \mu \vec{H}\end{aligned}\quad (1)$$

where

$$\vec{\xi} = \vec{\zeta} = \frac{1}{c} \begin{bmatrix} 0 & -ju & 0 \\ ju & 0 & 0 \\ 0 & 0 & 0 \end{bmatrix}. \quad (2)$$

The reciprocity condition is satisfied because $\vec{\xi} = -\vec{\zeta}^T$ [20]. We note here that the tensors used in the previous reports [13]–[16] are different with respect to (2) since they have only one off-diagonal element. The reason for this difference lies in the fact that the transmission line has an inhomogeneous field structure in the transverse plane, unlike the plane wave. The form of (2) ensures that magneto-electric coupling does not depend on polarization of the transverse field, which leads to a much simpler solution than in the opposite case, as will become clear later on.

Now, let us assume that a guided wave propagates along the z -axis, with all quantities depending on the z coordinate as $e^{-\gamma z}$, and on time as $e^{j\omega t}$.¹ We also assume that the wave is of a TEM type, i.e., z components of \vec{E} and \vec{H} vectors are zero. Now we can derive the following relations from the curl Maxwell's equations:

$$\begin{aligned}\vec{i}_z \times (-\gamma \vec{H}) &= j\omega \vec{D} \\ \vec{i}_z \times (-\gamma \vec{E}) &= -j\omega \vec{B}\end{aligned}\quad (3)$$

where \vec{i}_z is the unit vector in the z -direction. The constitutive relations can be rewritten as

$$\begin{aligned}\vec{D} &= \varepsilon_0 \varepsilon \vec{E} + \vec{i}_z \times \left(j \frac{u}{c} \vec{H} \right) \\ \vec{B} &= \mu_0 \mu \vec{H} + \vec{i}_z \times \left(j \frac{u}{c} \vec{E} \right).\end{aligned}\quad (4)$$

Combining (3) and (4) yields

$$\left(\gamma - \frac{\omega}{c} u \right) (\vec{i}_z \times \vec{H}) = -j\omega \varepsilon_0 \varepsilon \vec{E} \quad (5)$$

$$\left(\gamma + \frac{\omega}{c} u \right) (\vec{i}_z \times \vec{E}) = j\omega \mu_0 \mu \vec{H}. \quad (6)$$

Combining (5) and (6) yields the wave equation

$$\left(\gamma^2 + \frac{\omega^2}{c^2} (\varepsilon \mu - u^2) \right) \vec{E} = 0 \quad (7)$$

which gives the following dispersion relation:

$$\gamma = \pm j \frac{\omega}{c} \sqrt{\varepsilon \mu - u^2} \quad (8)$$

or, since $\gamma = j(\omega)/(c)n$,

$$n = \pm \sqrt{\varepsilon \mu - u^2}. \quad (9)$$

Different signs in (8) and (9) indicate two possible directions of propagation along the z -axis. The correct solution for a given direction should be chosen based on the passivity criterion.

¹The complex quantities are defined as, e.g., $n = n' - jn''$.

The characteristic impedance of the medium (i.e., the ratio between the electric and magnetic field strengths) can be obtained by substituting (8) in (5), yielding (normalized by $z_0 = \sqrt{\mu_0/\epsilon_0}$)

$$z_{1,2} = \frac{n \pm ju}{\epsilon} \quad (10)$$

where $z_{1,2}$ correspond to propagation along the positive and negative z -direction, respectively. From (10), it is clear that the impedance value is different for propagation in different directions, thus giving different reflections.

From (5) and (6), we deduce that the electric and magnetic field vectors are proportional and normal to each other in every point of transverse plane. Furthermore, polarization vectors \vec{D} and \vec{B} are proportional to \vec{E} and \vec{H} , respectively. Therefore, Maxwell's equations governing the field distribution in the transverse plane will not change, except for the factor of proportionality, compared with transmission line filled with air. Consequently, the line characteristic impedance (i.e., the voltage to current ratio) will change proportionally,

$$Z_{c1,2} = z_{1,2} Z_{\text{air}} \quad (11)$$

where Z_{air} is the of transmission line characteristic impedance in the air. Alternatively, the characteristic impedances can be written as

$$Z_{c1,2} = Z_c \pm \eta \quad Z_c = \frac{Z_{c1} + Z_{c2}}{2} \quad (12)$$

where $Z_c = (n)/(\epsilon)Z_{\text{air}}$ represents their mean value, and $\eta = (ju)/(\epsilon)Z_{\text{air}}$, based on (10), represents the offset from the mean value. We will use this form later, as it allows us a more convenient formulation.

B. Conditions for Negative Index of Refraction

In his seminal paper, Veselago proved that a material without losses will exhibit negative refractive index when ϵ and μ are simultaneously negative [1]. However, this condition is too strict, when we take into account losses, which exist in all natural materials. The necessary condition in the lossy case is found to be [21], [22]

$$\epsilon' \mu'' + \mu' \epsilon'' < 0. \quad (13)$$

This condition was derived using the standard dispersion relation, $n = \sqrt{\epsilon\mu}$. For bianisotropic media, however, the proper relation is given by (9), and the condition for negative index has to be derived starting from that.

To obtain a negative refractive index, we have to have a solution of (9) with $n'' > 0$ and $n' < 0$ (to ensure a positive power flow and negative phase velocity, respectively) [21]. In other words, n has to lie in the second quadrant of the complex plane. This implies that n^2 will necessarily lie in the lower half-plane, i.e., $\text{Im}\{n^2\} < 0$. By substituting (9), we obtain

$$\epsilon' \mu'' + \mu' \epsilon'' < 2u'u''. \quad (14)$$

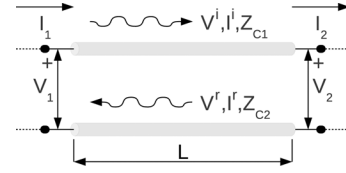


Fig. 1. Section of an asymmetric transmission line of length L .

An important consequence of (14) is that it shows it is possible to have both ϵ' and μ' negative and still not obtain a negative refractive index if the product $u'u''$ is negative.

C. Network Parameters of a Transmission-Line Section

Let us assume that we have a transmission-line section of length l , filled with bianisotropic medium having ϵ *hbox*-, μ -, and u -parameters. We can regard this section as a two-port network, which can be described by its scattering parameters (S -parameters), or any other type of network parameters (impedance, admittance, etc.). We will use the $ABCD$ -parameter description as we found it most convenient for our discussion. The $ABCD$ -parameter matrix is defined by [23]

$$\begin{bmatrix} V_1 \\ I_1 \end{bmatrix} = \begin{bmatrix} A & B \\ C & D \end{bmatrix} \begin{bmatrix} V_2 \\ I_2 \end{bmatrix} \quad (15)$$

with referent directions for voltages and currents indicated in Fig. 1.

Our aim is to obtain $ABCD$ -parameters as a function of transmission-line properties derived in Section II-B, namely, propagation constant γ (the same for both directions), defined by (8), and characteristic impedances Z_{c1} and Z_{c2} (for incident and reflected wave, respectively), defined by (12). To this end, we represent the state at arbitrary point of transmission line with voltages of incident and reflected waves, V^i and V^r , respectively. The relation between these voltages at ports 1 and 2, written in matrix form, will be

$$\begin{bmatrix} V_1^i \\ V_1^r \end{bmatrix} = \begin{bmatrix} e^{\gamma l} & 0 \\ 0 & e^{-\gamma l} \end{bmatrix} \begin{bmatrix} V_2^i \\ V_2^r \end{bmatrix}. \quad (16)$$

Total voltage and total current anywhere along the line can be expressed as

$$\begin{bmatrix} V \\ I \end{bmatrix} = \begin{bmatrix} 1 & -1 \\ \frac{1}{Z_{c1}} & -\frac{1}{Z_{c2}} \end{bmatrix} \begin{bmatrix} V^i \\ V^r \end{bmatrix} = Q \begin{bmatrix} V^i \\ V^r \end{bmatrix}. \quad (17)$$

The inverse relation is

$$\begin{bmatrix} V^i \\ V^r \end{bmatrix} = Q^{-1} \begin{bmatrix} V \\ I \end{bmatrix}. \quad (18)$$

By substituting (18) into (16) and multiplying by Q from the left side, we obtain the $ABCD$ matrix

$$ABCD = Q \begin{bmatrix} e^{\gamma l} & 0 \\ 0 & e^{-\gamma l} \end{bmatrix} Q^{-1} \quad (19)$$

which, after substituting value of Q and some manipulation, comes down to

$$\begin{bmatrix} \cosh \gamma l + \frac{\eta}{Z_c} \sinh \gamma l & \left(Z_c - \frac{\eta^2}{Z_c} \right) \sinh \gamma l \\ \frac{\sinh \gamma l}{Z_c} & \cosh \gamma l - \frac{\eta}{Z_c} \sinh \gamma l \end{bmatrix}. \quad (20)$$

It can be seen from (20) that when $\eta = 0$, i.e., in the symmetric case, $ABCD$ -parameters are reduced to those of the standard transmission line.

D. Parameter Retrieval

Scattering parameters (S -parameters) are usually obtained as a result of measurements or EM simulation and can be unambiguously transformed to the $ABCD$ matrix [23]. Once we have it, we can easily see from (20) that we can obtain the effective parameters as

$$\gamma = \pm \cosh^{-1} \frac{A + D}{2} \quad (21)$$

$$Z_c = \frac{\sinh \gamma l}{C} = \pm \frac{1}{C} \sqrt{1 - \left(\frac{A + D}{2} \right)^2} \quad (22)$$

$$\eta = \frac{A - D}{2C}. \quad (23)$$

If the unit cell is symmetric,² we can substitute S -parameters and simplify the expressions to obtain

$$\gamma = \pm \frac{1}{L} \cosh^{-1} \frac{1 - S_{11}^2 + S_{21}^2}{2S_{21}} \quad (24)$$

$$Z_c = \pm \sqrt{\frac{(1 + S_{11})^2 - S_{21}^2}{(1 - S_{11})^2 - S_{21}^2}} \quad (25)$$

and $\eta = 0$, which, as expected, agrees with the previous reports on the NRW procedure [9], [11], [24].

The NRW_{avg} procedure proposed in [12] was intended to circumvent the problem of dealing with asymmetric unit cells by using a standard retrieval technique (for symmetric structures, i.e., (24) and (25) or similar ones), but with the averaged value of reflections S_{11} and S_{22} , i.e., $S_{11\text{avg}} = \sqrt{S_{11}S_{22}}$. However, it can be shown that the NRW_{avg} approach gives the correct value of index of refraction, but the characteristic impedance is different from the true mean value, as defined in (12) and (22). The disagreement between the impedances calculated both ways is expected to be proportional to the degree of asymmetry. As the characteristic impedance is crucial for the retrieval of effective EM parameters, this disagreement will translate to them as well, as will be shown later.

A few additional comments are needed about the given relations. First, the sign in (21) should be chosen based on the passivity criterion

$$\text{Re}\{\gamma\} > 0. \quad (26)$$

²Symmetry implies $A = D$ for $ABCD$ -parameters, and $S_{11} = S_{22}$ for S -parameters.

However, the problem of branching for $\cosh^{-1} z$, which leads to ambiguity in the imaginary part of γ (or, equivalently, in the real part of n) remains. This is the consequence of the fact that it is not possible to differentiate the phase change of ϕ from $\phi + 2k\pi$, $k \in \mathbb{Z}$. One approach to solving this problem is to use Kramers–Kronig relations to estimate the correct branch [25].

In most previous reports [7]–[11], the sign of the characteristic impedance in (22) or (25) is chosen based on the criterion $\text{Re}\{Z_c\} > 0$ or a similar one, which can be very sensitive to small numerical errors [24]. However, it is clearly visible from (22) that the characteristic impedance sign is related to the sign chosen for the propagation constant in (21), and, therefore, only one criterion is sufficient, as is found in [24].

E. Effective Parameters of the Equivalent Medium

Once we have found the propagation constant γ and characteristic impedance of an equivalent transmission line $Z_{c1,2}$, we can readily obtain the index of refraction n and characteristic impedance of the equivalent medium $z_{1,2}$ as

$$n = -j \frac{c}{\omega} \gamma \quad z_{1,2} = \frac{Z_{c1,2}}{Z_{\text{air}}}. \quad (27)$$

The bianisotropic medium effective parameters ε , μ , and u can be expressed in terms of n and $z_{1,2}$ by rearranging (9) and (10),

$$\varepsilon = \frac{2n}{z_1 + z_2} \quad \mu = 2n \frac{z_1 z_2}{z_1 + z_2} \quad u = -jn \frac{z_1 - z_2}{z_1 + z_2}. \quad (28)$$

Combining (27) and (28) with the expressions linking them with S -parameters derived in previous sections enables us to retrieve effective parameters from simulated or experimental data. We will refer to this relation as the GA.

Another option for describing asymmetric unit cells would be to use ε and μ that depend on the direction of propagation. They could be obtained as

$$\varepsilon_{1,2} = \frac{n}{z_{1,2}} \quad \mu_{1,2} = n z_{1,2}. \quad (29)$$

While mathematically equivalent, we feel that this approach is less physically justified. For the sake of comparison, we will include these values in our practical examples of extraction, and we will refer to them as the GA with a wave incoming from port 1 and port 2 (GA₁ and GA₂, respectively).

III. ASYMMETRIC UNIT CELLS

Here we investigate the EM properties of the metamaterial transmission line consisting of a microstrip line loaded with broadside-coupled asymmetric split-ring resonators (ASRRs) placed on one side of the transmission line.

It is shown that rotating the individual split rings significantly affects EM properties of the metamaterial transmission line due to different electrical and magnetic interactions that are caused by different mutual orientations of the SRRs in space and by their different orientation relative to the transmission line [26], [27].

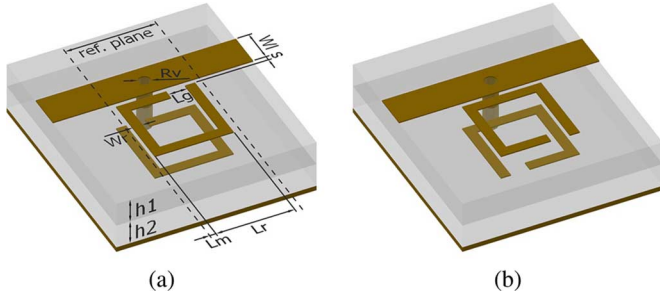


Fig. 2. Asymmetric unit cells with gaps oppositely displaced from the middle of the ring side. (a) Gaps near the microstrip line. (b) Gaps far from the microstrip line. Relevant dimensions: $h_1 = 0.635$ mm, $h_2 = 1.575$ mm, $\epsilon_{r,1} = 10.2$, $\epsilon_{r,2} = 2.2$, $L_r = 3.15$ mm, $L_g = 0.75$ mm, $L_a = 2$ mm, $L_m = 0.25$ mm, $L = L_r + 2L_m$, $W_l = 1.4$ mm, $W_r = 0.4$ mm, $R_v = 0.5$ mm, $s = 0.2$ mm.

Using the proposed generalized retrieval procedure, we explore novel asymmetric unit cells realized on a two-layer substrate. Gap-bearing sides of the SRRs are placed one above the other, not opposite to each other, as is the case with standard BSC SRRs. Unlike the standard design, novel SRRs exhibit the resonant frequencies much closer to each other (about 500 MHz), which is suitable for modern wireless systems.

We examine two types of SRRs with gap-bearing sides parallel to the microstrip line and perpendicular to it. The gaps can be moved symmetrically with respect to the center of SRR branches, to the left and to the right sides, as shown in Fig. 2 for SRRs with gaps parallel to the microstrip line.

To investigate the effectiveness of the proposed extraction procedure with respect to the NRW method, we study the metamaterial unit cells that are not distinctly asymmetric as those consisting of SRRs with gaps parallel to the microstrip line, and also the highly asymmetric unit cells with gaps perpendicular to the microstrip line.

A. Unit Cell With Gaps Parallel to the Microstrip Line

This type of unit cells can be designed with gap bearing sides near the microstrip line and far from it, as shown in Fig. 2. Unit cells comprise BSC SRRs with gaps symmetrically displaced from the center. Their asymmetry is caused only by the fact that gaps are placed at different substrate layers (top and bottom). Microstrip line is connected to the ground plane with cylindrical via, R_v , placed in the center between reference planes (denoted by dash lines).

Unit cells are simulated using the WIPL-D Pro 10.0 3-D EM solver,³ which is based on the method of moments, and S -parameters are de-embedded at the reference planes.

For the extraction of the effective parameters, we use the GA procedure that gives two different values for the effective permittivity, permeability, and characteristic impedance. The effective EM parameters of an asymmetric unit cell can also be presented by bianisotropic parameters u and η and average values of effective permittivity, permeability, and characteristic impedance (GA) that is more suitable for the direct comparison with the NRW_{avg} approach. It should be pointed out that the

³[Online]. Available: <http://www.wipl-d.com/>

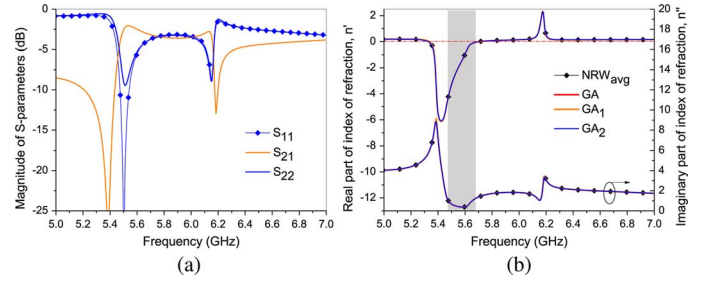


Fig. 3. Unit cell with ASRRs with gaps near the microstrip line. (a) Magnitude of S -parameters. (b) Extracted index of refraction. The rectangular bar denotes the frequency range with double negative effective parameters.

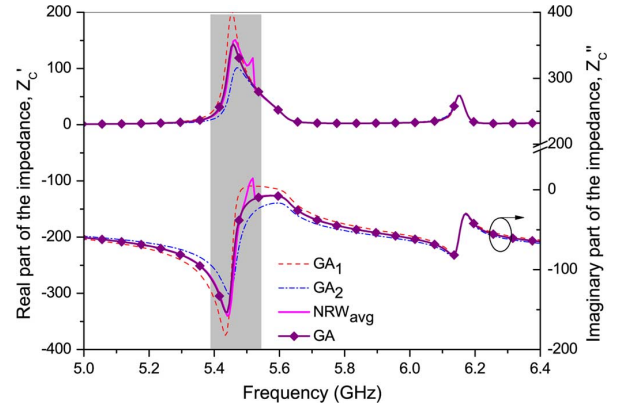


Fig. 4. Characteristic impedance extracted using different retrieval procedures for the unit cell with ASRRs with gaps near the microstrip line.

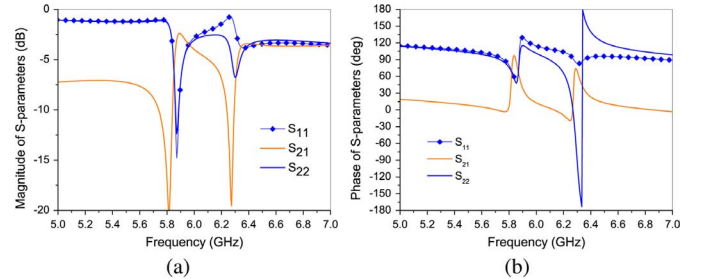


Fig. 5. (a) Magnitude and (b) phase of S -parameters for ASRRs with gaps far from the microstrip line.

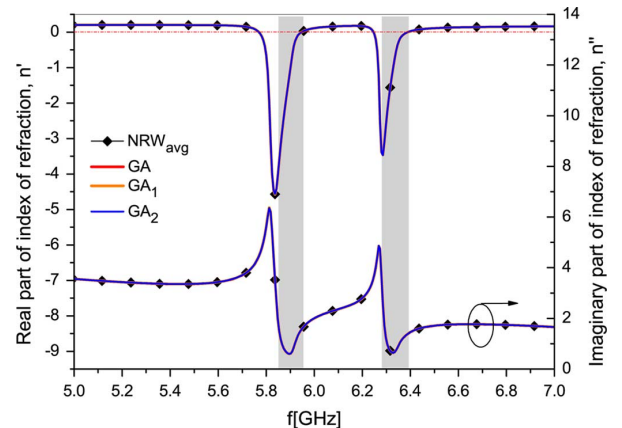


Fig. 6. Effective index of refraction extracted using different retrieval procedures for unit cell with ASRRs with gaps far from the microstrip line. Rectangular bars denote the frequency ranges with double-negative effective parameters.

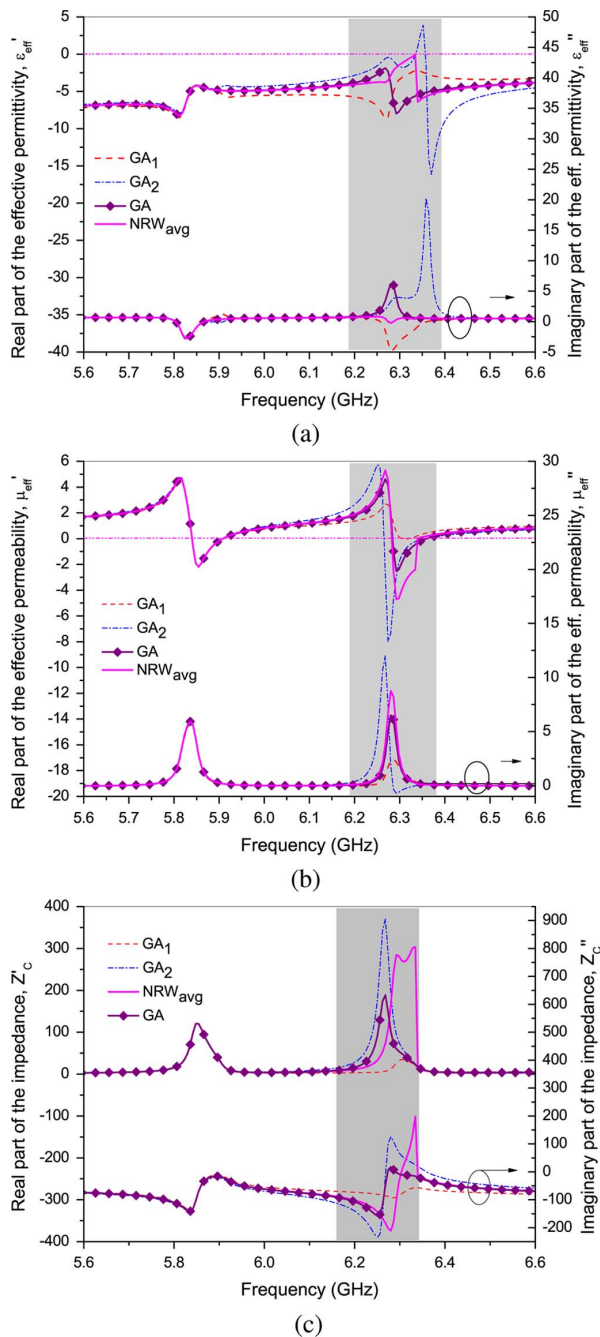


Fig. 7. (a) Effective permittivity, (b) permeability, and (c) characteristic impedance extracted for ASRRs with gaps far from the microstrip line. Rectangular bars denote the frequency range in which the NRW_{avg} and GA give different results.

NRW_{avg} method describes the asymmetric unit cell with the single value of the effective permittivity, permeability, and characteristic impedance as if it were symmetric. We compare GA₁, GA₂, and the GA with the NRW_{avg} approach.

The magnitude of S -parameters for the unit cells with gaps near the microstrip line [see Fig. 2(a)] is shown in Fig. 3(a). It can be seen that the difference between reflection coefficients S_{11} and S_{22} exists only around the first resonance. The extracted index of refraction in Fig. 3(b) is the same for the GA and NRW_{avg} approaches thanks to the conveniently defined average reflection coefficient used for the NRW_{avg} extraction. The unit

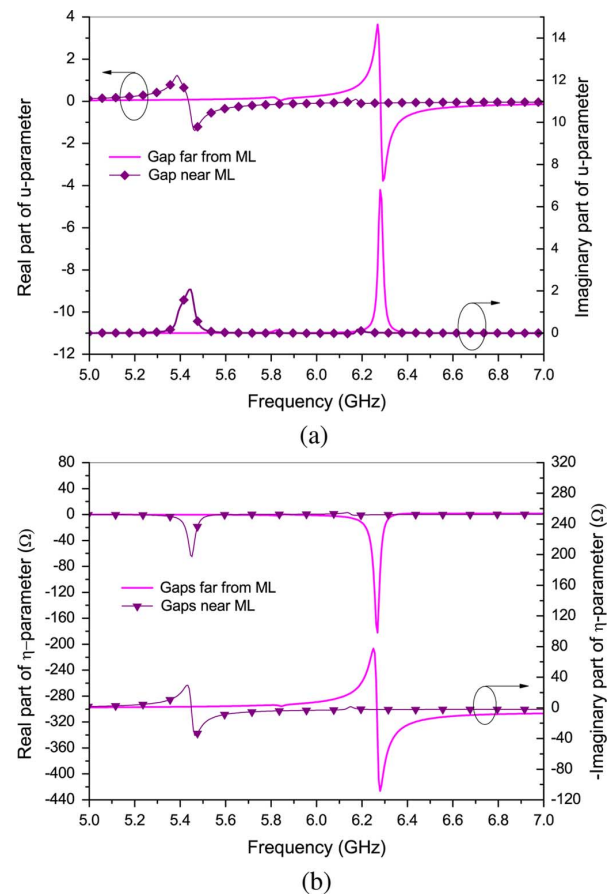


Fig. 8. Comparison of the extracted parameters. (a) Bianisotropy parameter u and (b) difference between effective characteristic impedances η for unit cells with gaps parallel to microstrip line.

cell exhibits the LH band around 5.5 GHz denoted with a rectangular bar and also the right-handed (RH) band around 6.15 GHz that corresponds to the second resonance.

The characteristic impedances extracted using three different methods are compared in Fig. 4. It can be seen that the values extracted by the GA fit exactly between the two corresponding values extracted by GA₁ and GA₂, as was expected according to (12). It is important to point out that, only at the first resonance, the characteristic impedance extracted by the NRW_{avg} method is different, but not considerably, from those extracted using the GA approach, which means that asymmetry is not much pronounced.

B. Unit Cell With Gaps Far From the Microstrip Line

The unit cell with gaps far from the microstrip line [see Fig. 2(b)] has very different S -parameters and extracted index of refraction than the unit cell with gaps near the microstrip line [see Figs. 5 and 6]. The difference between the reflection coefficients at port 1 and port 2 appears near the second resonance, which is evident from their phase in Fig. 5(b). The extracted index of refraction in Fig. 6 has two LH bands around 5.9 and 6.35 GHz that are marked by rectangular bars.

The effective permittivity, permeability, and characteristic impedance extracted using GA₁, GA₂, GA, and NRW_{avg} are shown in Fig. 7. It can be seen that all four retrieval procedures give the same results in the frequency range where symmetrical

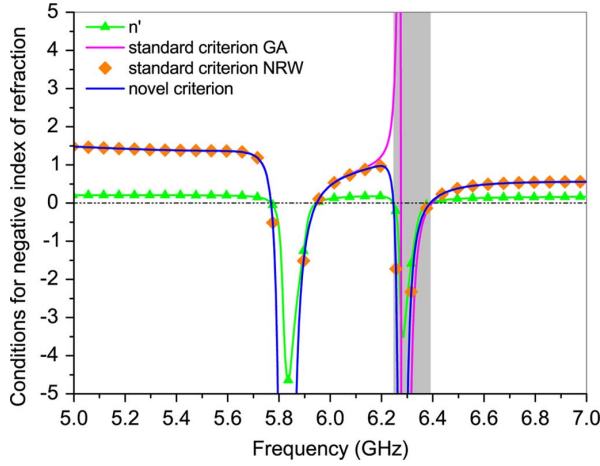


Fig. 9. Comparison of standard and novel criteria for negative index of refraction for the unit cell with parallel gaps far from the microstrip line. Effective parameters are extracted using the GA approach. The rectangular bar denotes the range in which the cell has asymmetric response and two criteria also predict different ranges of negative index of refraction.

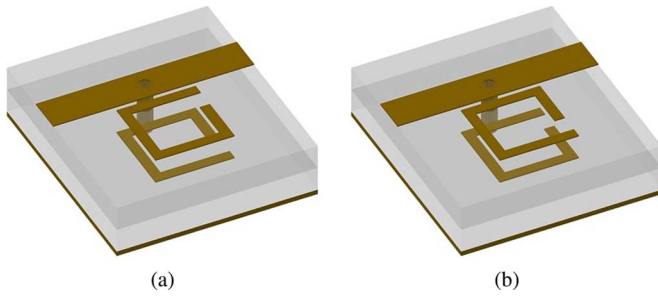


Fig. 10. Layout of unit cells consisting of ASRRs with gap-bearing side perpendicular to the microstrip line. (a) Upper gap close to the microstrip line. (b) Upper gap far from the microstrip line.

response exists ($S_{11} = S_{22}$). Effective parameters extracted by the GA and NRW_{avg} are different only around the second resonance, where the asymmetry is most significant, as it is marked by rectangular bars at Fig. 7. In the whole frequency range of interest, the effective permittivity extracted applying the NRW_{avg} and GA is negative, while the effective permeability changes the sign at two resonances that correspond to the LH bands.

The generalized extraction procedure introduces two novel parameters as a measure of unit cells asymmetry: u - and η -parameters. Fig. 8 clearly shows that the unit cell with gaps far from the microstrip line exhibits the maximum value of u - and η -parameters about three times greater than the unit cell with gaps near the microstrip line. It is also seen that bianisotropy occurs in the vicinity of either the first or the second resonance of the corresponding unit cells. It is interesting to mention that bianisotropy is considerably smaller if gaps are placed at the opposite sides of SRRs like standard BSC SRRs, even if they are oppositely displaced from the center. In that case, bianisotropy occurs at both resonances.

In Fig. 9, we compare the standard condition for negative index of refraction (13), which is valid for symmetrical unit cells, and consequently for the effective parameters extracted by the NRW_{avg} method, and the novel condition (14), which

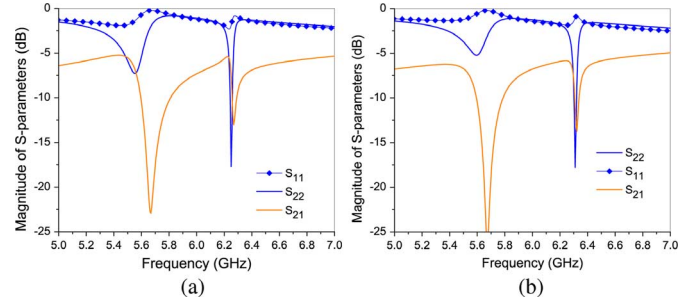


Fig. 11. Magnitude of S -parameters for unit cells with the gap perpendicular to the microstrip line. (a) Upper gap close to the microstrip line. (b) Upper gap far from the microstrip line.

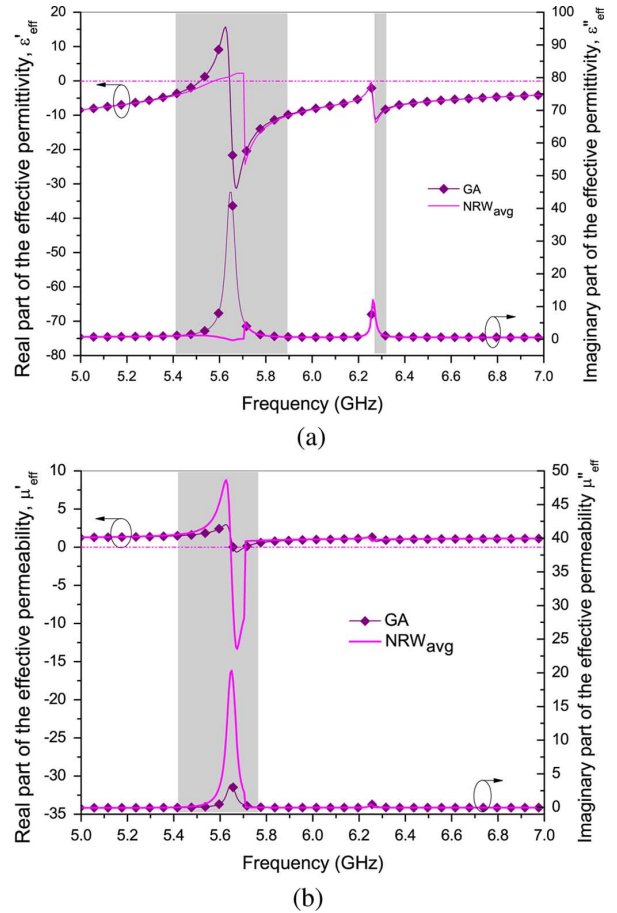
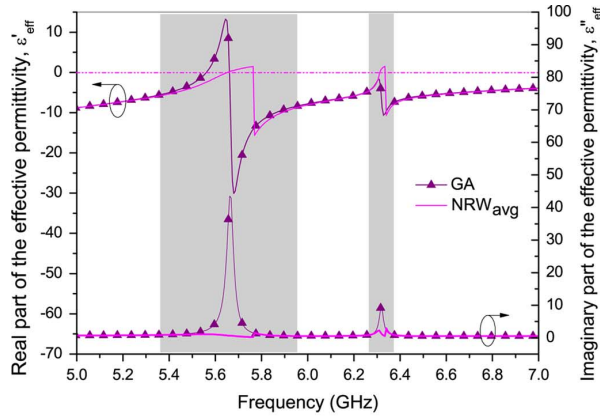
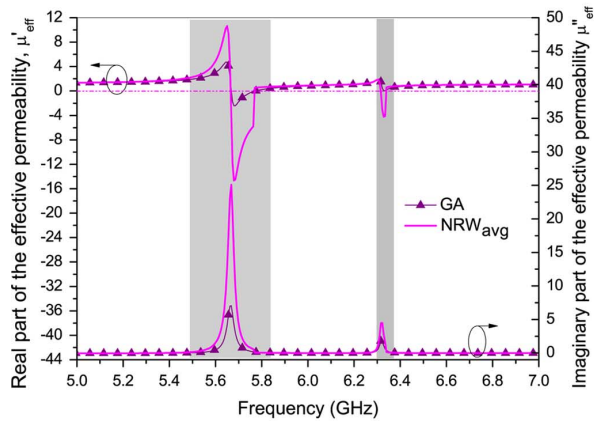


Fig. 12. Effective parameters extracted using the GA and NRW_{avg} methods for unit cell with upper gap close to the microstrip line. (a) Permittivity. (b) Permeability. Rectangular bars denote the frequency range in which the NRW_{avg} and GA give different results.

is derived for asymmetric unit cells. Both conditions are calculated using the effective parameters extracted by the GA method. In case of the unit cell with parallel gaps far from the microstrip line, it can be seen that around the first resonance both curves, for standard and novel criteria, are overlapped as was expected since the cell is symmetrical in that range. Around the second resonance, the curve corresponding to the novel criterion crosses the axis exactly at the points where the real part of the index of refraction is equal to zero, which was not the case with the curve corresponding to the standard criterion. In this case, the standard criterion predicts a somewhat narrower



(a)



(b)

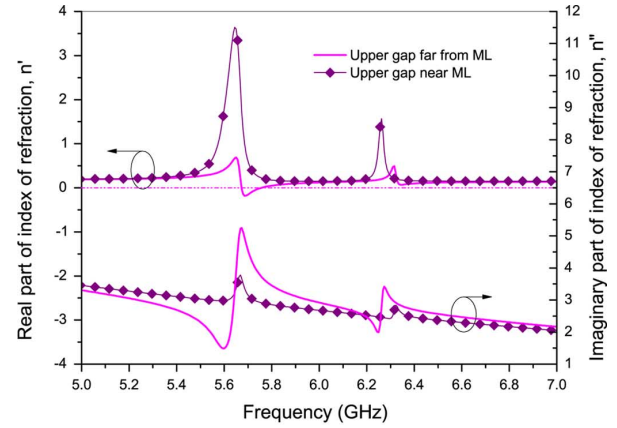
Fig. 13. Effective parameters extracted using the GA and NRW_{avg} methods for unit cell with upper gap far from the microstrip line. (a) Permittivity. (b) Permeability. Rectangular bars denote the frequency range in which the NRW_{avg} and GA give different results.

range of the negative index. Finally, we applied the standard condition using the parameters extracted by the NRW_{avg} method and showed that it completely overlapped with the novel criterion. This proves validity of the novel criterion since both methods give the same index of refraction not only for the symmetric response, but also for the asymmetric one.

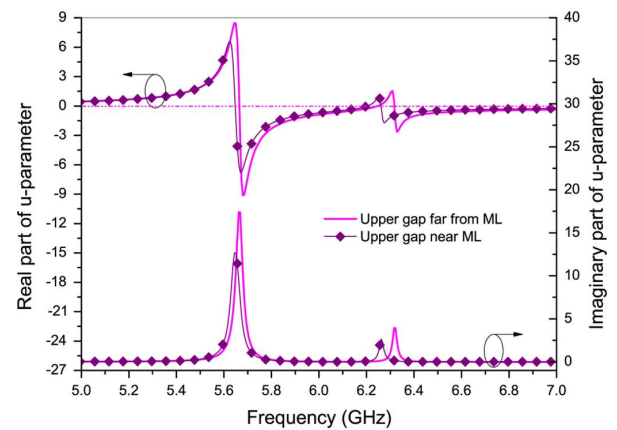
C. Unit Cells With Gaps Perpendicular to the Microstrip Line

Unit cells with gaps perpendicular to the microstrip line are shown in Fig. 10, and we can distinguish two cases in respect to the position of the upper gap: (a) when it is near the microstrip line and (b) when it is far from the microstrip line. In both cases, gaps are placed near port 1 of the unit cell. If we interchange the ports by putting port 1 instead of port 2, only the sign of u - and η -parameters will be changed.

Magnitude of S -parameters for the unit cells with perpendicular gaps are shown in Fig. 11. The extracted effective permittivity and permeability for unit cells with the upper gap near and far from the microstrip line are presented in Figs. 12 and 13, respectively. It can be seen that the position of perpendicular gaps does not influence resonant frequencies too much. S_{11} is also different from S_{22} around both resonances, but more pronounced at the first resonance. Extracted effective permittivity and permeability using the GA and NRW_{avg} are significantly



(a)



(b)

Fig. 14. (a) Extracted index of refraction and (b) u -parameter for unit cells with gaps perpendicular to the microstrip line.

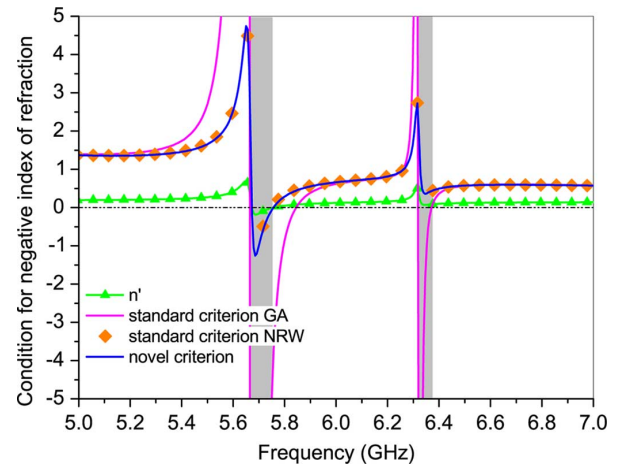


Fig. 15. Comparison of standard and novel criteria for negative index of refraction for unit cell with perpendicular gaps far from the microstrip line. Rectangular bars denote the range in which the cell has asymmetric response and two criteria predict different ranges of negative index of refraction.

different around 5.7 GHz, not only that the values are different, but also they have the opposite signs.

Characteristics of unit cells with perpendicular gaps are compared in Fig. 14. It can be seen that the real part of the index of refraction is positive in the whole range of interest for the unit cell with the gap near the microstrip line, while the unit cell with the gap far from the microstrip line exhibits a narrow band

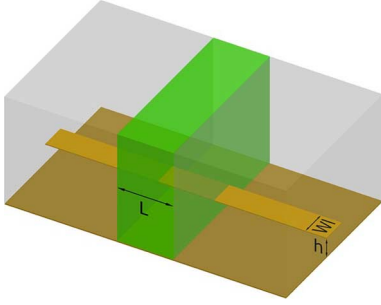
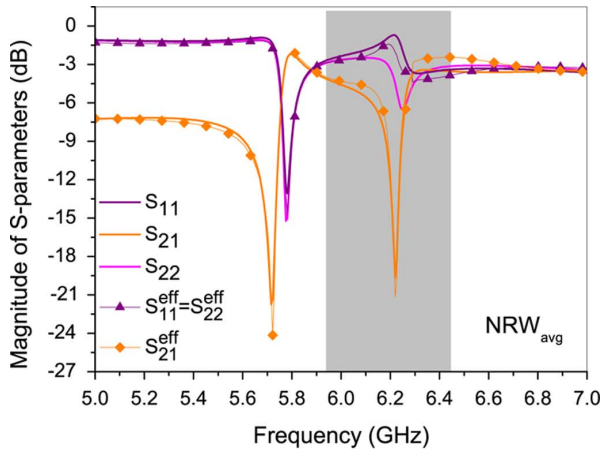
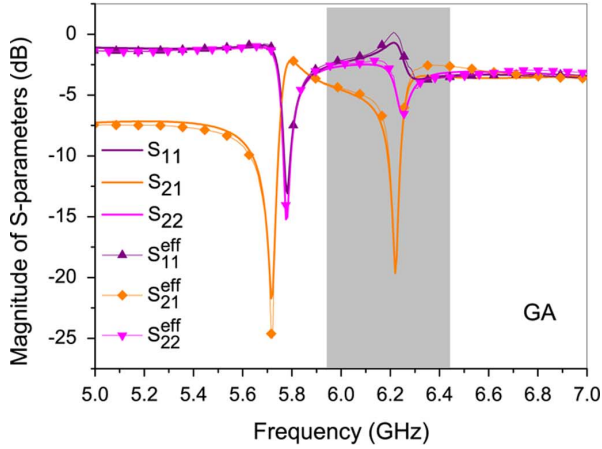


Fig. 16. Effective medium slab of the asymmetric unit cell (green box in online version) and input microstrip lines immersed in the effective dielectric (light gray boxes). Relevant dimensions: $L = L_r + 2L_m$, $h = h_1 + h_2$, where L_r , L_m , h_1 , h_2 and W_l are given in Fig. 2.



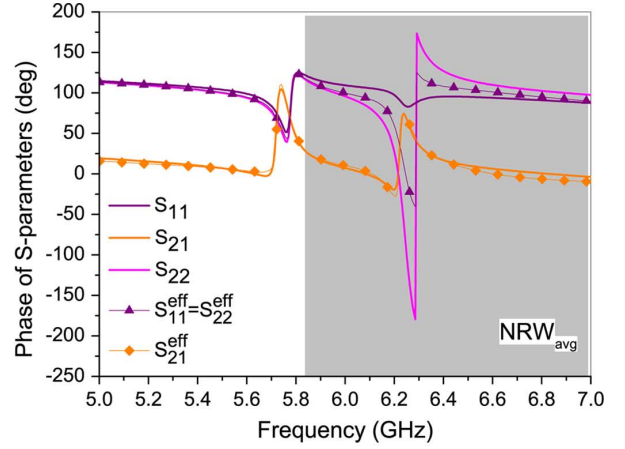
(a)



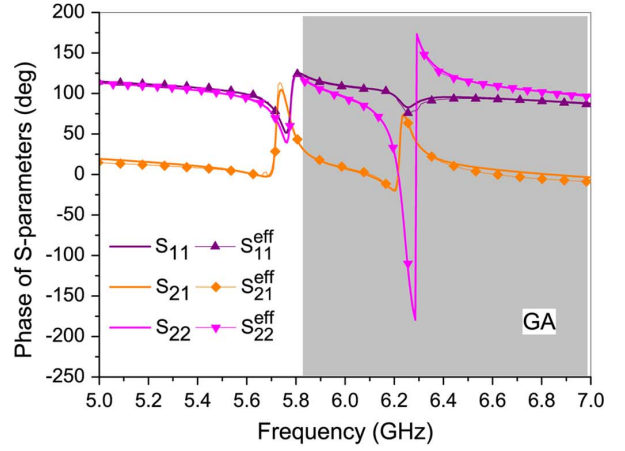
(b)

Fig. 17. Magnitudes of S -parameters simulated and recovered using the effective parameters. (a) NRW_{avg} and (b) GA retrieval methods. Rectangular bars denote the range of different magnitudes of S_{11} and S_{22} .

with the negative index of refraction. Asymmetry is also much more pronounced if the gaps are far from the microstrip line, as was also the case with the unit cells containing the gaps parallel to the microstrip line. For both unit cells with perpendicular gaps, the maximum value of u -parameter ($u_{\text{far}} = 8.6$ and $u_{\text{near}} = 6.6$) is considerably greater than in the case of gaps parallel to the microstrip line ($u_{\text{far}} = 3.69$ and $u_{\text{near}} = 1.21$).



(a)



(b)

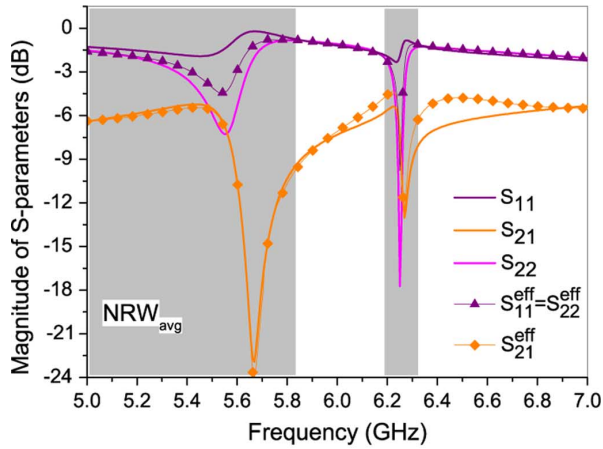
Fig. 18. Phases of S -parameters simulated and recovered using effective parameters. (a) NRW_{avg} and (b) GA retrieval methods.

In Fig. 15, we compare the standard condition for the negative index of refraction and the novel condition for the unit cell with the upper gap far from the microstrip line. For calculating both conditions, we used the effective parameters extracted by the GA method. It can be seen that around the first resonance the novel criterion exactly coincides with points where the real part of the negative index of refraction becomes zero. That is not the case with the standard criterion, which predicts considerably wider range of negative index. Around the second resonance at 6.3 GHz, the standard criterion predicts negative index of refraction while the real part of the index is positive. As a proof of validity of the novel criterion, we added the curve that corresponds to the standard criterion, but with data extracted by means of the NRW_{avg} method, which completely overlaps the novel criterion.

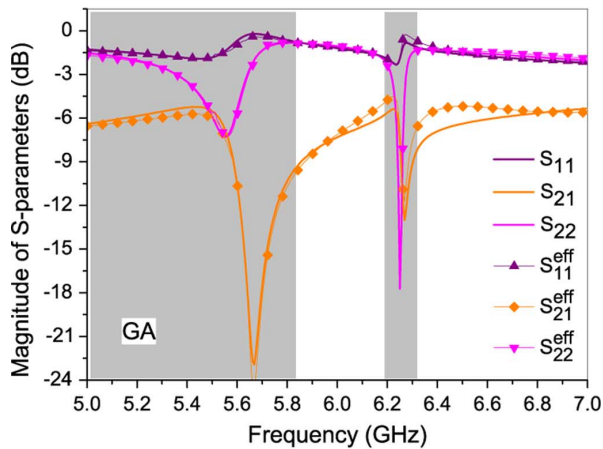
IV. VALIDATION OF THE EXTRACTION METHODS

A. Decomposition Method

In order to validate the proposed method, an independent simulation of the microstrip line immersed in a slab of homogeneous material with the extracted effective parameters can be used, as depicted in Fig. 16. Input microstrip lines are immersed in the effective dielectric $\epsilon_{\text{eff}}^{\text{ML}} = 3.15$. When calculating S -parameters of the effective medium slab, input microstrip lines are



(a)



(b)

Fig. 19. Magnitudes of S -parameters simulated and recovered using the effective parameters. (a) NRW_{avg} and (b) GA retrieval methods. Rectangular bars denote the range of different magnitudes of S_{11} and S_{22} .

de-embedded. We can readily apply this procedure to restore the S -parameters for the NRW extraction, which uses an isotropic medium described by ϵ and μ , but to the authors' best knowledge, there is no EM solver capable of handling bianisotropic media.

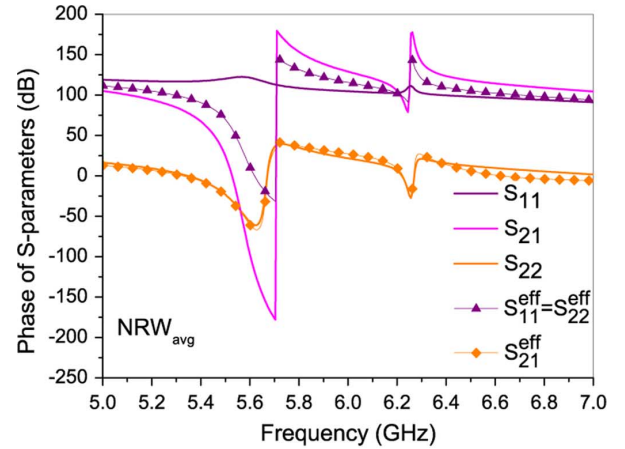
Therefore, we propose the following work-around: we simulate two isotropic slabs corresponding to the GA_1 - and GA_2 -parameters described above, to obtain two sets of $ABCD$ -parameters, denoted $ABCD_{\text{GA}_1}$ and $ABCD_{\text{GA}_2}$, respectively. Now, if we observe (19) more closely, we note that it represents what is known as *eigendecomposition* of a matrix in linear algebra, where $e^{\pm\gamma l}$ represents eigenvalues, and columns of matrix Q represent eigenvectors. From (17) and (19), it follows that the matrices $ABCD_{\text{GA}_1,2}$, since they imply a single value of impedance $Z_{c1,2}$, respectively, will decompose in the following form:

$$ABCD_{\text{GA}_1,2} = Q_{1,2} \text{diag}(e^{\gamma l}, e^{-\gamma l}) Q_{1,2}^{-1} \quad (30)$$

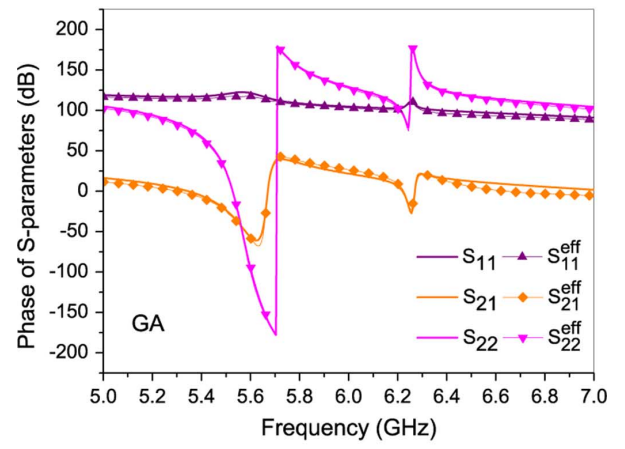
where

$$Q_{1,2} = \begin{bmatrix} 1 & 1 \\ \frac{1}{Z_{c1,2}} & -\frac{1}{Z_{c1,2}} \end{bmatrix} \quad (31)$$

respectively. Note that the eigenvalues $e^{\pm\gamma l}$ are the same for all three matrices.



(a)



(b)

Fig. 20. Phases of S -parameters simulated and recovered using the effective parameters. (a) NRW_{avg} and (b) GA retrieval methods.

From the simulation of the slabs GA_1 and GA_2 , we obtain two sets of S -parameters, which can be converted to $ABCD_{\text{GA}_1,2}$. We then perform the eigendecomposition of these matrices to obtain the form of (30). This decomposition is readily available in software packages like MATLAB, and we only need to arrange eigenvalues and eigenvectors in the same order as in (30), which can be done according to the passivity criterion (26). Now we can obtain the matrix Q as

$$Q = \begin{bmatrix} Q_1(1,1) & Q_2(1,2) \\ Q_1(2,1) & Q_2(2,2) \end{bmatrix} \quad (32)$$

and finally, the resulting $ABCD$ matrix according to (19).

B. Unit Cell With Gaps Parallel to the Microstrip Line

The S -parameters resulting from the described approach for the unit cell with gaps parallel and far from the microstrip line [see Fig. 2(b)], compared with the original simulations, are shown on Figs. 17 and 18, for both the NRW_{avg} and GA method. The NRW_{avg} method [see Figs. 17(a) and 18(a)] results in symmetric response (therefore only one reflection coefficient $S_{11}^{\text{eff}} = S_{22}^{\text{eff}}$ is reconstructed), which clearly fails to reproduce reflection in the range of pronounced asymmetry correctly (marked with a rectangular bar). This is most visible in phase, where the obtained value behaves as mean of the

original phases of S_{11} and S_{22} (this is expected because of the used averaging procedure).

The GA method, however, clearly distinguishes two different values of reflection coefficients, which are very close to the original values [see Figs. 17(b) and 18(a)]. It is clearly visible that the effective parameters extracted by the GA method allow the recovery of all S -parameters, which is not the case with the parameters retrieved by the NRW_{avg} method, that can restore only S_{21} , but not S_{11} and S_{22} in the range where asymmetry is present. The unit cell has symmetric response out of that range and both methods work correctly. We believe that the presented results clearly show that the GA method is advantageous over the NRW_{avg} when asymmetry is present, while it gives exactly the same results as the well-established NRW method for symmetric response.

C. Unit Cell With Gaps Perpendicular to the Microstrip Line

Results for the unit cell with gaps perpendicular to, and upper gap near the microstrip line [see Fig. 10(b)], compared with the original simulations, are shown in Figs. 19 and 20, for the NRW_{avg} and GA methods. Again, the NRW_{avg} method [see Figs. 19(b) and 20(b)] reproduces only the mean value of reflection, the disparity here being even more striking, due to the greater asymmetry of the unit cell. The GA method closely reproduces both reflection coefficients once again [see Figs. 19(b) and 20(b)]. To conclude, the GA method is able to restore all S -parameters in the whole frequency range of interest, while the NRW_{avg} method recovers them only in the range of symmetric response. Especially good agreement is obtained in the phases of S -parameters. There are small discrepancies in the recovered magnitude of S_{21} around the second resonance, which appear equally in both methods.

V. CONCLUSION

In this paper, we have presented the GA for the extraction of effective parameters for the metamaterial transmission line loaded with asymmetric unit cells. To describe the asymmetry, we have introduced an equivalent bianisotropic medium, which emulates the effect of asymmetric unit cells. Besides standard constitutive parameters such as permittivity, permeability, and characteristic impedance, the equivalent medium is described by two additional parameters, u and η , which are very useful as a measure of asymmetry.

We derived a novel condition necessary for achieving a negative index of refraction in the bianisotropic medium. According to it, the criterion valid for isotropic medium is relaxed in the range in which the real and imaginary part of the u -parameter are both negative or positive, while the criterion becomes more strict if they have different signs.

The proposed generalized extraction procedure and the NRW_{avg} method, adopted for asymmetric unit cells, are applied to novel dual-band unit cells. They consist of BSC SRRs with gaps displaced from the center (to the left and to the right or up and down), along two gap-bearing sides, which are placed one above the other. It was shown that unit cells with gaps parallel with the microstrip line exhibit asymmetry only around one resonance. Unit cells with gaps perpendicular to

the microstrip line have a very asymmetric response around both resonances. Therefore, the effective permittivity and permeability extracted using the GA and NRW_{avg} methods are significantly different.

To conclude, we have shown that the NRW_{avg} procedure gives the correct index of refraction in the whole frequency range, but wrong effective permittivity, permeability, and characteristic impedance in the range of asymmetric response.

This was proven through the validation procedure where the asymmetric unit cell was replaced by effective medium slabs with the parameters extracted by the proposed GA method. The all original S -parameters were successfully restored, which was not the case when the parameters extracted by the approximate NRW_{avg} method are used.

ACKNOWLEDGMENT

The authors would like to thank WIPL-D Belgrade for the use of software licenses.

REFERENCES

- [1] V. G. Veselago, "Electrodynamics of substances with simultaneously negative ϵ and μ ," *Sov. Phys.-Usp.*, vol. 10, no. 4, pp. 509–514, 1968.
- [2] J. B. Pendry, "Negative refraction makes a perfect lens," *Phys. Rev. Lett.* vol. 85, pp. 3966–3969, Oct. 2000. [Online]. Available: <http://link.aps.org/doi/10.1103/PhysRevLett.85.3966>
- [3] C. Caloz and T. Itoh, *Electromagnetic Metamaterials: Transmission Line Theory and Microwave Applications: The Engineering Approach*. New York, NY, USA: Wiley, 2006.
- [4] L. Landau, E. Lifshits, and L. Pitaevskii, *Electrodynamics of Continuous Media*, 2nd ed. Oxford, U.K.: Pergamon, 1984.
- [5] J. B. Pendry, A. J. Holden, W. J. Stewart, and I. Youngs, "Extremely low frequency plasmons in metallic mesostructures," *Phys. Rev. Lett.* vol. 76, pp. 4773–4776, Jun. 1996. [Online]. Available: <http://link.aps.org/doi/10.1103/PhysRevLett.76.4773>
- [6] J. Pendry, A. Holden, D. Robbins, and W. Stewart, "Magnetism from conductors and enhanced nonlinear phenomena," *IEEE Trans. Microw. Theory Techn.*, vol. 47, no. 11, pp. 2075–2084, Nov. 1999.
- [7] A. M. Nicolson and G. F. Ross, "Measurement of the intrinsic properties of materials by time-domain techniques," *IEEE Trans. Instrum. Meas.*, vol. IM-19, no. 4, pp. 377–382, Nov. 1970.
- [8] W. Weir, "Automatic measurement of complex dielectric constant and permeability at microwave frequencies," *Proc. IEEE*, vol. 62, no. 1, pp. 33–36, Jan. 1974.
- [9] D. R. Smith, S. Schultz, P. Markoš, and C. M. Soukoulis, "Determination of effective permittivity and permeability of metamaterials from reflection and transmission coefficients," *Phys. Rev. B, Condens. Matter* vol. 65, Apr. 2002. [Online]. Available: <http://link.aps.org/doi/10.1103/PhysRevB.65.195104>, Art. ID 195104
- [10] P. Markos and C. Soukoulis, "Transmission properties and effective electromagnetic parameters of double negative metamaterials," *Opt. Exp.* vol. 11, no. 7, pp. 649–661, Apr. 2003. [Online]. Available: <http://www.opticsexpress.org/abstract.cfm?URI=oe-11-7-649>
- [11] S.-G. Mao, S.-L. Chen, and C.-W. Huang, "Effective electromagnetic parameters of novel distributed left-handed microstrip lines," *IEEE Trans. Microw. Theory Techn.*, vol. 53, no. 4, pp. 1515–1521, Apr. 2005.
- [12] D. R. Smith, D. C. Vier, T. Koschny, and C. M. Soukoulis, "Electromagnetic parameter retrieval from inhomogeneous metamaterials," *Phys. Rev. E, Stat. Phys. Plasmas Fluids Relat. Interdiscip. Top.* vol. 71, Mar. 2005. [Online]. Available: <http://link.aps.org/doi/10.1103/PhysRevE.71.036617>, Art. ID 036617
- [13] R. Marqués, F. Medina, and R. Rafii-El-Idrissi, "Role of bianisotropy in negative permeability and left-handed metamaterials," *Phys. Rev. B, Condens. Matter* vol. 65, Apr. 2002. [Online]. Available: <http://link.aps.org/doi/10.1103/PhysRevB.65.144440>, Art. ID 144440
- [14] X. Chen, B.-I. Wu, J. A. Kong, and T. M. Grzegorzczak, "Retrieval of the effective constitutive parameters of bianisotropic metamaterials," *Phys. Rev. E, Stat. Phys. Plasmas Fluids Relat. Interdiscip. Top.* vol. 71, pp. –, Apr. 2005. [Online]. Available: <http://link.aps.org/doi/10.1103/PhysRevE.71.046610>, Art. ID 046610

- [15] C. Kriegler, M. Rill, S. Linden, and M. Wegener, "Bianisotropic photonic metamaterials," *IEEE J. Sel. Top. Quantum Electron.*, vol. 16, no. 2, pp. 367–375, Mar.–Apr. 2010.
- [16] A. Kildishev, J. Borneman, X. Ni, V. Shalaev, and V. Drachev, "Bianisotropic effective parameters of optical metamagnetics and negative-index materials," *Proc. IEEE*, vol. 19, no. 10, pp. 1691–1700, Oct. 2011.
- [17] A. Alù, "First-principles homogenization theory for periodic metamaterials," *Phys. Rev. B, Condens. Matter* vol. 84, Aug. 2011. [Online]. Available: <http://link.aps.org/doi/10.1103/PhysRevB.84.075153>, Art. ID 075153
- [18] T. Koschny, P. Markoš, E. N. Economou, D. R. Smith, D. C. Vier, and C. M. Soukoulis, "Impact of inherent periodic structure on effective medium description of left-handed and related metamaterials," *Phys. Rev. B, Condens. Matter* vol. 71, Jun. 2005. [Online]. Available: <http://link.aps.org/doi/10.1103/PhysRevB.71.245105>, Art. ID 245105
- [19] A. Alù, "Restoring the physical meaning of metamaterial constitutive parameters," *Phys. Rev. B, Condens. Matter* vol. 83, Feb. 2011. [Online]. Available: <http://link.aps.org/doi/10.1103/PhysRevB.83.081102>, Art. ID 081102
- [20] A. Sihvola and I. V. Lindell, F. Capolino, Ed., "Bianisotropic materials and PEMC," in *Theory and Phenomena of Metamaterials*. Boca Raton, FL, USA: CRC Press, 2009, pp. 26.1–26.7.
- [21] M. W. McCall, A. Lakhtakia, and W. S. Weiglhofer, "The negative index of refraction demystified," *Eur. J. Phys.* vol. 23, no. 3, pp. 353–, 2002. [Online]. Available: <http://stacks.iop.org/0143-0807/23/i=3/a=314>
- [22] A. Lakhtakia, M. W. McCall, and W. S. Weiglhofer, W. Weiglhofer and A. Lakhtakia, Eds., "Negative phase-velocity mediums," in *Introduction to Complex Mediums for Optics and Electromagnetics*, ser. SPIE Press Monograph. Bellingham, WA, USA: SPIE Press, 2003, pp. 347–363.
- [23] D. Pozar, *Microwave Engineering*, 3rd ed. New York, NY, USA: Wiley, 2005.
- [24] X. Chen, T. M. Grzegorzczak, B.-I. Wu, J. Pacheco, and J. A. Kong, "Robust method to retrieve the constitutive effective parameters of metamaterials," *Phys. Rev. E, Stat. Phys. Plasmas Fluids Relat. Interdiscip. Top.* vol. 70, Jul. 2004. [Online]. Available: <http://link.aps.org/doi/10.1103/PhysRevE.70.016608>, Art. ID 016608
- [25] Z. Szabo, G.-H. Park, R. Hedge, and E.-P. Li, "A unique extraction of metamaterial parameters based on Kramers–Kronig relationship," *IEEE Trans. Microw. Theory Techn.*, vol. 58, no. 10, pp. 2646–2653, Oct. 2010.
- [26] N. Liu, H. Liu, S. Zhu, and H. Giessen, "Stereometamaterials," *Nat. Photon.*, vol. 3, pp. 157–162, Mar. 2009.
- [27] R. Bojanic, B. Jokanovic, and V. Milosevic, "Multiband delay lines with reconfigurable split-ring resonators," in *10th Int. Telecommun. in Modern Satellite Cable and Broadcast. Services Conf.*, 2011, vol. 1, pp. 31–34.



Vojislav Milosevic was born in Belgrade, Serbia, on April 5, 1986. He received the Dipl. Ing. and M.Sc. degrees in electrical engineering from the University of Belgrade, Belgrade, Serbia, in 2009 and 2012, respectively, and is currently working toward the Ph.D. degree at the University of Belgrade.

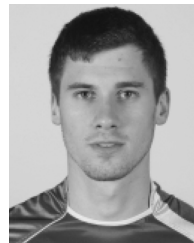
In 2010, he became a Research Assistant with the Photonic Center, Institute of Physics, University of Belgrade. His research interests include EM metamaterials and homogenization theory.



Branka Jokanovic (M'89) received the Dipl. Ing., M.Sc., and Ph.D. degrees in electrical engineering from the University of Belgrade, Belgrade, Serbia, in 1977, 1988, and 1999, respectively.

She is currently a Research Professor with the Institute of Physics, University of Belgrade. Prior to joining the Photonic Center, Institute of Physics, she was the Head of the Microwave Department, Institute IMTEL, Belgrade, Serbia. She is a Corresponding Member of the Serbian Academy of Engineering Sciences. She initiated the Yugoslav microwave theory and techniques journal *Microwave Review* for which she was the editor for six years (1994–2000). Her current research interests include modeling, simulation, and characterization of microwave and photonic metamaterials for wireless communications and sensors.

Dr. Jokanovic was one of the founders of the Yugoslav IEEE Microwave Theory and Techniques Society (IEEE MTT-S) Chapter and its chairperson from 1989 to 2000. She also founded the Yugoslav Association for Microwave Techniques and Technology in 1994. She was the recipient of the 1996 IMTEL Institute Award for Scientific Contribution, the 2000 IEEE Third Millennium Award, and the 2005 Yugoslav IEEE MTT-S Distinguished Service Award.



Radovan Bojanic was born in Knin, Croatia, in 1986. He received the Dipl. Ing. and M.Sc. degrees in electrical engineering from the University of Belgrade, Belgrade, Serbia, in 2009 and 2012, respectively, and is currently working toward the Ph.D. degree at the University of Belgrade.

Since 2010, he has been with the Institute of Physics, University of Belgrade, as Research Assistant with the Photonic Center, where he has been involved in modeling and simulation of microwave circuits.

Retrieval and validation of the effective constitutive parameters of bianisotropic metamaterials

This content has been downloaded from IOPscience. Please scroll down to see the full text.

2014 Phys. Scr. 2014 014046

(<http://iopscience.iop.org/1402-4896/2014/T162/014046>)

View [the table of contents for this issue](#), or go to the [journal homepage](#) for more

Download details:

IP Address: 147.91.83.219

This content was downloaded on 27/09/2016 at 16:15

Please note that [terms and conditions apply](#).

You may also be interested in:

[Transmission lines emulating moving media](#)

J Vehmas, S Hrabar and S Tretyakov

[Analysis of ultra-broad band metamaterial absorber based on simplified multi-reflection interference theory](#)

Xiaojun Huang, Xiaoling He, Linyan Guo et al.

[Bianisotropic metamaterials based on twisted asymmetric crosses](#)

J A Reyes-Avenidaño, M P Sampedro, E Juárez-Ruiz et al.

[The strong non-reciprocity of metamaterial absorber: characteristic, interpretation and modelling](#)

Yuanxun Li, Yunsong Xie, Huaiwu Zhang et al.

[Metamaterial analogue of EIT in two orthogonal directions](#)

F-Y Meng, J-H Fu, K Zhang et al.

[Negative refraction and partial focusing in an anisotropic metamaterial](#)

Xiaohua Teng, Junming Zhao, Tian Jiang et al.

[Three-dimensional magnetic terahertz metamaterials using a multilayer electroplating technique](#)

Kebin Fan, Andrew C Strikwerda, Richard D Averitt et al.

Retrieval and validation of the effective constitutive parameters of bianisotropic metamaterials

V Milosevic, B Jokanovic and R Bojanic

Institute of Physics, University of Belgrade, Pregrevica 118, 11080 Belgrade, Serbia

E-mail: vojislav@ipb.ac.rs

Received 20 September 2013

Accepted for publication 12 February 2014

Published 19 September 2014

Abstract

In this paper we present the exact bianisotropic parameter retrieval procedure for the case of transmission line metamaterials. The procedure assigns two different sets of effective parameters for two directions of propagation, which can be modelled by a bianisotropic medium. The procedure is applied to a microstrip line loaded with asymmetric edge-coupled split-ring resonators with gaps parallel and perpendicular to the line. The standard Nicolson-Ross-Weir procedure based on averaging of the S -parameters is not applicable to this case due to pronounced asymmetry. We also present the reverse procedure, which recovers the original S -parameters using the extracted effective permittivity and permeability, that fully validates the correctness of the proposed retrieval method.

Keywords: asymmetric unit cell, split-ring resonator (SRR), effective material parameters, bianisotropic medium, metamaterial transmission line

(Some figures may appear in colour only in the online journal)

1. Introduction

Metamaterials are most frequently characterized by their effective electromagnetic parameters, under the assumption that the homogenization procedure can be applied to them [1]. The effective parameters are usually obtained through the Nicolson–Ross–Weir (NRW) extraction procedure [2]. Almost the same procedure can be applied in the case of transmission line metamaterials, where we assume that the conductors of the line are immersed in the effective dielectric [3].

The NRW procedure is based on the isotropic medium model, described only with scalar ϵ and μ , which will always have symmetric response. If the metamaterial sample under study has asymmetric response ($S_{11} \neq S_{22}$), which can happen due to several factors (magneto-electric coupling, spatial dispersion, asymmetric positioning of elements within the unit cell), the NRW procedure is inappropriate. Some

authors suggested an NRW_{avg} method based on averaging of the scattering parameters (i.e. $S_{11avg} = \sqrt{S_{11}S_{22}}$), but it is acceptable only for a small asymmetry [4]. An improved procedure is based on using a bianisotropic medium model [5, 6].

In the previous paper [7] we derived the exact parameter extraction procedure based on a bianisotropic model for the case of transmission line metamaterials. We demonstrated that for the reciprocal medium this model will represent an equivalent transmission line having the same propagation constant for both directions, but different characteristic impedances.

In this paper, we explore the causes of differences between the NRW_{avg} method and bianisotropic parameter (BP) retrieval. They both give the same index of refraction, but different characteristic impedances, which affect the effective parameters ϵ and μ .

2. Asymmetric transmission line

2.1. Network parameters of the line section

Consider the transmission line with propagation constant γ and characteristic impedances Z_{c1} and Z_{c2} for the incident and reflected waves, respectively. Anywhere on the line, the total voltage and current can be expressed as functions of voltages of individual waves [7]:

$$\begin{bmatrix} V \\ I \end{bmatrix} = \begin{bmatrix} 1 & 1 \\ \frac{1}{Z_{c1}} & -\frac{1}{Z_{c2}} \end{bmatrix} \begin{bmatrix} V^i \\ V^r \end{bmatrix} = Q \begin{bmatrix} V^i \\ V^r \end{bmatrix}. \quad (1)$$

For the section of such a line of length l we can write the following relationship between voltages of incident and reflected waves at ports 1 and 2:

$$\begin{bmatrix} V_1^i \\ V_1^r \end{bmatrix} = \begin{bmatrix} e^{\gamma l} & 0 \\ 0 & e^{-\gamma l} \end{bmatrix} \begin{bmatrix} V_2^i \\ V_2^r \end{bmatrix}. \quad (2)$$

By combining (1) with (2) we obtain the $ABCD$ matrix of the section

$$ABCD = Q \begin{bmatrix} e^{\gamma l} & 0 \\ 0 & e^{-\gamma l} \end{bmatrix} Q^{-1}. \quad (3)$$

2.2. Extraction of the effective parameters

From equation (3), we can derive the inverse relation for transmission line parameters from the $ABCD$ parameters, which can be obtained from measurement or simulations:

$$\gamma = \pm \cosh^{-1} \frac{A + D}{2},$$

$$Z_{c1,2} = \frac{A - D}{2C} \pm \frac{1}{C} \sqrt{1 - \left(\frac{A + D}{2} \right)^2}. \quad (4)$$

Now we can calculate the effective electromagnetic parameters using propagation constant γ and normalized characteristic impedance $z_{1,2} = Z_{c1,2}/Z_{air}$, where Z_{air} is the characteristic impedance of the transmission line filled with air:

$$n = -j \frac{c}{\omega} \gamma, \quad \epsilon_{1,2} = \frac{n}{z_{1,2}}; \quad \mu_{1,2} = n z_{1,2}. \quad (5)$$

We will label sets of parameters for the two directions as BP_1 and BP_2 , each of which represents an isotropic medium. Another option is to use the mean value of characteristic impedance $z_{avg} = (z_1 + z_2)/2$, in which case an additional parameter must be used to take account of the asymmetry [7]. We will denote these averaged parameters $\epsilon_{avg} = n/z_{avg}$, $\mu_{avg} = n z_{avg}$ as BP_{avg} .

2.3. Characteristic impedances in BP and NRW methods

The main reason for the differences in the extracted permittivity and permeability using the exact BP and approximate NRW_{avg} methods are caused by different characteristic

impedances. In the BP method, the mean value of characteristic impedance, using $ABCD$ parameters, is

$$z_{avg}^{BP} = \pm \frac{1}{Z_{air}} \frac{1}{C} \sqrt{1 - \left(\frac{A + D}{2} \right)^2}, \quad (6)$$

which can be converted to S -parameters:

$$z_{avg}^{BP} = \frac{Z_0}{Z_{air}} \frac{2S_{12}}{1 - S_{11} - S_{22} + S_{11}S_{22} - S_{12}^2} z'_c, \quad (7)$$

where Z_0 is the characteristic impedance of the transmission line, and

$$z'_c = \sqrt{1 - \left(\frac{1 - S_{11}S_{22} + S_{12}^2}{S_{12}} \right)^2}. \quad (8)$$

When we apply the averaging procedure, we actually substitute both reflection coefficients $S_{11avg} = \sqrt{S_{11}S_{22}}$. It can be shown that, when $S_{11} = S_{22}$, relation (7) reduces to the standard expression for characteristic impedance in the NRW method [7]. Therefore, we can obtain impedance z_{avg}^{NRW} for the NRW_{avg} method by substituting S_{11avg} in (7), which comes down to

$$z_{avg}^{NRW} = \frac{Z_0}{Z_{air}} \frac{2S_{12}}{1 - 2\sqrt{S_{11}S_{22}} + S_{11}S_{22} - S_{12}^2} z'_c. \quad (9)$$

Therefore, we can express the relative difference between two impedances:

$$\frac{z_{avg}^{NRW}}{z_{avg}^{BP}} = \frac{S_{11} + S_{22} - S_{11}S_{22} + S_{12}^2 - 1}{2\sqrt{S_{11}S_{22}} - S_{11}S_{22} + S_{12}^2 - 1}$$

$$= \frac{(S_{11} + S_{22})/2 - F}{\sqrt{S_{11}S_{22}} - F}, \quad (10)$$

where $F = (S_{11}S_{22} - S_{12}^2 + 1)/2$.

Here we have derived the ratio between the characteristic impedances for BP and NRW_{avg} methods, that is proportional to the difference between geometric and arithmetic means of S_{11} and S_{22} . This ratio is a consequence of the averaging in the NRW method ($S_{11avg} = \sqrt{S_{11}S_{22}}$), which was necessary to provide the correct value of the index of refraction:

$$n = \mp \frac{jc}{\omega l} \cosh \frac{1 - S_{11}S_{22} + S_{12}^2}{2S_{12}}$$

$$= \mp \frac{jc}{\omega l} \cosh \frac{1 - S_{11avg}^2 + S_{12}^2}{2S_{12}}. \quad (11)$$

This is the main reason why the exact retrieved permittivity and permeability are different from those obtained with the NRW_{avg} method.

3. Asymmetric unit cells

We applied the proposed retrieval procedure to the asymmetric unit cell consisting of a microstrip line loaded with

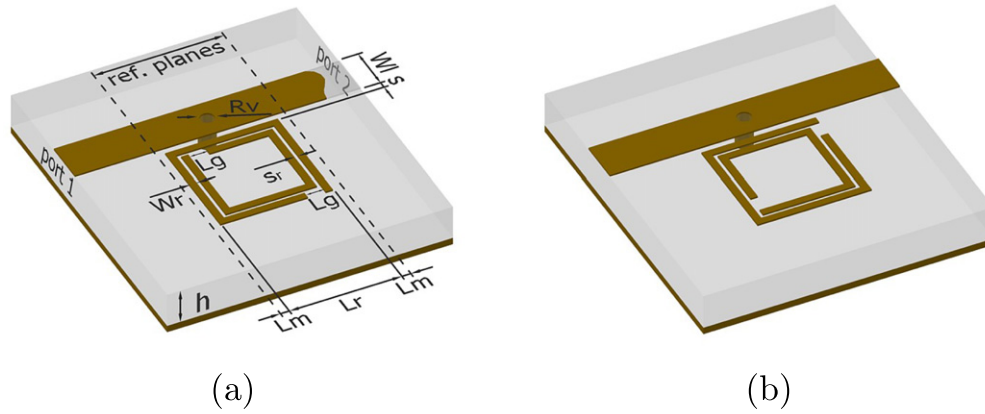


Figure 1. Asymmetric unit cells: (a) gaps parallel, (b) gaps perpendicular. Relevant dimensions: $h = 1.27$ mm, $L_r = 3$ mm, $L_g = 0.5$ mm, $L_m = 0.25$ mm, $W_l = 1.2$ mm, $W_r = 0.2$ mm, $R_v = 0.5$ mm, $s = 0.1$ mm, $s_r = 0.1$ mm, and substrate relative permittivity is $\epsilon_r = 10.2$.

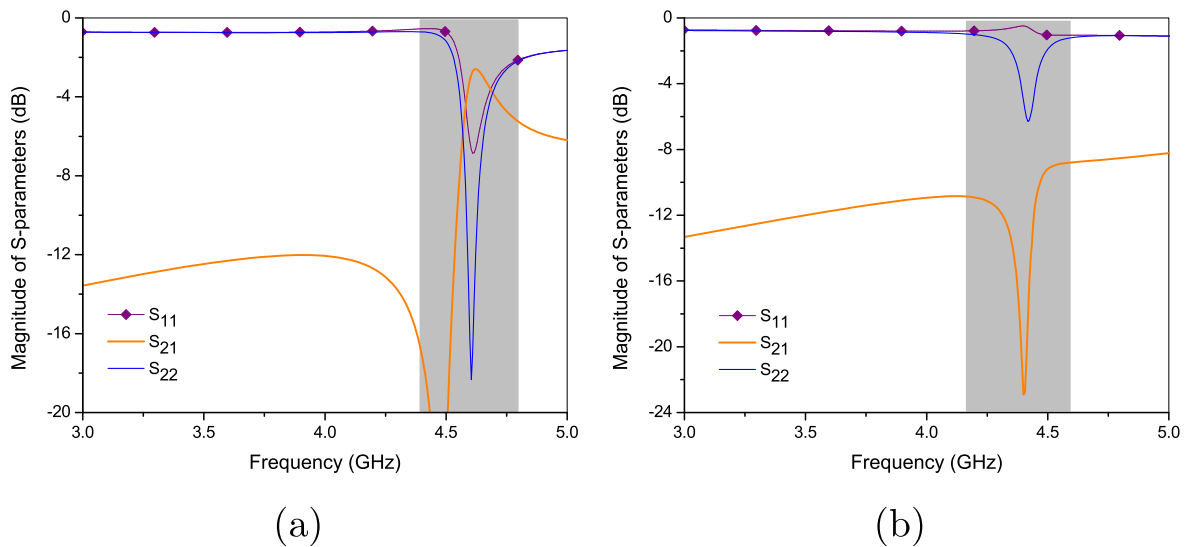


Figure 2. Magnitude of the S -parameters: (a) gaps parallel, (b) gaps perpendicular. Rectangular bars denote regions where asymmetry is present.

edge-coupled split-ring resonators (SRRs), and connected to ground with via holes. We examined two types of edge-coupled SRR with gap-bearing sides parallel to the microstrip line and perpendicular to it. The gaps are moved symmetrically with respect to the center, to the opposite sides (figure 1).

Magnitudes of the simulated S -parameters given in figure 2, and phases in figure 3, are obtained using full-wave electromagnetic simulations based on method of moments [8]. We can see that S_{11} is different from S_{22} in both magnitude and phase only around the resonance, but that asymmetry is most pronounced in the case with perpendicular gaps which are displaced from the center up and down.

3.1. Effective parameters

The extracted effective index of refraction, characteristic impedance, permittivity and permeability are shown in figures 4–7. It can be seen from figure 4 that an SRR with parallel gaps has a considerably wider frequency range with

negative index of refraction than an SRR with perpendicular gaps.

The impedance $Z_{\text{avg}}^{\text{BP}}$ is the mean value of impedances Z_{c1} and Z_{c2} , which is also visible in figure 5. The characteristic impedance $Z_{\text{avg}}^{\text{NRW}}$ has a completely different shape and values, that is a consequence of the averaging of S_{11} and S_{22} parameters. For both structures the impedance $Z_{\text{avg}}^{\text{NRW}}$ exhibits very unnatural behavior at some frequencies around resonance. This will result in an unusual shape of the extracted ϵ and μ , which can be seen in figures 6(b) and 7(b).

The asymmetry is weaker in the case of SRRs with parallel gaps, which leads to smaller differences in extracted effective parameters for two different directions, which can be seen in figures 6(a) and 7(a) (in this case the results for the NRW_{avg} method are not shown, as they would not give significant differences compared to the BP method). In contrast to this, the asymmetry in SRRs with perpendicular gaps is more pronounced because Z_{c1} considerably differs from Z_{c2} .

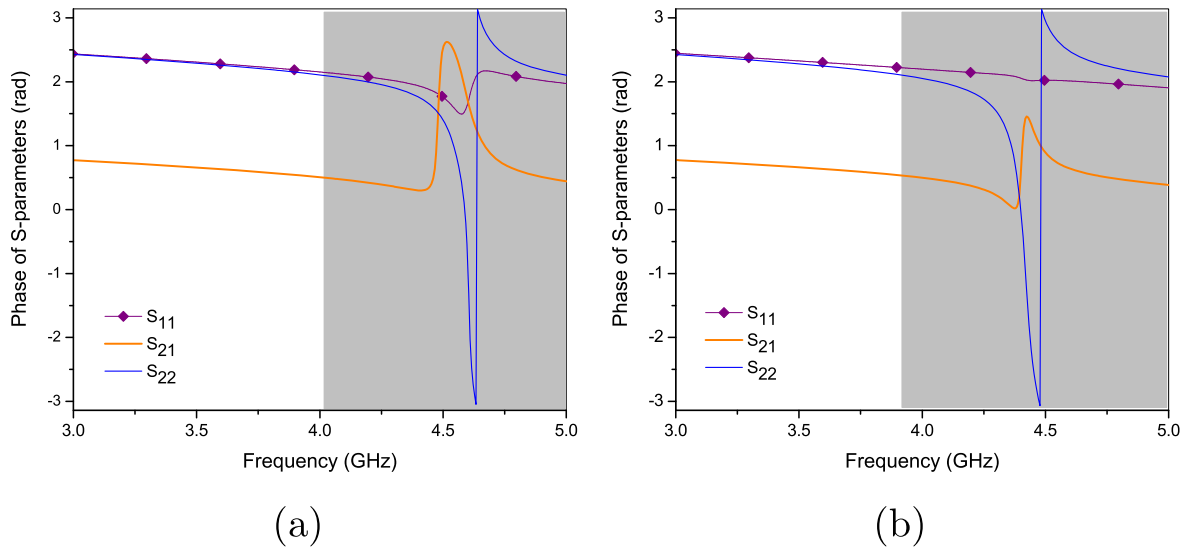


Figure 3. Phase of the S -parameters: (a) gaps parallel, (b) gaps perpendicular. Rectangular bars denote regions where asymmetry is present.

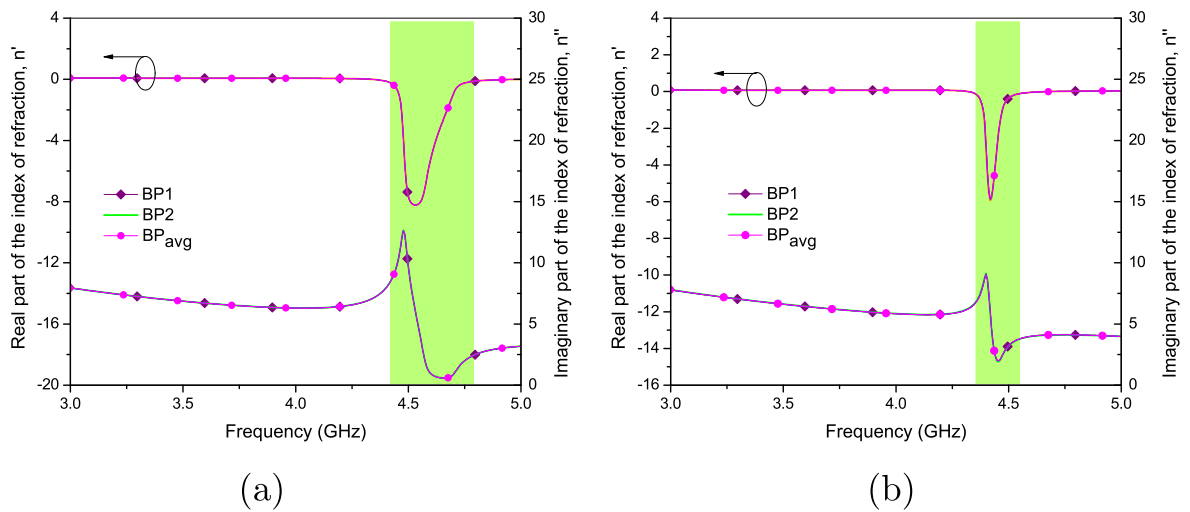


Figure 4. Extracted index of refraction: (a) gaps parallel, (b) gaps perpendicular. Rectangular bars denote the frequency range with double-negative effective parameters.

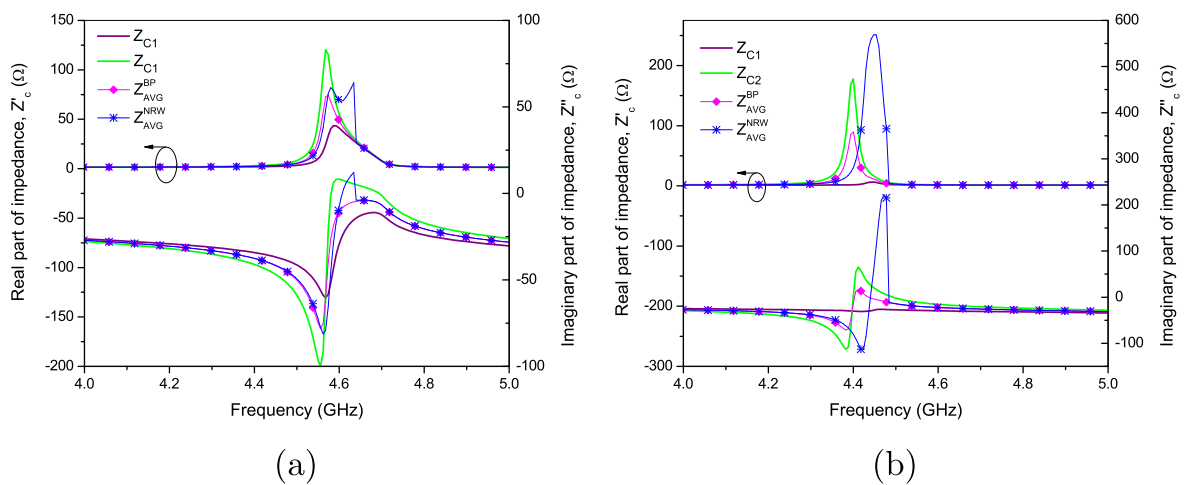


Figure 5. Extracted characteristic impedances using BP and NRW_{avg} methods: (a) gaps parallel, (b) gaps perpendicular.

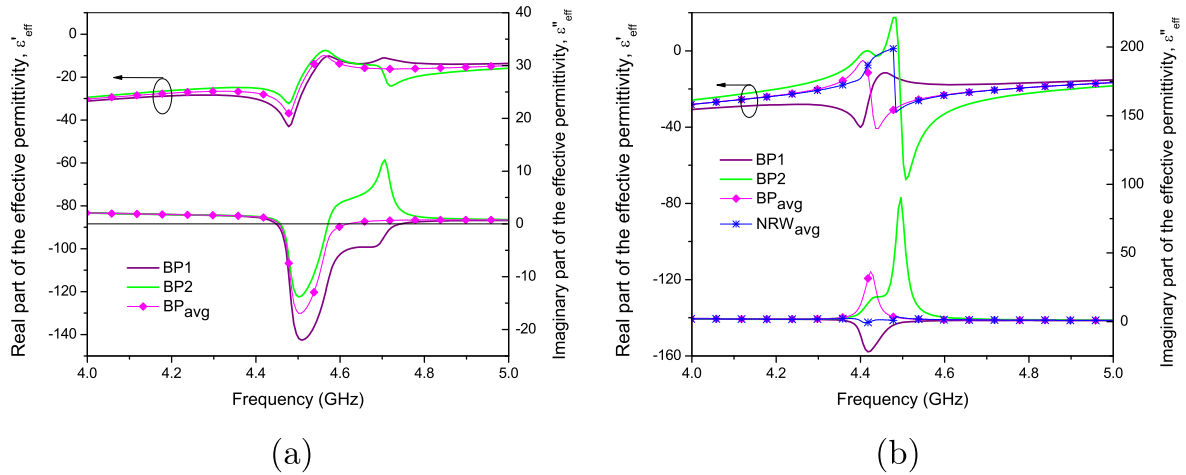


Figure 6. Extracted effective permittivity: (a) gaps parallel, (b) gaps perpendicular.

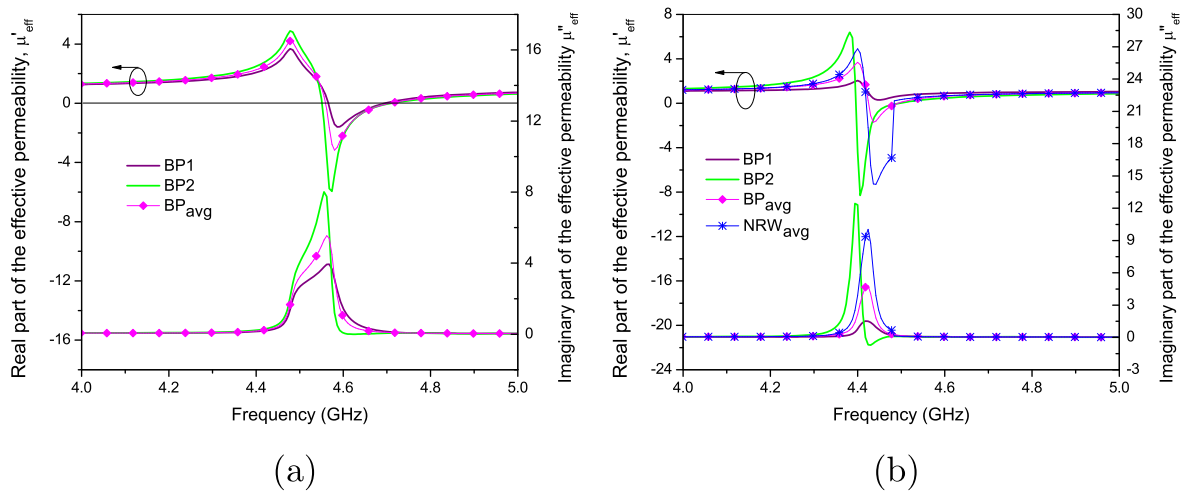


Figure 7. Extracted effective permeability: (a) gaps parallel, (b) gaps perpendicular.

As a consequence, the extracted effective parameters $\epsilon_{1,2}$ and $\mu_{1,2}$ for different directions are greatly different, as can be seen in figures 6(b) and 7(b).

4. Validation of the extracted parameters

To validate the effectiveness of the proposed method we simulated two homogeneous slabs with parameters that correspond to the extracted BP_1 and BP_2 sets. The resulting $ABCD$ parameters, which we will denote as $ABCD_{1,2}$, respectively, can be decomposed to a form like equation (3), which is known as eigendecomposition in linear algebra. The resulting matrix Q is calculated as

$$Q = \begin{bmatrix} Q_1(1, 1) & Q_2(1, 2) \\ Q_1(2, 1) & Q_2(2, 2) \end{bmatrix}, \quad (12)$$

and the final $ABCD$ parameters are obtained using relation (3).

These recovered parameters are converted to S -parameters and compared with the original S -parameters in figures 8 and 9. We can see that a very good agreement is obtained, even in the areas of pronounced asymmetry. Some discrepancies exist near the end of the band, especially in the magnitude, and we are working to improve the stability of the presented method.

5. Conclusion

We have presented the exact extraction procedure for retrieval of the effective parameters for a metamaterial transmission line loaded with asymmetric SRRs, which is based on describing each direction of propagation with an independent set of parameters. This can be interpreted as a consequence of a bianisotropic medium causing different characteristic impedances for different directions. We derived the ratio of the real mean value of the characteristic impedances and that obtained by the NRW_{avg} method, and showed that the main

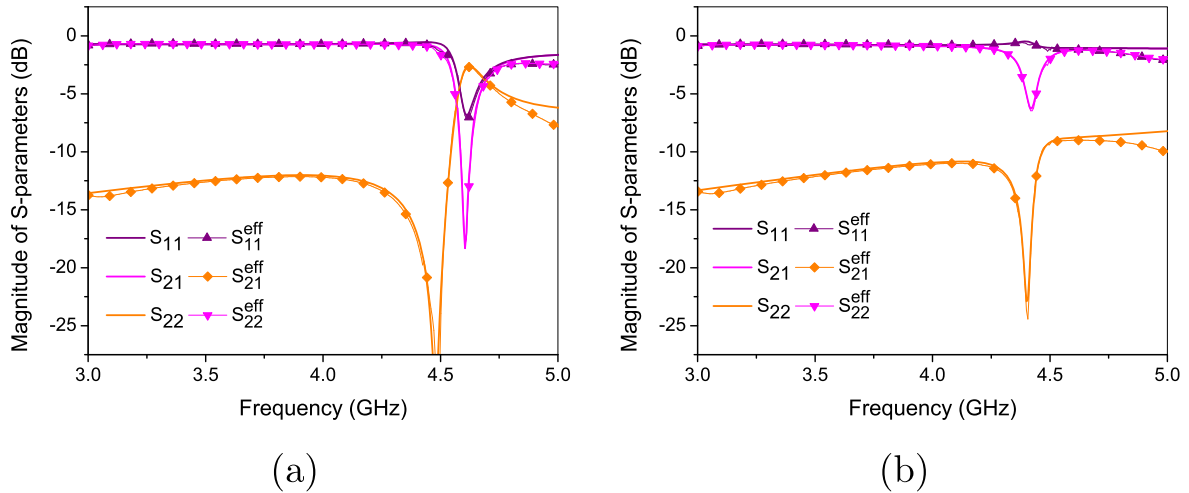


Figure 8. Magnitudes of S -parameters simulated and recovered using the effective bianisotropic parameters: (a) gaps parallel, (b) gaps perpendicular.

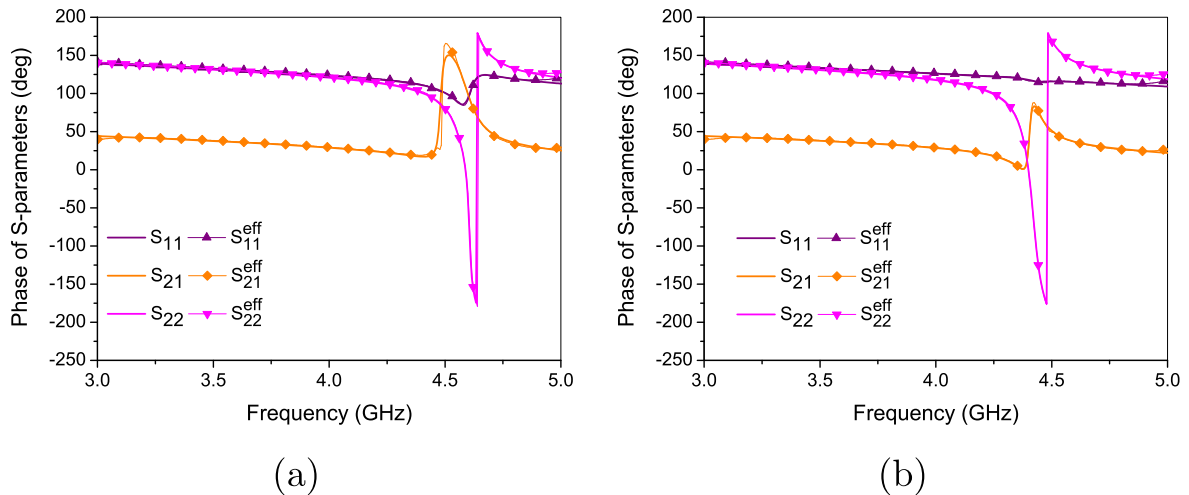


Figure 9. Phases of S -parameters simulated and recovered using the effective bianisotropic parameters: (a) gaps parallel, (b) gaps perpendicular.

difference is a consequence of the averaging of S -parameters in the NRW_{avg} method.

The validation of the BP method is confirmed by using independent simulation of two isotropic homogeneous slabs with the extracted effective permittivity and permeability for the different directions of propagation, and then combining them to recover the original S -parameters. All original S -parameters were successfully restored, which is proof of the validity of our method.

Acknowledgments

This work was financed by the Serbian Ministry for Education, Science and Technological Development through projects TR-32024 and III-45016.

The authors would like to thank WIPL-D Belgrade for the use of software licenses. Numerical results were obtained

on the PARADOX cluster at the Scientific Computing Laboratory of the Institute of Physics Belgrade, supported in part by the Serbian Ministry of Education, Science and Technological Development under projects ON-171017 and III-43007, and by the European Commission under FP7 projects PRACE-3IP and EGI-InSPIRE.

References

- [1] Smith D R, Schultz S, Markoš P and Soukoulis C M 2002 Determination of effective permittivity and permeability of metamaterials from reflection and transmission coefficients *Phys. Rev. B* **65** 195104
- [2] Nicolson A M and Ross G F 1970 Measurement of the intrinsic properties of materials by time-domain techniques *IEEE Trans. Instrum. Meas.* **19** 377–82
- [3] Mao S-G, Chen S-L and Huang C-W 2005 Effective electromagnetic parameters of novel distributed left-handed

- microstrip lines *IEEE Trans. Microw. Theory Tech.* **53** 1515–21
- [4] Smith D R, Vier D C, Koschny Th and Soukoulis C M 2005 Electromagnetic parameter retrieval from inhomogeneous metamaterials *Phys. Rev. E* **71** 036617
- [5] Kildishev A V, Borneman J D, Ni X, Shalaev V M and Drachev V P 2011 Bianisotropic effective parameters of optical metamagnetics and negative-index materials *Proc. IEEE* **99** 1691–700
- [6] Kriegler C E, Rill M S, Linden S and Wegener M 2010 Bianisotropic photonic metamaterials *IEEE J. Sel. Topics Quantum Electron.* **16** 367–75
- [7] Milosevic V, Jokanovic B and Bojanic R 2013 Effective electromagnetic parameters of metamaterial transmission line loaded with asymmetric unit cells *IEEE Trans. Microw. Theory Tech.* **61** 2761–72
- [8] <http://wipl-d.com/>

Enhanced Modelling of Split-Ring Resonators Couplings in Printed Circuits

Radovan Bojanic, Vojislav Milosevic, Branka Jokanovic, *Member, IEEE*, Francisco Medina-Mena, *Fellow, IEEE*, and Francisco Mesa, *Fellow, IEEE*

Abstract—An enhanced equivalent circuit approach for the magnetic/electric interaction of single split-ring resonators (SRRs) with printed lines is presented in this paper. A very simple and efficient lumped-element network is proposed to model the behavior of metamaterial-based printed lines over a wide frequency band. The same circuit topology can be used for the single- and two-mirrored SRRs loaded microstrip line. The corresponding circuit parameters are obtained from the multiconductor transmission line theory as well as from closed-form expressions that make use of just the resonance frequency and minimum of the reflection coefficient (which should be previously extracted from experiments or full-wave simulations). The comparison of our equivalent circuit results with measurements and full-wave simulations has shown a very good agreement in a considerably wider frequency band than other previously proposed simple equivalent circuits.

Index Terms—Coupled transmission lines, equivalent circuit, metamaterial, microstrip line, split-ring resonator.

I. INTRODUCTION

METAMATERIAL-BASED guiding structures have been intensively investigated in the past decade with the purpose of extending the operational capabilities of diverse passive and active components in antennas and microwave circuits [1]. A great deal of effort has specifically been devoted to the study of printed transmission lines loaded with parallel inductive or series capacitive elements [2]–[5]. Resonant-type metamaterial-based transmission lines (MMTLs) with double split ring resonators (SRRs) and complementary SRRs (CSRRs) have also been considered in the frame of the development of filters, sensors, and RFID tags [6]–[8], among other applications. One of the most interesting properties of the SRR is that the

orientation and position of its gap with respect to the hosting transmission line has significant influence on the overall performance of the loaded transmission line. This topic has been previously studied by some of the authors of the present work [9] and has found potential application in designing reconfigurable delay lines and scanning antennas [10], [11].

Metamaterial transmission lines (like many other electromagnetic structures) can be reasonably modeled by lumped-element equivalent circuits. This approach is a useful tool for better understanding of the physics underlying the propagation phenomena in MMTLs. Also, a very important benefit of using the equivalent circuit is in independent parameter tuning and optimization of cascaded structures. These are still very time-consuming, despite the enormous progress in computational resources, especially if a great number of individual resonators is involved.

Equivalent circuits of MMTLs loaded with double SRRs with passband and stopband characteristics can be found, for instance, in [12] and [13], where coplanar waveguides (CPWs) were used as the background transmission lines. MMTLs based on microstrip lines mostly involve coupling with CSRRs [14] or fractal and multiple CSRRs [15] etched in the ground plane (right beneath the line) so that they are excited by the electric field perpendicular to the plane of the CSRR. The equivalent circuit of a double-SRR-loaded microstrip line with a vertical via was reported in [16] to explain its passband response. In all of these previous papers, the gaps of the double SRRs and CSRRs were oriented parallel to the transmission line. The cross-coupling effects resulting from the different orientations of double SRRs and CSRRs coupled to CPW and microstrip lines have been studied using the equivalent circuit approach in [17].

It should be noted that all of the examples mentioned above (except those in [16]) are double-sided structures, which are difficult to fabricate and assemble with other planar devices. This fact might limit their wide application in modern wireless systems, in which reduced size, cost, and simple integration are principal concerns. For these reasons, microstrip technology is possibly the best choice for integrating MMTLs and related components.

The present work studies square-shaped SRRs coupled to the microstrip line lying in the same plane. Gaps in the SRRs are either parallel (near to or far from the line) or perpendicular to the microstrip line, with the latter having cross-coupling effects. Both a single SRR placed at one side of the line and a pair of SRRs symmetrically/asymmetrically placed at both sides are

Manuscript received December 25, 2013; revised March 29, 2014; accepted June 12, 2014. Date of publication July 08, 2014; date of current version August 04, 2014. This work was supported by the Serbian Ministry of Education, Science and Technological Development through Projects TR-32024 and III-45016 and the project of bilateral cooperation between the Kingdom of Spain and the Republic of Serbia PRI-AIBSE-2011-1119. The work of F. Mesa and F. Medina-Mena was supported by the Spanish Ministry of Economy and Competitiveness under Projects TEC2010-16948 and CSD2008-00066. (*Corresponding author: Francisco Medina-Mena.*)

R. Bojanic, V. Milosevic, and B. Jokanovic are with the Institute of Physics, University of Belgrade, 11080 Belgrade, Serbia (e-mails: radovan@ipb.ac.rs; vojislav@ipb.ac.rs; brankaj@ipb.ac.rs).

F. Medina-Mena is with the Department of Electronics and Electromagnetism, Faculty of Physics, University of Seville, Seville, Spain (e-mail: medina@us.es).

F. Mesa is with the Department of Applied Physics 1, University of Seville, Seville, Spain (e-mail: mesa@us.es).

Color versions of one or more of the figures in this paper are available online at <http://ieeexplore.ieee.org>.

Digital Object Identifier 10.1109/TMTT.2014.2332302

considered. An equivalent circuit model is proposed and validated for an arbitrarily oriented single-SRR-loaded microstrip line. The topology of the circuit is slightly more complicated than other proposed approaches, in order to increase the bandwidth of the model. The new models make use of the same number of independent parameters as in previous simpler proposals, although they are now interconnected in a different way in order to capture the distributed nature of the original loaded transmission line more efficiently. The approximation to the distributed behavior could be further improved by adding more elements to the lumped-circuit representation, but this would increase the complexity of the model and the number of parameters to be determined.

The proposed unit cells exhibit a stopband response, and they can be used as basic components in the design of high-performance compact filters. The validity of the equivalent circuit models is confirmed by the S -parameters obtained from the measurements of laboratory samples and from full-wave electromagnetic simulations. The proposed circuit topology is also very suitable for the unit cells with passband response since via inductance can easily be taken into account without increasing the complexity of the model.

This paper is organized as follows. Section II presents the circuit parameter extraction using a coupled-lines model to obtain the parameters of the host line coupled to SRR. In Section III, the remaining parameters are calculated employing closed-form expressions that make use of the resonance frequencies and the reflection coefficient minimum obtained by full-wave simulations. Two types of equivalent circuit are considered for the loaded transmission line: with one and with two LC cells. The latter is found to provide a bandwidth two times wider. The equivalent circuit model is validated by comparison with full-wave simulations and measurements in Section IV. A very good agreement is found in a wide frequency range, not only for structures with a single unit cell but also for structures with a cascade of SRR unit cells.

II. CIRCUIT PARAMETERS EXTRACTION USING A COUPLED-LINES MODEL

In order to obtain the equivalent circuit models of microstrip lines loaded with arbitrarily oriented SRRs, having their gaps parallel or perpendicular to the line (both near and far from the line), two configurations are examined: 1) a single SRR at one side of the microstrip line and 2) two SRRs at both sides of the line. The equivalent circuit of an arbitrarily oriented single-SRR-loaded microstrip line has not been considered so far, with the exception of the modeling of the mutual coupling between SRRs themselves reported in [18].

The SRR-loaded microstrip line with the gap parallel (and close) to the line is shown in Fig. 1, together with the relevant dimensions. A similar structure, but involving double SRRs, has been studied in [16], where the equivalent circuit shown in Fig. 2(a) is proposed. The transmission line is represented by a single Π -cell. In this paper, we propose the enhanced model shown in Fig. 2(b), where the line is represented by two Π -cells. We will demonstrate that this circuit, which has the same number of independent parameters as the previous one,

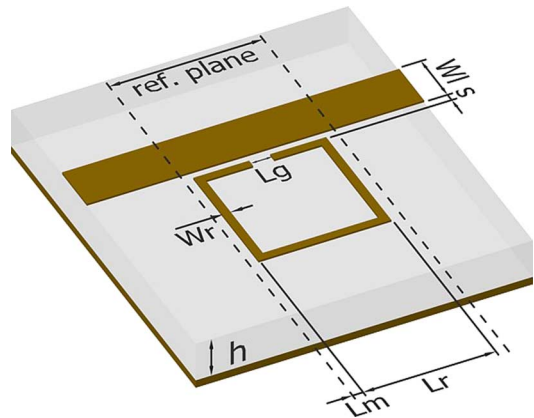


Fig. 1. Layout of the microstrip line loaded with SRR with the relevant dimensions: $h = 1.27$ mm, $L_r = 3$ mm, $L_m = 0.25$ mm, $L_g = 0.5$ mm, $W_r = 0.2$ mm, $W_l = 1.2$ mm, $S = 0.1$ mm. The metalization thickness is $t = 17$ μ m, and the dielectric permittivity $\epsilon_r = 10.2$.

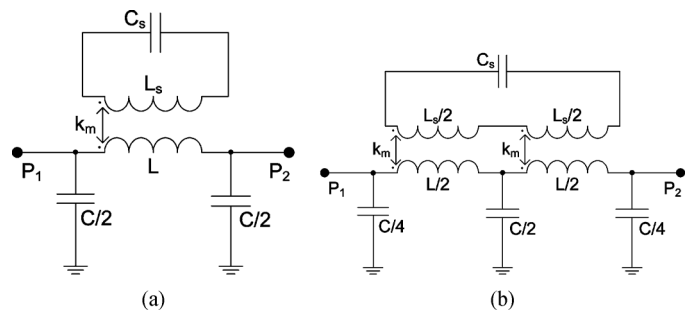


Fig. 2. Equivalent circuit of the microstrip line loaded with SRR consisting of (a) one and (b) two Π -cells.

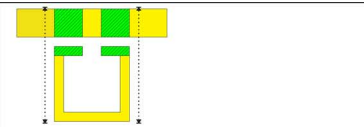
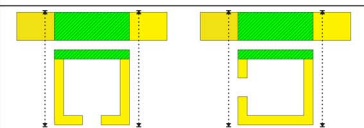
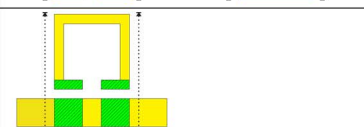
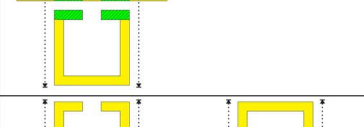
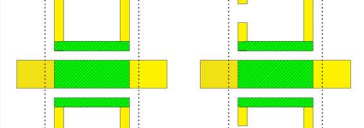
allows much better matching with full-wave simulations and measurements.

To extract the parameters L and C of the transmission line (Fig. 2), taking into account the coupling between the line and the nearest SRR arm, the system is modeled as a section of the multiconductor transmission line. LINPAR software [19] is employed for the numerical evaluation of the quasistatic line parameters. LINPAR provides the per unit length (p.u.l.) inductance and capacitance matrices from which the required parameters of the finite-length coupled-line sections are obtained.

According to the coupling geometry between the SRRs and the transmission line, the structures under study have been divided into five groups, as shown in Table I. Depending on the orientation of the SRR, the microstrip line is coupled with the whole SRR side or by two parts of the side separated by the gap.

In Table I, three types of marked sections can be distinguished: the isolated section and the coupled section with one or two SRR arms. The parameters of each section have been calculated using diagonal elements of the p.u.l. inductance and capacitance matrices. The resulting parameters L and C of the microstrip line (given in the second column of Table I) are obtained by summing the parameters of individual sections. It can be seen that the transmission-line inductance L is very similar for all configurations, but the capacitance C varies much more (15%) depending on the configuration, i.e., on the coupling between the SRR and the line. The SRR

TABLE I
CONFIGURATIONS OF SRRs COUPLED WITH THE MICROSTRIP LINE AND EXTRACTED PARAMETERS. COUPLING HAS BEEN TAKEN INTO ACCOUNT ONLY BETWEEN THE SECTIONS MARKED BY HATCHING. REFERENCE PLANES ARE DENOTED BY DOTTED LINES

(a)		$L = 1.51 \text{ nH}$ $C = 0.72 \text{ pF}$ $L_s = 7.97 \text{ nH}$
(b)		$L = 1.51 \text{ nH}$ $C = 0.74 \text{ pF}$ $L_s = 7.92 \text{ nH}$
(c)		$L = 1.5 \text{ nH}$ $C = 0.82 \text{ pF}$ $L_s = 7.97 \text{ nH}$
(d)		$L = 1.5 \text{ nH}$ $C = 0.86 \text{ pF}$ $L_s = 7.92 \text{ nH}$
(e)		$L = 1.5 \text{ nH}$ $C = 0.84 \text{ pF}$ $L_{s1} = 7.97 \text{ nH}$ $L_{s2} = 7.92 \text{ nH}$

inductance L_S consists of two parts: 1) from the section that is coupled with the transmission line, which is calculated using the corresponding diagonal element of the inductance matrix, and 2) from an isolated transmission line with length equal to the remaining uncoupled part of the SRR length. Values of L_S given in Table I are slightly different due to the fact that coupled-line sections have a somewhat lower p.u.l. inductance than isolated ones. Hereinafter, we adopt the same values for the inductances, $L = 1.5 \text{ nH}$ and $L_S = 8 \text{ nH}$, for all of the considered configurations.

III. CIRCUIT PARAMETERS EXTRACTION USING FULL-WAVE ANALYSIS

It has been found that different configurations of SRR loaded microstrip line can be modeled by the same circuit topology, but with different values of the circuit parameters. According to the circuit topology, all considered configurations can be divided into three groups: 1) SRRs with gaps parallel to the line; 2) two SRRs with parallel gaps near and far from the line; and 3) SRRs with gaps perpendicular to the line. For each topology, closed-form expressions for the resonance frequency and the minimum reflection frequency can be obtained. Those expressions are then used to determine the remaining circuit parameters (magnetic coupling coefficient k_m and SRR capacitance C_s), based on the

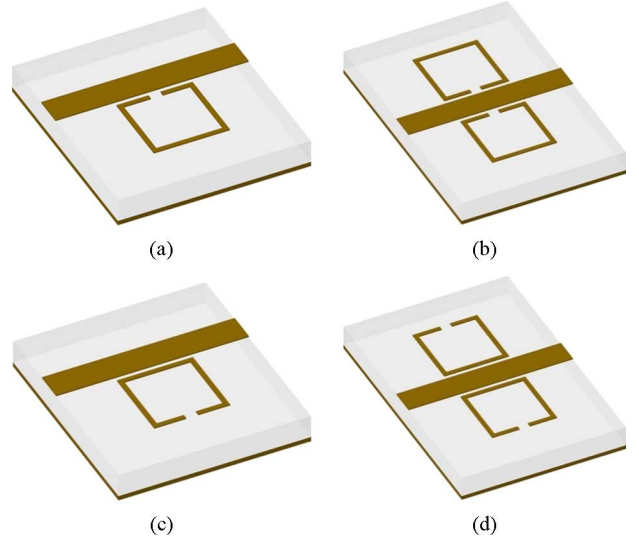


Fig. 3. Microstrip line loaded with SRRs with gaps parallel to the line. (a) One SRR with gap near the line. (b) Two SRRs with gaps near the line. (c) One SRR with gap far from the line. (d) Two SRRs with gaps far from the line. These configurations can be modeled by the equivalent circuits in Fig. 2.

frequencies computed through full-wave simulations. The only parameter that has to be fitted is the electric coupling coefficient k_e ; i.e., coupling capacitance $C_m = k_e \sqrt{CC_s}$, in the case of SRR with perpendicular gaps (this coefficient is introduced in Section III-C).

A. Microstrip Line Loaded With SRRs With Gaps Parallel to the Line

Microstrip lines loaded with SRRs with gaps parallel to the line are shown in Fig. 3. The equivalent circuit parameters L , C , and L_S are given in Table I for each configuration in Fig. 3 (they depend on their geometry and material characteristics). The remaining parameters C_S and k_m are determined using the S -parameters obtained by full-wave simulation. It should be noted that, in the frequency range of interest, the full-wave simulation only shows one S_{11} minimum that is located below the resonance frequency while both equivalent circuits exhibit two S_{11} minima: one below and the other above the resonance. The presence of this upper spurious parasitic S_{11} minimum certainly reduces the bandwidth, where it is possible to obtain a good matching between simulations and equivalent circuit analysis. However, the equivalent circuit with two II-cells [Fig. 2(b)] moves that minimum to higher frequencies with respect to the one cell model, as will be discussed later.

The capacitance C_S is obtained from the SRR resonance frequency $f_r = \omega_r/2\pi$ as follows:

$$f_r = \frac{1}{2\pi\sqrt{L_S C_S}}. \quad (1)$$

1) S_{11} Minimum of the Equivalent Circuit Model Below the Resonance: The magnetic coupling coefficient k_m is determined by the frequency of the first minimum of S_{11} , $f_{\min} = \omega_{\min}/2\pi$, for the equivalent circuits in Fig. 2. In order to simplify calculations, we can apply Bartlett's bisection

theorem [20]. The coupling coefficient k_m is then obtained as a function of f_{\min} , the resonance frequency f_r , and the line parameters L and C as follows:

$$k_m^2 = \left(1 - \frac{\omega_r^2}{\omega_{\min}^2}\right) (1 - a_{1,2}) \quad (2)$$

where a_1 corresponds to the circuit with one cell [Fig. 2(a)] and a_2 is for the two cells circuit [Fig. 2(b)]. These coefficients are given by

$$a_1 = \left[\frac{L}{C}Y_0^2 + 2b\right]^{-1} \quad (3)$$

$$a_2 = \left[\frac{L}{C}Y_0^2 \left(1 - \frac{b}{2-b}\right) + b\right]^{-1} \quad (4)$$

where Y_0 is the characteristic admittance of the microstrip line (20 mS in our case), and

$$b = \left(\frac{\omega_{\min}}{\omega_0}\right)^2; \quad \omega_0^2 = \frac{8}{LC}.$$

Full-wave simulations and measurements for all of the structures in Fig. 3 show that the S_{11} minimum appears before the resonance of the SRR f_r , making the first parenthesis in (2) negative. In order to obtain a real value of the coupling coefficient k_m (which allows for the matching between the frequencies of first minima of S_{11} obtained by full-wave simulation and those obtained by equivalent circuit analysis), it is necessary for the right-hand side of that equation to be positive, which requires $a_{1,2} > 1$.

In Fig. 4(a) and (b), we show a comparison of the a -coefficients calculated for one and two cells, respectively, for the SRR coupled to the 50- Ω microstrip line [Fig. 3(a)] on different substrates. From the position of the S_{11} minimum (corresponding markers), it can be seen that the condition $a > 1$ is not satisfied in any case in Fig. 4(a). On the other hand, that condition is fulfilled for all cases in Fig. 4(b). Also, the substrate with the highest permittivity (Rogers RO3010) exhibits the lowest upper frequency of the bandwidth in which k_m has a real value (3.51 GHz for one cell and 7.02 GHz for two cells). It should be noted that the a -coefficient is not a function of SRR parameters, but only of the S_{11} minimum frequency and the parameters of the background transmission line.

Fig. 4(a) and (b) clearly shows that the important advantage of the enhanced modeling of SRR loaded transmission line, compared with the one Π -cell equivalent circuit, is that it provides a bandwidth two times wider in which k_m has real values.

If a grounding via was present, a passband response would be obtained, and the S_{11} minimum would appear above the transmission zero in a full-wave simulation. In such case, a good agreement can be achieved with the equivalent circuit where the line is represented by only one cell [16]. In that case, our proposed equivalent circuit would become very similar to the

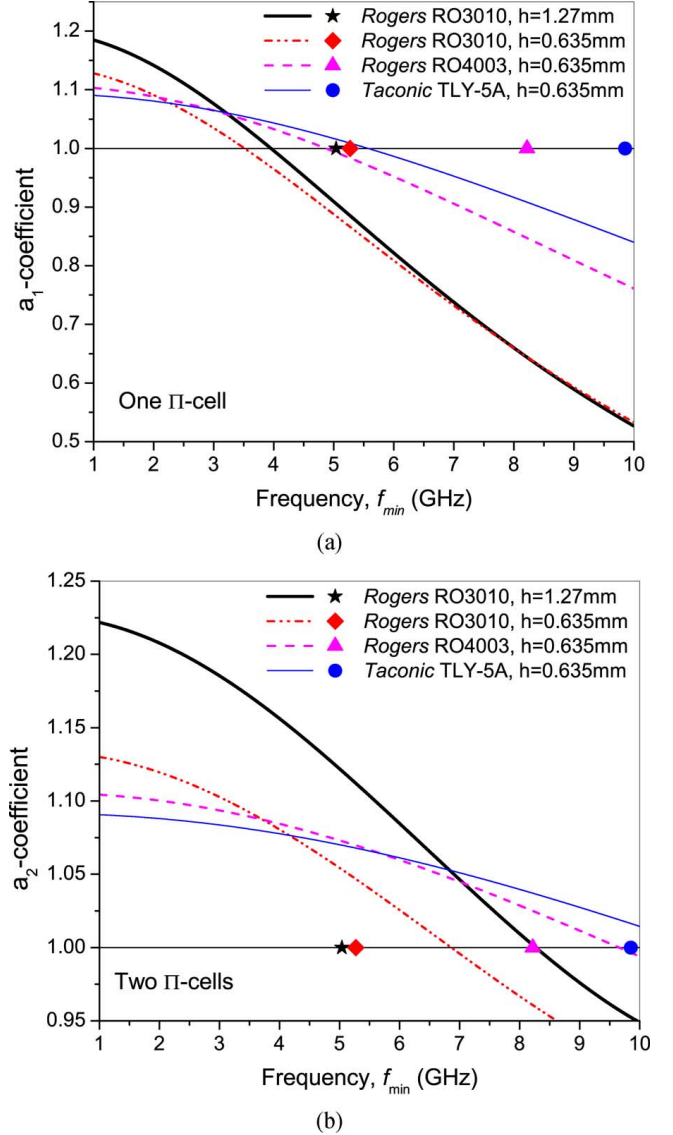


Fig. 4. Comparison of the a -coefficient for the equivalent circuit with (a) one and (b) two Π -cells for the case in Fig. 3(a). Horizontal black lines indicate the value of 1 on the vertical axis, and markers denote the frequency of S_{11} minimum for the corresponding substrates. For real values of the coupling coefficient k_m , the coefficients $a_{1,2}$ should be greater than 1.

improved model reported in [13], in which one cell is modified to allow for positioning of a centered via inductance.

2) S_{11} Minimum of the Equivalent Circuit Model Above the Resonance: Both equivalent circuit models in Fig. 2 exhibit a second S_{11} minimum above the resonance frequency of the SRR, which does not appear in the full-wave simulations or measurements. This spurious effect is a consequence of approximating a distributed circuit by lumped elements. In order to improve the bandwidth in which the equivalent circuit can be used, it is necessary to push that parasitic minimum towards high frequencies. This has been done by using the equivalent circuit with two Π -cells.

To clarify this, we start from the condition of perfect matching (minimum of S_{11}) for the symmetric circuit (following Bartlett's theorem): $Y_{\text{in,even}}Y_{\text{in,odd}} = Y_0^2$, where even and odd admittances are calculated by placing an open/short

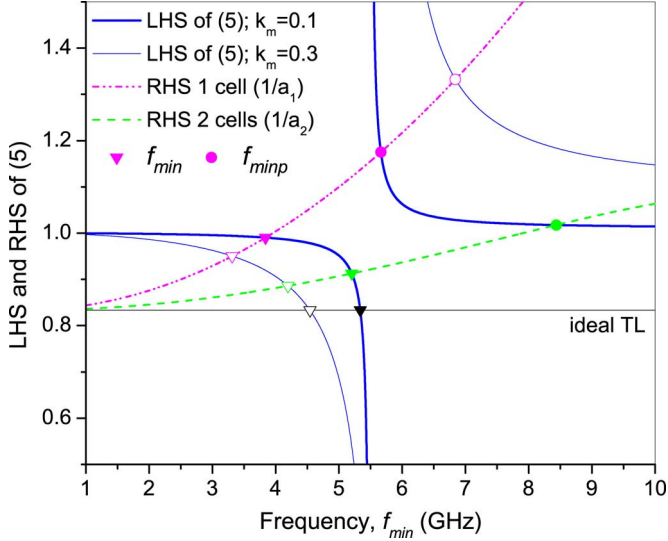


Fig. 5. Plotted LHS (solid curves) and RHS (dashed curves) of (5). Crossings indicate S_{11} minima for corresponding cases.

termination at the symmetry plane. After some rearrangements, the equivalent condition can be reformulated as

$$\frac{\omega_r^2 - \omega_{\min}^2}{\omega_r^2 - (1 - k_m^2)\omega_{\min}^2} = a_{1,2}^{-1} \quad (5)$$

where values of $a_{1,2}$ correspond to (3) and (4) for one and two cells, respectively. At low frequencies, a_2 can be approximated as $a_2^{-1} \approx (L/C)Y_0^2 + (b/2)$. Comparing this expression with (3), it is observed that the coefficient accompanying the term b is four times smaller. Since b is proportional to the square of the frequency [see (4)], this implies that a_2 varies two times slower with frequency than a_1 , thus showing a frequency behavior closer to that expected for an ideal transmission line (which should give a constant value of the a -coefficient).

In Fig. 5 the left-hand side (LHS) and right-hand side (RHS) of (5) are plotted for one and two cells and for two different coupling coefficients [the transmission line parameters correspond to the case in Fig. 3(a)]. The crossings of the corresponding curves for LHS and RHS indicate solutions of (5) and, therefore, frequencies of S_{11} minima. Crossings below the SRR resonance are marked with triangles, and they represent the real minima of the S_{11} parameter, while the crossings above the resonance, marked with circles, are the parasitic minima $f_{\min p}$, absent in full-wave simulation. The LHS of this equation does not depend on the number of cells but only on the coupling coefficient k_m and resonance f_r (solid curves). By increasing the coupling strength, this curve “widens” (compare thick and thin curves) so that it is possible to adjust the frequencies of both S_{11} minima in a given range. Moreover, the RHS depends only on the transmission line parameters L and C (which are basically determined by the choice of the substrate and characteristic impedance), and it has a completely different slope for the simple and the enhanced equivalent circuits. It can readily be observed from the figure that the RHS corresponding to the enhanced equivalent circuit is much more favorable in regards to the parasitic minimum, $f_{\min p}$, of S_{11} , as it appears at much higher frequencies

TABLE II
EXTRACTED PARAMETERS FOR THE CONFIGURATIONS IN FIG. 3

Configurations	f_r (GHz)	f_{\min} (GHz)	C (pF)	C_S (pF)	k_m
Fig. 3(a)	5.47	5.04	0.72	0.107	0.14
Fig. 3(b)	5.48	5.14	0.82	0.106	0.167
Fig. 3(c)	6.19	4.84	0.74	0.084	0.28
Fig. 3(d)	6.14	4.72	0.86	0.088	0.41

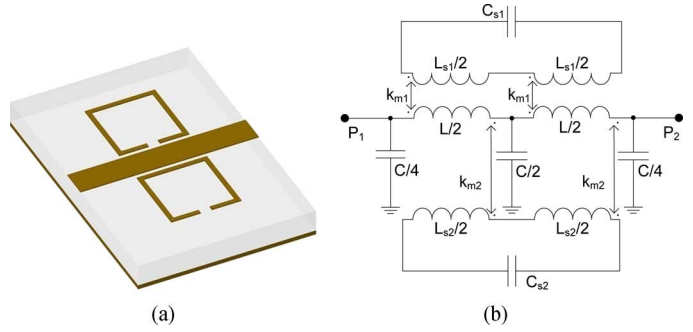


Fig. 6. (a) Microstrip line loaded with two SRRs with parallel gaps near and far from the line. (b) Corresponding equivalent circuit.

than those corresponding to the conventional circuit. In particular, for small values of the coupling coefficient ($k_m \sim 0.1$), the second S_{11} minimum appears right above the one-cell circuit resonance, therefore severely reducing its usable bandwidth, as opposed to the case of the enhanced equivalent circuit.

3) *Extracted Equivalent Circuit Parameters*: Extracted parameters for the two-cell equivalent circuit [Fig. 2(b)] are given in Table II for all configurations in Fig. 3. The difference in C_S is due to different resonance frequencies, according to (1). The magnetic coupling coefficient k_m is very different and is much greater for the structures without gaps in the arm near the line, where the coupling is the most pronounced.

B. Microstrip Line Loaded With Two SRRs With Parallel Gaps Near and Far From the Line

A microstrip line loaded with two SRRs with parallel gaps near and far from the line [Fig. 6(a)] has a more complex equivalent circuit [Fig. 6(b)] than in the previous case. It is a superposition of two equivalent circuits given in Fig. 2(b), because the SRRs have two different magnetic couplings and resonance frequencies.

The values of the extracted parameters $C_{s1} = 0.105$ pF and $C_{s2} = 0.081$ pF have been determined from the resonance frequencies f_{r1} and f_{r2} , computed with a full-wave simulator.

The magnetic coupling coefficients $k_{m1,2}$ are determined by applying Bartlett’s theorem to the circuit in Fig. 6(b), in a similar way as for the circuit in Fig. 2(b). To obtain $k_{m1,2}$, the following system of two equations has to be solved (since there are two S_{11} minima, $f_{\min 1,2}$):

$$\begin{aligned} \frac{\omega_{\min 1}^2}{\omega_{r1}^2 - \omega_{\min 1}^2} k_{m1}^2 + \frac{\omega_{\min 1}^2}{\omega_{r2}^2 - \omega_{\min 1}^2} k_{m2}^2 &= a_2^{(1)} - 1 \\ \frac{\omega_{\min 2}^2}{\omega_{r1}^2 - \omega_{\min 2}^2} k_{m1}^2 + \frac{\omega_{\min 2}^2}{\omega_{r2}^2 - \omega_{\min 2}^2} k_{m2}^2 &= a_2^{(2)} - 1 \end{aligned} \quad (6)$$

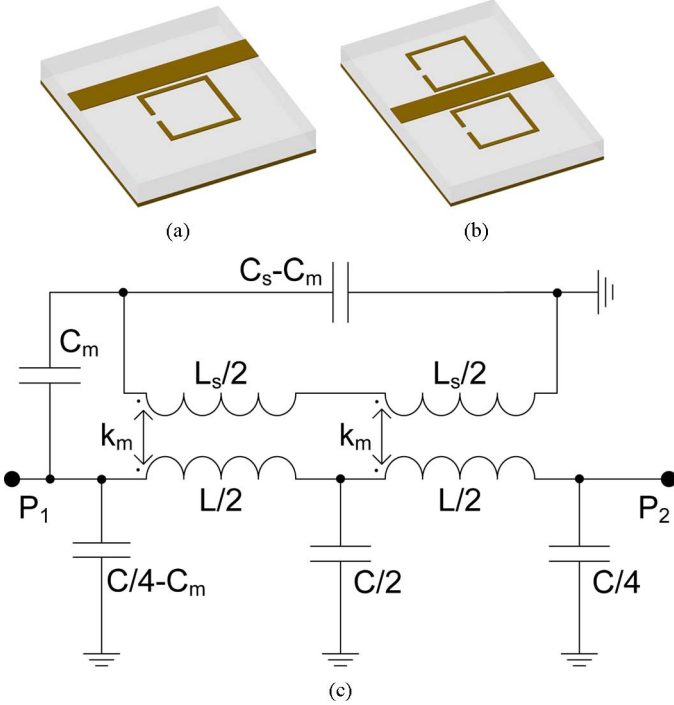


Fig. 7. Microstrip line loaded with SRRs with gaps perpendicular to the line. (a) Single SRR. (b) Two SRRs mirrored with respect to the line, which can be modeled by (c) the same equivalent circuit.

where $a_2^{(1),(2)}$ are calculated according to (4). Finally, it is obtained $k_{m1} = 0.14$ and $k_{m2} = 0.26$.

For the equivalent circuit with one II-cell, the system (6) will remain the same, except that a_2 is replaced by a_1 , calculated according to (3). In this case, the first equation in (6) corresponds to the first minimum of S_{11} below the resonances. Thus the coefficients on the LHS will be positive, and the RHS turns out to be negative, which is impossible to solve. Consequently, it is impossible to overlap the first minimum with full-wave simulations and measurements. The second minimum, however, falls between two resonances; therefore, one of the coefficients at LHS in the second equation in (6) is negative, so it is possible to overlap this minimum. For this case, it is found the following relation between coupling coefficients:

$$k_{m1}^2 = (\omega_{\min 2}^2 - \omega_{r1}^2) \left(\frac{k_{m2}^2}{\omega_{r2}^2 - \omega_{\min 2}^2} - \frac{a_1^{(2)} - 1}{\omega_{\min 2}^2} \right). \quad (7)$$

When solving (7), which has multiple solutions, it should be taken into account that k_{m2} (corresponding to the SRR with the gap far from the line) should be greater than k_{m1} .

C. Microstrip Line Loaded With SRRs With Gaps Perpendicular to the Line

The SRRs depicted in Fig. 7 differ from the previous configurations as they have been rotated 90° , which means that the structure is no longer symmetric with respect to the microstrip line. In this case, the electric field of the line is parallel to the gap, which causes additional electric coupling, included in the equivalent circuit model shown in Fig. 7(c).

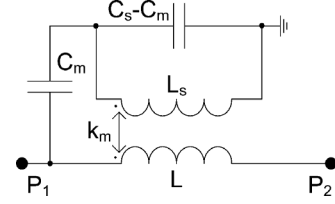


Fig. 8. Simplified circuit for the calculation of the resonance frequency.

A microstrip line loaded with one SRR with the gap perpendicular to the line [Fig. 7(a)] has the same equivalent circuit as two mirrored SRRs symmetrically placed at both sides of the line [Fig. 7(b)], but with different values of circuit elements.

The corresponding equivalent circuit parameters L , C and L_S are given in Table I for each configuration in Fig. 7. The magnetic coupling coefficient k_m for the structures in Fig. 7(a) and (b) are approximated by the values obtained for the corresponding SRRs with gaps parallel and far from the microstrip line [Fig. 3(c) and (d), respectively], since they have very similar surface current distributions. The remaining parameters, C_S and C_m , are determined using the resonance frequency (C_S is determined as function of C_m , which is derived through a fitting procedure with full-wave simulation).

To calculate the approximate resonance frequency (i.e., minimum of S_{21}), we use the equivalent circuit shown in Fig. 8, in which the shunt capacitors are removed with respect to the circuit in Fig. 7(c). This makes the circuit analysis significantly easier while the resonance is hardly affected.

After writing the system of equations according to Kirchhoff's laws, the following matrix relation between currents and voltages at ports 1 and 2 is obtained:

$$\begin{bmatrix} j\omega \left(\frac{1-L_S}{L_m} \right) & 1 \\ \frac{j}{\omega L_m} (1 - \omega^2 L_S C_S) + j\omega C_m & 0 \end{bmatrix} \begin{bmatrix} V_1 \\ I_1 \end{bmatrix} = \begin{bmatrix} -\frac{j\omega C_m L_S}{L_m} & 1 - \omega^2 L_m C_m \left(\frac{1}{k_m^2} - 1 \right) \\ \frac{j}{\omega L_m} (1 - \omega^2 L_S C_S) & \frac{L}{L_m} (1 - \omega^2 L_S C_S (1 - k_m^2)) \end{bmatrix} \cdot \begin{bmatrix} V_2 \\ I_2 \end{bmatrix}. \quad (8)$$

The condition for the resonance can be expressed as having a nontrivial solution on the LHS when $V_2, I_2 = 0$ (i.e., the RHS should be equal to zero), which is only satisfied when the determinant of the matrix on LHS is equal to zero as follows:

$$\begin{aligned} & \frac{j}{\omega L_m} (1 - \omega^2 L_S C_S) + j\omega C_m \\ & = \frac{j}{\omega L_m} (1 - \omega^2 L_S C_S + \omega^2 L_m C_m) \\ & = 0 \end{aligned} \quad (9)$$

which gives the following resonance frequency:

$$f_r = \frac{1}{2\pi \sqrt{L_S C_S - L_m C_m}} \quad (10)$$

TABLE III
EXTRACTED PARAMETERS FOR THE CONFIGURATIONS IN FIG. 7

Configurations	f_r (GHz)	C (pF)	C_S (pF)	k_m	C_m (pF)
Fig. 7(a)	5.8	0.74	0.102	0.29	0.055
Fig. 7(b)	5.86	0.86	0.108	0.42	0.08

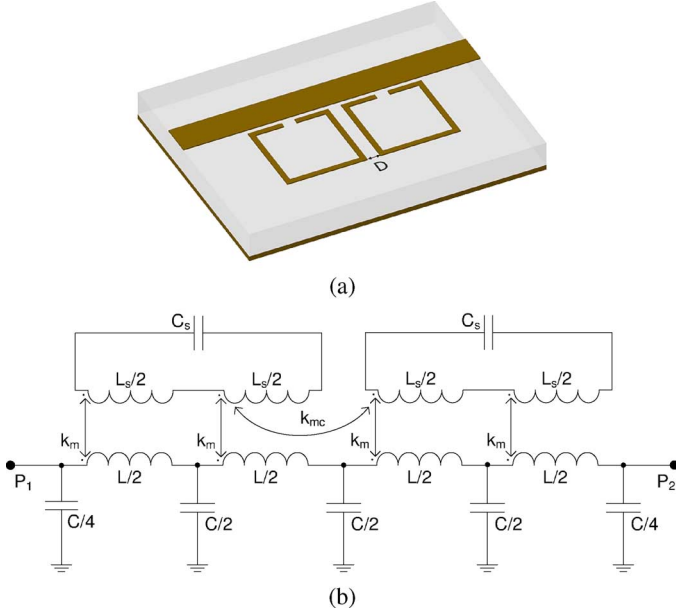


Fig. 9. (a) Cascaded SRRs. (b) Corresponding equivalent circuit.

with $L_m = k_m \sqrt{LL_S}$. It can be proved that, due to reciprocity ($S_{12} = S_{21}$), the LHS and RHS matrices of (8) have equal determinants, but it is simpler to consider the one on the LHS.

The extracted values of the equivalent circuit elements (Table III) are obtained after a slight optimization of C_s , C_m and k_m parameters, required because of the simplified circuit analysis. It can be seen that the values of L , C_s and L_s are very similar for both structures but C , C_m and k_m are different. The differences in C_m and k_m are a consequence of the stronger coupling in the case with two SRRs.

D. Cascaded Structures

The unit cells discussed above can be cascaded in order to design filters with improved bandwidth, as shown in Fig. 9(a) for SRRs with the gaps parallel and close to the line. This structure is modeled by the equivalent circuit shown in Fig. 9(b), with the previously extracted parameters, and with an additional inter-resonator coupling that depends on the distance D between the SRRs. The coupling coefficient k_{mc} is determined from full-wave simulation of two resonators, and can be used for modeling an arbitrary number of SRRs as long as non-adjacent resonator coupling can be neglected. The obtained coupling coefficients k_{mc} for different inter-resonator distances are shown in Table IV.

IV. VALIDATION OF THE MODEL AND RESULTS

To validate the proposed equivalent circuit models and the extracted circuit parameters, the magnitudes and phases of the

TABLE IV
EXTRACTED INTER-RESONATOR COUPLING COEFFICIENTS, k_{mc}

D (mm)	0.1	0.2	0.3	0.4	0.5
k_{mc}	0.155	0.102	0.078	0.052	0.03

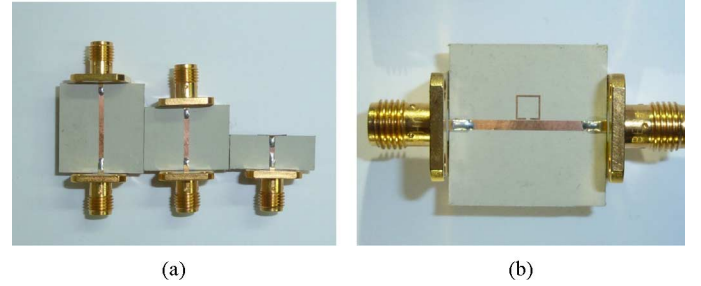


Fig. 10. (a) Fabricated custom designed LRL calibration set for the measurement of S -parameters at reference planes. (b) Microstrip line loaded with SRR with parallel gap close to the line.

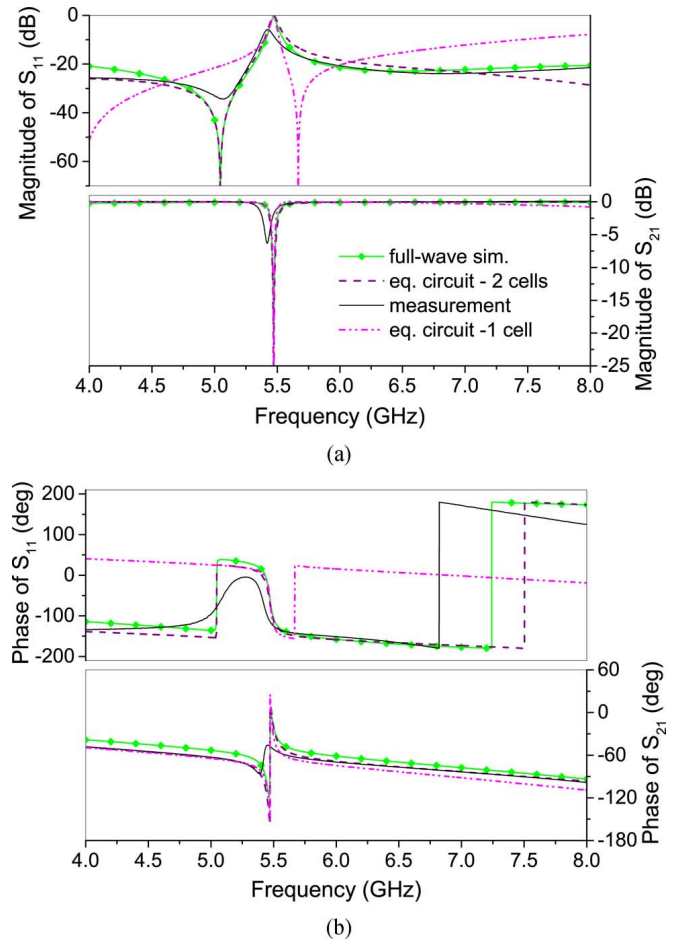
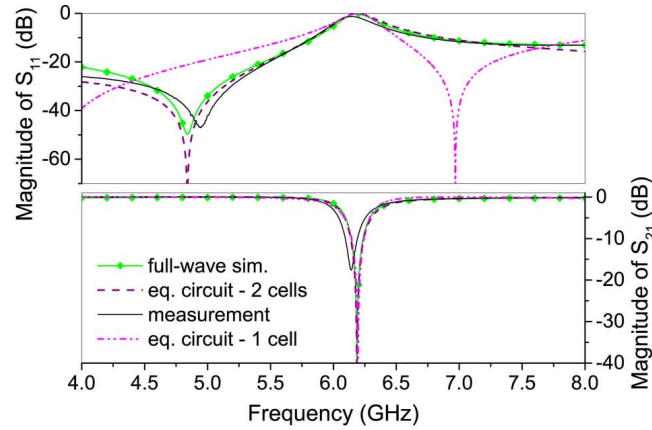
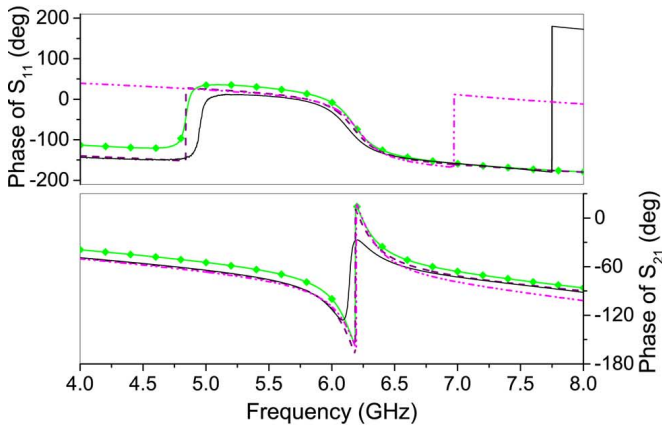


Fig. 11. Comparison of magnitudes (a) and phases (b) of S -parameters obtained by measurements, full-wave simulations, and equivalent circuit analysis with one and two Π -cells for the configuration in Fig. 3(a).

S -parameters obtained by measurements, full-wave simulations and equivalent circuit analysis are compared. Full-wave simulations are performed using lossless materials, since the equivalent circuit models do not include any losses. Nevertheless, some losses are still present both in full-wave simulations and measurements due to radiation. Certainly, the measured



(a)



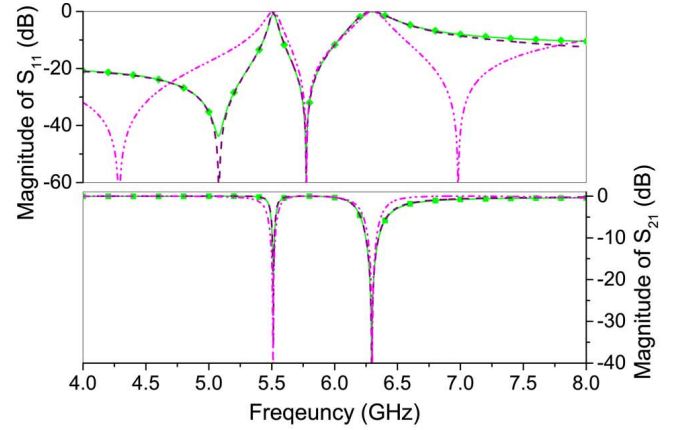
(b)

Fig. 12. Comparison of (a) magnitudes and (b) phases of S -parameters obtained by measurements, full-wave simulations, and equivalent circuit analysis with one and two Π -cells for the configuration in Fig. 3(c).

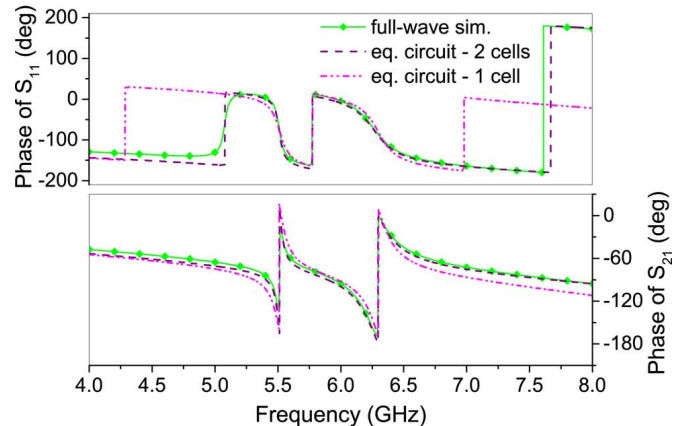
results include the actual losses in the metal and dielectric. All structures are simulated using WIPL-D software [21], and results are de-embedded at the reference planes marked in Fig. 1. Measured S -parameters are also de-embedded at the reference planes using the LRL (Line-Reflect-Line) calibration set shown in Fig. 10(a), and the Anritsu ME7838A VNA. A fabricated prototype of the microstrip line loaded with a single SRR with gap parallel (and close) to the line is shown in Fig. 10(b).

A. Microstrip Line Loaded With SRRs With Gaps Parallel to the Line

The results obtained by measurement, full-wave simulation, and equivalent circuit analysis using two Π -cells [Fig. 2(b)] for structures in Fig. 3(a) and (c) are shown in Figs. 11 and 12, respectively. They are in good agreement in the whole frequency range from 4 to 8 GHz. Small discrepancies in magnitude between the equivalent circuit model and measurements in Fig. 11 are found at the end of the swept band and are attributed to the presence of the parasitic S_{11} minimum. The frequency of this minimum is around 8.8 GHz due to relatively weak coupling (see Fig. 5). In contrast to that, the results obtained with the one-cell equivalent circuit model [Fig. 2(a)] show a big discrepancy with the full-wave simulations and measurements for



(a)



(b)

Fig. 13. Comparison of (a) magnitudes and (b) phases of S -parameters obtained by full-wave simulations and equivalent circuit analysis with one and two Π -cells for the configuration in Fig. 6(a).

any value of k_m . Actually, this simplified model only works properly at the resonance frequency and in a very small region around it. The first minimum of S_{11} occurs at a far lower frequency than the measured one, and it is not possible to overlap them for any real value of k_m , in accordance with (3). The coupling coefficients for the equivalent circuits with one cell are obtained by a fitting procedure and their values are $k_{m1} = 0.1$ in Fig. 11 and $k_{m1} = 0.23$ in Fig. 12, for SRR with the gap far from the line.

B. Microstrip Line Loaded With Two SRRs With Parallel Gaps Near and Far From the Line

Comparison between the full-wave simulation and the equivalent circuit analysis with one and two cells is given in Fig. 13. For the case of the equivalent circuit with two cells we can see that almost perfect agreement is obtained in magnitude and phase in the whole frequency range from 4 to 8 GHz.

For the one-cell equivalent circuit, the good matching is obtained only around the second minimum with the coupling coefficient $k_{m1} = 0.16$ and $k_{m2} = 0.18$, which is not expected since the coupling structures are very different (with and without the gap). It can be seen that around the second resonance there is discrepancy not only in S_{11} but also in S_{21} characteristics, since it

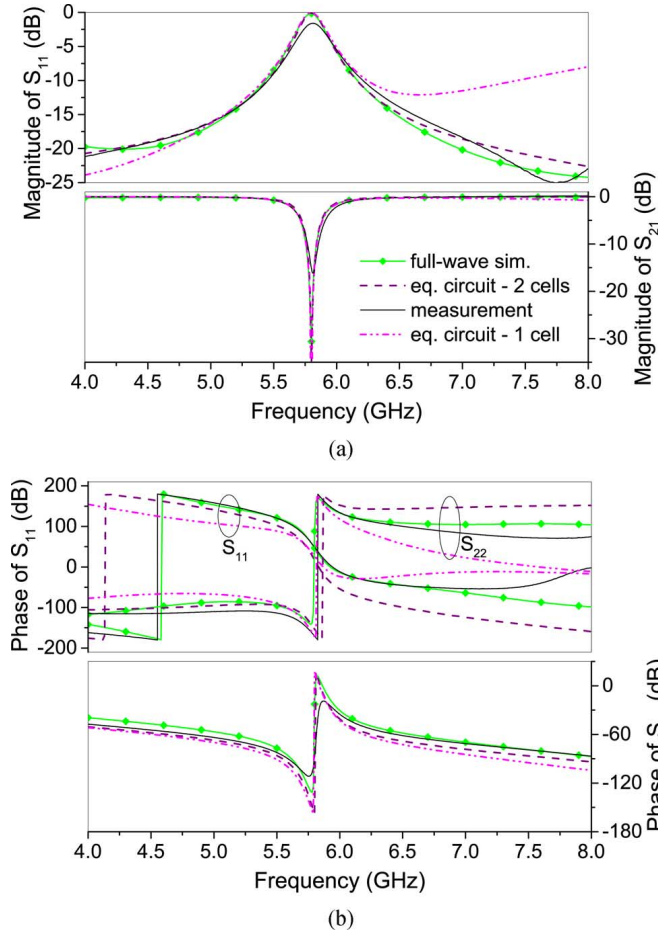


Fig. 14. Comparison of magnitudes (a) and phases (b) of S -parameters obtained by measurements, full-wave simulations, and equivalent circuit analysis with one and two Π -cells for the configuration in Fig. 7(a).

is not feasible to move the third minimum to a higher frequency. Also, the first minimum in the S_{11} characteristic is not possible to match at all with one-cell equivalent circuit, as we had already predicted in Section III-A.

C. Microstrip Line Loaded With SRRs With Gaps Perpendicular to the Line

To show the advantages of the proposed enhanced equivalent circuit [Fig. 7(c)] with respect to the one-cell model for the SRR with gap perpendicular to the line [Fig. 7(a)], we compared in Fig. 14 magnitudes and phases of S -parameters obtained by measurements, full-wave simulations, and equivalent circuit models with one and two Π -cells. Once again, the results for the two-cell equivalent circuit model are in very good agreement with full-wave simulation and measurements in the whole frequency range from 4 to 8 GHz. It is important to mention that SRRs with the gap perpendicular to the line do not exhibit the first minimum of reflection below the resonance as the SRR with the gap parallel to the line. Although the structure is asymmetric, only the magnitude of the reflection S_{11} is shown (the difference with S_{22} only concerns the phase). The one-cell equivalent circuit seems to perform now much better than in the

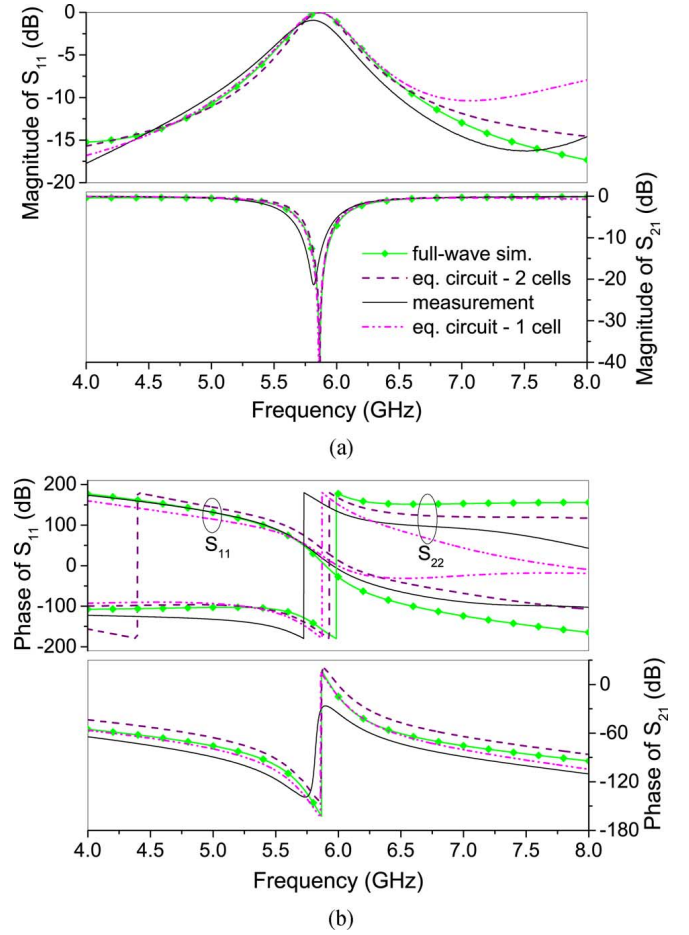


Fig. 15. Comparison of (a) magnitudes and (b) phases of S -parameters obtained by full-wave simulations and equivalent circuit analysis with one and two Π -cells for the configuration in Fig. 7(b).

case with the parallel gap, but the proposed two-cell model still works better in a wider frequency band. The extracted parameters of one-cell model are $k_m = 0.28$, $C_m = 0.062$ pF.

The results of full-wave simulations and equivalent circuit model analysis with one and two Π -cells for the configuration in Fig. 7(b) are shown in Fig. 15. The results from the equivalent circuit model with two cells are in very good agreement with full-wave simulations. The one-cell model fits the full-wave simulations in a wider frequency range than for the corresponding single SRR and matching is good up to 7.5 GHz. The extracted circuit parameters for one-cell model are $k_m = 0.39$ and $C_m = 0.095$ pF.

D. Cascaded SRRs With Gaps Parallel to the Line

The results of full-wave simulations and equivalent circuit model analysis with one and two Π -cells for the configuration in Fig. 9, for inter-resonator distance $D = 0.5$ mm, are shown in Fig. 16. A very good agreement is found in the whole frequency band of interest, both in magnitude and phase of the S -parameters, between the two Π -cell model and the full-wave simulations. In contrast to that, the one Π -cell model is unable to match the reflection except in a very narrow range around resonance.

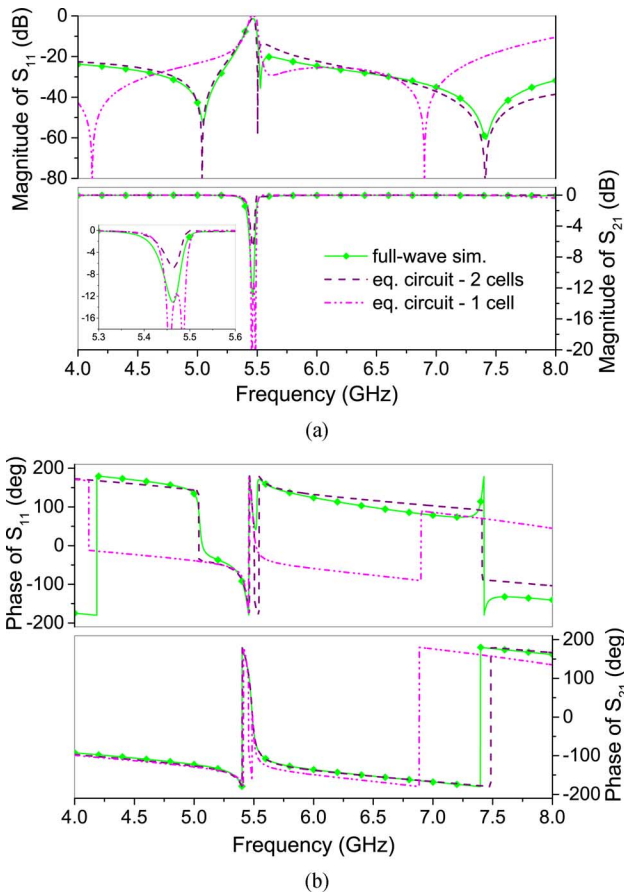


Fig. 16. Comparison of (a) magnitudes and (b) phases of S -parameters obtained by full-wave simulations and equivalent circuit analysis with one and two Π -cells for the configuration in Fig. 9, for distance $D = 0.5$ mm.

The values of magnetic coupling coefficients are obtained by fitting, and they are $k_m = 0.1$ and $k_{mc} = 0.015$.

V. CONCLUSION

Enhanced equivalent circuit models of microstrip lines loaded with single split-ring resonators have been proposed. Different orientations, not previously considered, of the SRR with respect to the line are analyzed: with the parallel gap near and far from the line, and with the gap perpendicular to the line. The printed line can be loaded with a single SRR at one side, or with two SRRs symmetrically/asymmetrically placed with respect to the line. This type of structures exhibits stop band response, but the proposed equivalent circuit model can easily be extended to structures with passband response by simply adding inductance between two Π -cells.

The single SRR (at one side of the line) and the two mirrored (with respect to the line) SRRs have the same equivalent circuit, although different circuit parameters. These are calculated using the multiconductor transmission-line model (L, C, L_s), while other necessary parameters (C_s and k_m) are obtained using closed-form expressions that relate them to the resonance frequency and minimum of reflection obtained by full-wave simulations. The only parameter to be optimized is the electric

coupling present in the case of SRRs with gap perpendicular to the line.

The main advantage of the proposed two-cell circuit model is that it provides a twice wider bandwidth in which it is possible to match the minimum of reflection obtained by full-wave simulations. This is achieved without increasing the number of circuit parameters with respect to the one-cell circuit model. Also, the enhanced equivalent circuit approximates the distributed nature of the background transmission line in a better way, and moves the parasitic minimum above the SRR resonance to significantly higher frequencies, compared to the one-cell model. Therefore, the achieved good matching bandwidth is considerably increased.

A number of samples have been fabricated and measured to validate the parameters extraction procedure. Very good agreement between measured S -parameters, full-wave simulations, and the proposed two-cell equivalent circuit has been demonstrated over a wide frequency range, both in magnitude and phase. In contrast, the conventional one-cell model has been shown to work only in a narrow frequency band. The proposed model is easily extendible to cascaded structures, as it has been exemplified with two unit cells with different inter-resonator spacing. The cascaded model is validated by comparison with full-wave simulations, and very good agreement is observed.

ACKNOWLEDGMENT

The authors would like to thank the Institute IMTEL, Belgrade, for the fabrication of the prototypes and WIPL-D Belgrade for the use of software licenses.

REFERENCES

- [1] A. Lay, T. Itoh, and C. Caloz, "Composite right/left-handed transmission line metamaterials," *IEEE Microw. Mag.*, vol. 5, no. 3, pp. 34–50, Mar. 2004.
- [2] A. K. Iyer and G. V. Eleftheriades, "Negative refractive index metamaterials supporting 2-D waves," in *IEEE MTT-S Int. Microw. Symp. Dig.*, 2002, vol. 2, pp. 412–415.
- [3] C. Caloz and T. Itoh, "Application of the transmission line theory of left-handed (LH) materials to the realization of a microstrip LH transmission line," in *Proc. IEEE-AP-S USNC/URSI Nat. Radio Sci. Meeting*, 2002, vol. 2, pp. 412–415.
- [4] A. A. Oliner, "A periodic-structure negative-refractive-index medium without resonant elements," in *IEEE-AP-S USNC/URSI Nat. Radio Sci. Meeting URSI Dig.*, 2002, vol. 2, p. 41.
- [5] C. Caloz and T. Itoh, *Electromagnetic Metamaterials: Transmission Line Theory and Microwave Applications*. New York, NY, USA: Wiley-IEEE Press, 2006.
- [6] J. García-García, J. Bonache, I. Gil, F. Martín, M. C. Velázquez-Ahmad, and J. Martel, "Miniaturized microstrip and CPW filters using coupled metamaterial resonators," *IEEE Trans. Microw. Theory Techn.*, vol. 54, no. 6, pp. 2628–2635, Jun. 2006.
- [7] J. Naqui, M. Durán-Sindreu, and F. Martín, "Alignment and position sensors based on split ring resonators," *Sensors*, vol. 12, no. 9, pp. 11790–11797, Sep. 2012.
- [8] F. J. Herraiz-Martínez, F. Paredes, G. Zamora, F. Martín, and J. Bonache, "Printed magnetoinductive-wave (MIW) delay lines for chipless RFID applications," *IEEE Trans. Antennas Propag.*, vol. 60, no. 11, pp. 5075–5082, Nov. 2012.
- [9] V. Milosevic, B. Jokanovic, and B. Kolundzija, "Microwave stereometamaterials and parameter extraction," in *Metamaterials 2010: Proc. 4th Int. Congr. Adv. Electromagn. Materials Microw. Opt.*, Karlsruhe, Germany, Sep. 13–16, 2010, pp. 474–477.
- [10] R. Bojanic, B. Jokanovic, and V. Milosevic, "Multiband delay lines with reconfigurable split-ring resonators," in *Proc. 10th Int. Conf. Telecommun. Modern Satellite, Cable and Broadcasting Services*, Nis, Serbia, Oct. 5–8, 2011, pp. 31–34.

- [11] N. Boskovic, B. Jokanovic, and A. Nestic, "Compact frequency scanning antenna array with SRR phase shifters," in *Proc. 11th Int. Conf. Telecommun. Modern Satellite, Cable and Broadcasting Services*, Nis, Serbia, Oct. 16–19, 2013, pp. 437–439.
- [12] J. D. Baena, J. Bonache, F. Martín, R. Marques, F. Falcone, T. Lepetegi, M. Laso, J. Garcia-Garcia, I. Gil, M. F. Portillo, and M. Sorolla, "Equivalent-circuit models for split-ring resonators and complementary split-ring resonators coupled to planar transmission lines," *IEEE Trans. Microw. Theory Techn.*, vol. 53, no. 4, pp. 1451–1461, Apr. 2005.
- [13] F. Aznar, M. Gil, J. Bonache, L. Jelinek, J. D. Baena, R. Marqués, and F. Martín, "Characterization of miniaturized metamaterial resonators coupled to planar transmission lines through parameter extraction," *J. Appl. Phys.*, vol. 104, Dec. 2008, Art. ID 114501.
- [14] F. Falcone, T. Lepetegi, J. D. Baena, R. Marqués, F. Martín, and M. Sorolla, "Effective negative-epsilon stopband microstrip lines based on complementary split ring resonators," *IEEE Microw. Wireless Compon. Lett.*, vol. 14, pp. 280–282, Jun. 2004.
- [15] V. Crnojevic-Bengin, V. Radonic, and B. Jokanovic, "Fractal geometries of complementary split-ring resonators," *IEEE Trans. Microw. Theory Techn.*, vol. 56, no. 10, pp. 2312–2321, Oct. 2008.
- [16] I. Gil, J. Bonache, J. García-García, F. Falcone, and F. Martín, "Metamaterials in microstrip technology for filter applications," in *Proc. APS-URSI*, Washington, DC, USA, Jul. 2005, vol. 1a, pp. 668–671.
- [17] J. Naqui, M. Durán-Sindreu, and F. Martín, "Modeling Split-Ring Resonator (SRR) and Complementary Split-Ring Resonator (CSRR) loaded transmission lines exhibiting cross-polarization effects," *IEEE Antennas Wireless Propag. Lett.*, vol. 12, no. 3, pp. 178–181, Mar. 2013.
- [18] J. S. Hong and M. J. Lancaster, "Couplings of microstrip square open-loop resonators for cross-coupled planar microwave filters," *IEEE Trans. Microw. Theory Techn.*, vol. 44, no. 12, pp. 2099–2109, Dec. 1996.
- [19] A. R. Djordjevic, M. B. Bazdar, T. K. Sarkar, and R. F. Harrington, *LINPAR for Windows: Matrix Parameters for Multiconductor Transmission Lines, Software and User's Manual*. Norwood, MA, USA: Artech House, 1995.
- [20] E. A. Guillemin, *Synthesis of Passive Networks: Theory and Methods Appropriate to the Realization and Approximation Problems*. Melbourne, FL, USA: Krieger, 1977, p. 207.
- [21] "Software and User's Manual," WIPL-D d.o.o, Belgrade, Serbia, 2010.



Radovan Bojanic was born in Knin, Croatia, in 1986. He received the Dipl.Ing. and M.Sc. degrees in electrical engineering from the University of Belgrade, Belgrade, Serbia, in 2009 and 2012, respectively, where he is currently working toward the Ph.D. degree.

Since 2010, he has been with the Institute of Physics, Belgrade, Serbia, as a Research Assistant with the Photonic Center, where he has been involved in modelling and simulation of microwave circuits.

Mr. Bojanic was the recipient of the Aleksandar Marincic Award from the Serbian National Society for Microwave Techniques, Technologies and Systems for the Best Paper in 2013.



Vojislav Milosevic was born in Belgrade, Serbia, on April 5, 1986. He received the Dipl. Ing. and M.Sc. degrees in electrical engineering from the University of Belgrade, Belgrade, Serbia, in 2009 and 2012, respectively, where he is currently working toward the Ph.D. degree.

In 2010, he became a Research Assistant with the Photonic Center, Institute of Physics, Belgrade, Serbia. His current research interests include electromagnetic metamaterials and homogenization theory.

Mr. Milosevic was the recipient of the Aleksandar Marincic Award from the Serbian National Society for Microwave Techniques, Technologies and Systems for the Best Paper in 2013.



Branka Jokanovic (M'89) received the Dipl. Ing., M.Sc., and Ph.D. degrees in electrical engineering from the University of Belgrade, Belgrade, Serbia, in 1977, 1988, and 1999, respectively.

She is currently a Research Professor with the Institute of Physics, University of Belgrade, Belgrade, Serbia. Before she joined the Photonic Center, Institute of Physics, she was the Head of the Microwave Department, Institute IMTEL, Belgrade. Her current research interests include modelling, simulation and characterization of microwave and photonic metamaterials for wireless communications and sensors.

Dr. Jokanovic was one of the founders of the Yugoslav IEEE Microwave Theory and Techniques Society (MTT-S) Chapter and its chairperson from 1989 to 2000. She also founded the Yugoslav Association for Microwave Techniques and Technology in 1994 and initiated the Yugoslav MTT journal *Microwave Review* for which she was the editor for six years (1994–2000). She received the IMTEL Institute Award for Scientific Contribution in 1996, the 2000 IEEE Third Millennium Award, the YU MTT Distinguished Service Award in 2005, and Aleksandar Marincic Award in 2013. She is a corresponding member of the Serbian Academy of Engineering Sciences.



Francisco Medina-Mena (M'90–SM'01–F'10) was born in Puerto Real, Cádiz, Spain, in November 1960. He received the Licenciado and Ph.D. degrees from the University of Seville, Seville, Spain, in 1983 and 1987, respectively, both in physics.

He is currently a Professor of electromagnetism with the Department of Electronics and Electromagnetism, University of Seville, Seville, Spain, and Head of the Microwaves Group. His research interest includes analytical and numerical methods for planar structures, anisotropic materials, and artificial media modelling. He has coauthored approximately 130 book chapters and journal papers on those topics as well as more than 250 conference contributions.

Prof. Medina-Mena acts as a reviewer for more than 40 IEEE, IEE, AIP and IoP journals among others and has been member of the TPCs of a number of local and international conferences on his topics.

Francisco Mesa (M'93–SM'11–F'14) was born in Cádiz, Spain. He received the Licenciado and Ph.D. degrees in physics from the University of Seville, Seville, Spain, in 1989 and 1991, respectively.

He is currently a Professor with the Department of Applied Physics, University of Seville, Seville, Spain. His research interests focus on electromagnetic propagation/radiation in planar structures.

Prof. Mesa is currently serving as an associate editor of the IEEE TRANSACTIONS ON MICROWAVE THEORY AND TECHNIQUES.



Enhanced Modelling of Asymmetric Split-Ring-Resonators in Printed Circuits

Radovan Bojanic¹, Branka Jokanovic¹, Vojislav Milosevic¹, Francisco Medina Mena², Francisco Mesa³

¹ Institute of Physics, University of Belgrade, Photonic Center, Pregrevica 118, 11080, Belgrade, Serbia

² Universidad de Sevilla, Electronica y Electromagnetismo, Reina Mercedes s/n, 41012, Sevilla, Spain

³ Universidad de Sevilla, Dept. Applied Physics 1, Reina Mercedes s/n, 41012, Sevilla, Spain

radovan@ipb.ac.rs

Abstract – We present an enhanced modelling of magnetic and electric interaction of single asymmetric split-ring resonators (ASRRs) with printed lines. Two simple lumped-element networks consisting of one and two Π -cells, which has the same number of independent parameters, are proposed to model the square-shaped ASRRs loaded microstrip line. The equivalent circuit parameters are obtained from the multi-conductor transmission line theory as well as from closed-form expression for the resonance frequency which is extracted from full-wave simulations. Comparison of proposed equivalent circuit results with full-wave simulations has shown that the network consisting of two Π -cells exhibits much better agreement in a much wider frequency band than one-cell model.

I. INTRODUCTION

Analysis and design of metamaterial-based transmission lines (MMTLs) require the use of long-lasting full-wave simulations that usually demand a lot of computational resources. However, MMTLs can be modelled by lumped-element equivalent circuits that provide a much better understanding of the electromagnetic properties and also simpler way of their design and optimization.

In this paper we study a single square-shaped ASRRs coupled to the microstrip line with gap parallel to the line and shifted from the center of the gap bearing side. It is shown that the orientation and position of the gap with respect to the hosting transmission line has significant influence to the overall performance of MMTL [1]. The proposed unit cells exhibit a stop band response and offer more flexibility in design of compact high-performance filters.

II. CIRCUIT PARAMETERS EXTRACTION

The ASRRs loaded microstrip line with parallel gap near and far from the line are shown in Figs. 1a. and 1b. respectively, together with the relevant dimensions. The proposed equivalent circuits that have the same number of independent parameters are given in Figs. 1c. and 1d. The first equivalent circuit represents transmission line by a single Π -cell while the enhanced model in Fig. 1d. uses two Π -cells for transmission line modelling. We will demonstrate that the equivalent circuit with two Π -cells, allows much better matching with full-wave simulations.

In order to extract the parameters L and C of the transmission line we considered coupling between the line and the nearest ASRR arm. This system is modeled as a section of the multi-conductor transmission line. LINPAR software [2] is employed for the numerical evaluation of the quasi-static line parameters. LINPAR provides the per unit length (p.u.l.) inductance and capacitance matrices from which the required parameters of the coupled line sections are obtained. Depending on the orientation of ASRRs, the microstrip line is coupled with the whole ASRR side or by the part of it. Extracted transmission line inductance, L is an equal for both unit cells in Figs. 1.a,b as well as the ASRR inductance L_S which consists of two parts: 1) from the section that is coupled with the transmission line and 2) from an isolated transmission line with the length equal to the remaining, uncoupled part of the ASRR length. Values of L_S are very similar for both configurations in Figs. 1a. and 1b. and we adopted the following values for the inductances, $L=1.5\text{nH}$ and $L_S=8\text{nH}$ for both unit cells. Capacitance C_S of ASRR is determined using the resonance frequency, $f_{r,S}$ obtained by full-wave simulation of

the corresponding symmetrical unit cell with gap positioned at the center of SRR side, since capacitance C_S changes a little when shifting the gap from the center:

$$f_{rs} = \frac{1}{2\pi\sqrt{L_S C_S}} \quad (1)$$

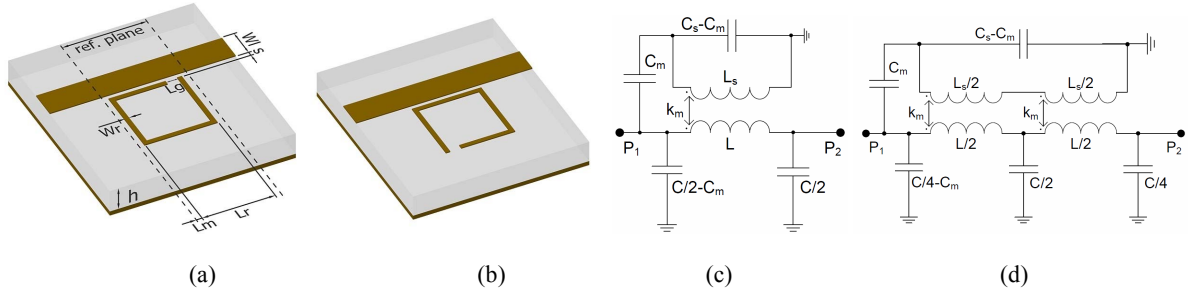


Fig. 1. Layouts of the microstrip line loaded with asymmetric SRRs (a) with gap near to the line and (b) with gap far from the line and the equivalent circuits consisting of (c) one and (d) two LC cells. Relevant dimensions are: $h=1.27\text{mm}$, $L_r=3\text{mm}$, $L_m=0.25\text{mm}$, $L_g=0.5\text{mm}$, $W_r=0.2\text{mm}$, $W_f=1.2\text{mm}$, $S=0.1\text{mm}$. The metallization thickness is $t=17\mu\text{m}$, and dielectric permittivity $\epsilon_r=10.2$.

To calculate the resonance of the circuit in Fig. 3c., we used simplified circuit with the shunt capacitors removed, as the resonant frequency is unaffected by this. This frequency turns out to be (for full details of calculation see [3]):

$$f_r = \frac{1}{2\pi\sqrt{L_S C_S - L_m C_m}}, \text{ where } L_m = k_m \sqrt{L L_S}; \quad (2)$$

which enables us to obtain the ratio between mutual capacitance C_m and mutual inductance L_m by using the resonant frequency obtained by full-wave simulation. In this way, only one parameter needs to be optimized. For the circuit in Fig. 1d the resonance will be a little shifted compared to the value given by (2), so the same procedure can be used with an additional slight optimization due to this shift.

III. VALIDATION OF THE MODEL AND RESULTS

To validate the proposed equivalent circuit models and the extracted circuit parameters, we compared the magnitudes and phases of the S -parameters obtained by full-wave simulations and equivalent circuit analysis in Figs. 2. and 3.

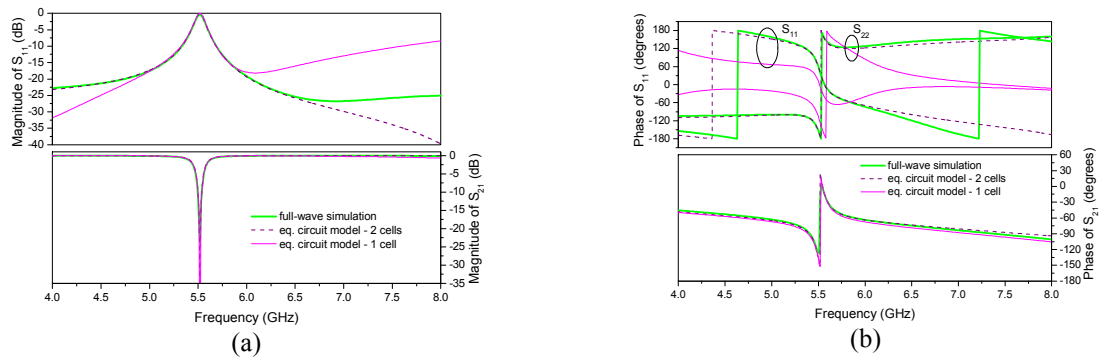


Fig. 2. Comparison of magnitudes (a) and phases (b) of S -parameters obtained by full-wave simulation and equivalent circuit analysis with one and two Π -cells for the configuration in Fig. 1a. The extracted circuit parameters for the enhanced circuit model are: $C_S=0.109\text{pF}$, $k_m=0.216$ and $C_m=0.049\text{pF}$.

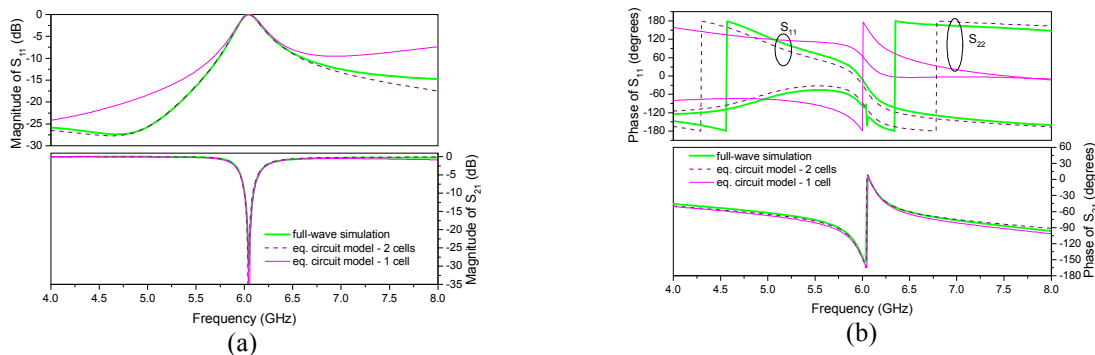


Fig. 3. Comparison of magnitudes (a) and phases (b) of S -parameters obtained by full-wave simulation and equivalent circuit analysis with one and two Π -cells for the configuration in Fig. 1b. The extracted circuit parameters for the enhanced circuit model are: $C_s=0.09\text{pF}$, $k_m=0.31$ and $C_m=0.02\text{pF}$.

It can be seen that the equivalent circuit with single Π -cell can match the full-wave simulation only in a narrow band around the resonance, while two-cell equivalent circuit achieves a very good matching in a considerably wider frequency band from 4-8GHz. It is due to fact that two Π -cell equivalent circuit is able to capture more efficiently the distributed nature of the original loaded transmission line. The topology of this enhanced circuit model is a slightly more complicated, but number of independent circuit parameters to be determined is the same for the both circuit topologies.

IV. CONCLUSION

We present the equivalent circuit models for single asymmetric SRRs loaded microstrip line with gap parallel to the line, but shifted from the center of the gap-bearing side. Two circuit models are considered: with one and two Π -cells and is shown that circuit with two Π -cells is able to match full-wave simulation in a considerably wider frequency range, since its topology captures the distributed nature of the transmission line in a better way than one-cell model. Even the topology of two-cell circuit is a slightly more complicated, the number of unknown parameters that should be extracted is the same as for one Π -cell model.

ACKNOWLEDGEMENT

This work was financed by the Serbian Ministry for Education, Science and Technological Development through the projects TR-32024, III-45016 and through the project of bilateral cooperation between Kingdom of Spain and Republic of Serbia PRI-AIBSE-2011-1119.

The authors would like to thank to WIPL-D Belgrade for the use of software licenses.

REFERENCES

- [1] V. Milosevic, B. Jokanovic and B.Kolundzija, "Microwave stereomatamaterials and parameter extraction," in *Proc. Metamaterials' 2010*, pp. 474-477, Karlsruhe, Germany, 13-16 September 2010.
- [2] A.R. Djordjevic, M.B. Bazdar, T.K. Sarkar and R.F. Harrington, *LINPAR for Windows: Matrix Parameters for Multiconductor Transmission Lines*, Software and User's Manual, Norwood, USA: Artech House, 1995.
- [3] R. Bojanic, V. Milosevic, B. Jokanovic, F. Medina, F. Mesa, "Enhanced modelling of split-ring resonators couplings in printed circuits", submitted to *IEEE Trans. Microw. Theory Tech*.
- [4] WIPL-D Pro v8.0, *Software and User's Manual*, WIPL-D d.o.o., Belgrade, 2010.



Coupled-mode Theory Approach for Analysis of Resonant Transmission Line

V. Milošević¹, G. Isić¹ and B. Jakanović¹

¹University of Belgrade, Institute of Physics, 11080, Belgrade, Serbia
vojislav@ipb.ac.rs

Abstract – In this paper we apply the framework of temporal coupled-mode theory on the case of resonant transmission line (TL) consisting of microstrip line coupled to split-ring resonators (SRR). In particular, we study the system which breaks the mirror symmetry by moving the slit in the SRR. The combination of two such SRRs in anti-symmetric configuration is shown to possess two orthogonal resonant modes which both couple to the line with controllable coupling strengths and corresponding Q -factors. Such an approach could prove to be useful in microstrip filter design, classical electromagnetically induced transparency (EIT) and slow wave structures.

I. INTRODUCTION

Most of the metamaterials presented in the literature are of a so-called resonant-type, i.e. they derive their properties from the interaction of constituent sub-wavelength resonators with the propagating wave [1]. More generally, it can be said that they belong to a broad class of systems where the discrete localized states interact with the propagating continuum states. Temporal coupled-mode theory provides first-order perturbation approach for treating the dynamics of such systems [2]. Qualitative description of the scattering spectra using only a few parameters can be obtained, as well as important constraints on those parameters coming from the symmetries of the system [3]. Theory can easily be extended to the case of multiple resonators, with possible couplings between them [4].

In this paper we apply the coupled-mode formalism to microstrip line edge-coupled with one or two SRRs. Usually such systems possess mirror symmetry, however in our previous work we demonstrated that interesting effects arise when the slit is moved to the perpendicular SRR arm, causing electric coupling (in addition to the magnetic coupling with the line), and negative values of extracted effective ε [5].

We should note that another approach for approximately describing SRRs coupled with TL would be use of the equivalent circuit model, which was extensively studied [1] and can be extended to include the electrical coupling [6]. While each approach has its merits, we feel that the equivalent circuit is more cumbersome in the case of asymmetric SRR, while coupled-mode approach can treat such case naturally, as it will be shown below.

II. THEORY AND RESULTS

A. Investigated structure

Structures under consideration are shown in Fig. 1. They consist of $50\ \Omega$ microstrip line printed on top of the substrate Rogers RO3010 with height 1.27 mm and permittivity $\varepsilon = 10.2$ (bottom layer is metallised). In the first case, shown in Fig. 1a, one SRR is asymmetrically placed next to the line, while in the second case [Fig. 1b] two such SRRs are placed anti-symmetrically. It should be noted that the structure in Fig. 1b, while not having mirror symmetry, possess the 180° -rotation symmetry with respect to the center, which causes reflection from both directions to be the same. The structure operates at about 5 – 6 GHz, which is suitable for microwave applications.

B. Coupled-mode approach

In the case of one SRR we have one resonant mode edge-coupled with the channel, as schematically depicted in Fig. 2a. For our purposes it can be assumed that all the interaction takes place in the center plane, which divides



Fig. 1: Microstrip line coupled with a) one SRR with the gap in a perpendicular arm; b) two such SRRs placed anti-symmetrically. Dimensions: $L_r = 3$ mm, $L_g = 0.5$ mm, $W_r = 0.2$ mm, $W_l = 1.2$ mm, $s = 0.1$ mm.

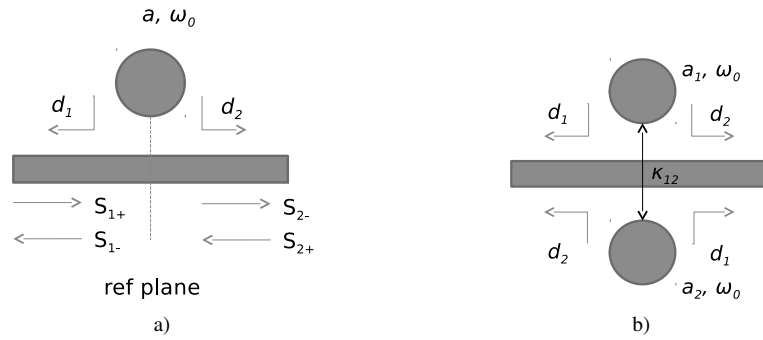


Fig. 2: Schematic of a) one; b) two anti-symmetric resonant modes edge-coupled to the transmission line.

the line in two parts. Due to lack of mirror symmetry, the coupling coefficient in both directions is generally not the same. Following references [3, 4], we can write

$$\frac{da}{dt} = j\omega_0 a + D^T |s_+\rangle; \quad |s_-\rangle = C |s_+\rangle + Da; \quad C = \begin{pmatrix} & 1 \\ 1 & \end{pmatrix}; \quad D = \begin{pmatrix} d_1 \\ d_2 \end{pmatrix}. \quad (1)$$

Interpretation of (1) is following: resonant mode is described with complex quantity a , whose magnitude squared is proportional to the energy, and phase is equal to the phase of the oscillating field. Time evolution of a has homogeneous part, which represents resonant frequency, and forcing term due to excitation by incoming waves through coupling. The scattered wave, $|s_-\rangle$, has two components, one from the direct scattering (i.e. without the influence of the resonator), represented by matrix C , and indirect caused by the coupling with the resonant mode. Due to energy conservation and time reversal symmetry constraints, it can be shown that $d_{1,2} = \delta e^{\pm j\theta}$. Total transmission coefficient can be calculated:

$$S_{21} = \langle s_{2-} | s_{1+} \rangle = 1 - \frac{\delta^2}{j(\omega - \omega_0) + \delta^2}. \quad (2)$$

The case of two anti-symmetric SRRs is schematically represented in Fig. 2b. We can now write the same equation as (1), only now a is no longer a scalar, but becomes a vector $\vec{a} = \begin{pmatrix} a_1 & a_2 \end{pmatrix}^T$, and D becomes the appropriate square matrix. Transmission is now

$$S_{21} = 1 - \frac{2\delta^2 \cos^2 \theta}{j(\omega - \omega_0 - \kappa) + 2\delta^2 \cos^2 \theta} - \frac{2\delta^2 \sin^2 \theta}{j(\omega - \omega_0 + \kappa) + 2\delta^2 \sin^2 \theta}. \quad (3)$$

We note that the two terms in (3) represent scattering due to symmetric and anti-symmetric mode, which form orthogonal basis for two coupled resonators. Interesting feature of (3) is that the coupling strengths and corresponding Q -factors of the two modes can be tuned by tuning θ , which may be useful for synthesising the desired response.



C. Comparison with numerical results

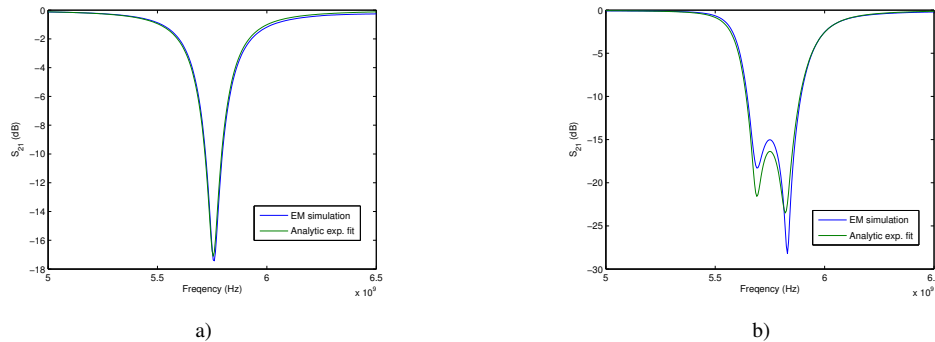


Fig. 3: Comparison of expressions (2), (3) and numeric results for S_{21} for structures from a) Fig. 1a; b) Fig. 1b.

Formulae (2), (3) are fitted to the results of electromagnetic simulations in Mentor Graphics IE3D package. In (2), fitting constants are ω_0 and δ . From the reflection coefficient θ also can be resolved, leading to full set of S -parameters, which excellently agrees with simulations, however due to space limitations only magnitude of transmission is shown in Fig. 3a. Then, data for single SRR are used in (3), with *only* fitting parameter being the mutual coupling κ , and the results are shown in Fig. 3b. The discrepancies in the resonance depths in our opinion can be attributed to different radiation properties of symmetric and anti-symmetric modes, leading to slightly different Q -factors.

III. CONCLUSION

Temporal coupled-mode theory has been applied to the two configurations of SRR coupled with microstrip line: one asymmetric ring, and two such rings in anti-symmetric arrangement. Analytical expressions for transmission in both cases are derived, and their good agreement with numerical simulations is shown.

ACKNOWLEDGEMENT

This work is supported by Serbian Ministry of Education, Science and Technological Development through the projects TR-32024 and III-45015.

REFERENCES

- [1] R. Marqués, F. Martín, and M. Sorolla, *Metamaterials with Negative Parameters: Theory, Design and Microwave Applications*, ser. Wiley Series in Microwave and Optical Engineering. Wiley, 2011.
- [2] H. Haus, *Waves and fields in optoelectronics*, ser. Prentice-Hall Series in Solid State Physical Electronics. Prentice Hall, Inc, 1984.
- [3] S. Fan, W. Suh, and J. D. Joannopoulos, “Temporal coupled-mode theory for the fano resonance in optical resonators,” *J. Opt. Soc. Am. A*, vol. 20, no. 3, pp. 569–572, Mar 2003.
- [4] W. Suh, Z. Wang, and S. Fan, “Temporal coupled-mode theory and the presence of non-orthogonal modes in lossless multimode cavities,” *Quantum Electronics, IEEE Journal of*, vol. 40, no. 10, pp. 1511–1518, Oct 2004.
- [5] R. Bojanic, B. Jokanovic, and V. Milosevic, “On the orientation of split-ring resonators excited by guided waves,” in *Proc. of Metamaterials’2012*, St. Petersburg, Russia, September 2012.
- [6] R. Bojanic, V. Milosevic, B. Jokanovic, F. Medina-Mena, and F. Mesa, “Enhanced modelling of split-ring resonators couplings in printed circuits,” *Microwave Theory and Techniques, IEEE Transactions on*, vol. 62, no. 8, pp. 1605–1615, Aug 2014.

Classical Electromagnetically Induced Transparency in Metamaterials

Vojislav Milošević, Branka Jokanović, Radovan Bojanić and Brana Jelenković

Abstract – Electromagnetically induced transparency (EIT) is a quantum mechanical phenomenon that creates a narrow transparency window in otherwise absorbing medium. An analogous classical effect can be observed in various systems due to resonators coupling. In this paper, we present a review of metamaterials employing this feature in order to achieve low losses, high dispersion and extreme values of group delay.

Keywords – Metamaterials, Electromagnetically Induced Transparency (EIT).

I. INTRODUCTION

In laser physics, EIT has been known as a method to eliminate the effect of the medium on a propagating beam [1]. Typically, it involves three-level atomic system (so called Λ -configuration, depicted in Fig. 1), where the transition between states $|1\rangle$ and $|3\rangle$ is dipole-forbidden (i.e. state $|3\rangle$ is meta-stable). Then, two lasers, probe beam and a considerably stronger pump beam, are tuned to the transitions $|1\rangle \rightarrow |2\rangle$ and $|1\rangle \rightarrow |3\rangle$, respectively. If proper coherence is achieved, it can result in vanishing probability for electrons to be found in the excited state due to quantum mechanical interference, and therefore the probe beam can propagate without any absorption. Classically, the resulting effect can be explained as a consequence of two driving forces acting on electrons, having equal magnitude and opposite sign [1].

Electromagnetically induced transparency is not restricted to quantum mechanics and can be observed in classical mechanical, electrical and plasmonic systems. Classical EIT relies on asymmetrically coupled resonators in respect to the external field. One of the resonators is weakly coupled and is called “dark” element, while the other is strongly coupled and is called “bright” element. To obtain the EIT effects, it is necessary that the “dark” resonator has a considerably greater Q-factor in respect to the “bright” resonator.

In the case of metamaterials consisting from coupled electromagnetic microresonators, this effect results in a sharp transmission peak appearing within wider absorption band [2-7]. This results in a very steep dispersion, which in turn creates very high value of group delay, i.e. very small value of group velocity. It was observed more than 200 times slower wave propagation in metamaterials than the velocity of light in free space, making this type of material suitable for slow-wave applications in terahertz region, [2,3], and for delay-lines in microwave region [7]. Also, due to high Q-factor and strong field confinement, the EIT-like resonance is very sensitive to refractive index of surrounding medium, making it desirable for refractive index-based sensors.

The authors are with the Institute of Physics, University of Belgrade, Pregrevice 118, 11080 Belgrade, Serbia. E-mail: vojislav@ipb.ac.rs

This paper is organized as follows. First, we present the coupled oscillators model that allows us to study the classical EIT phenomenologically. Then, we present a review of recent papers that demonstrate the EIT-like effects in metamaterials.

II. COUPLED OSCILLATORS MODEL

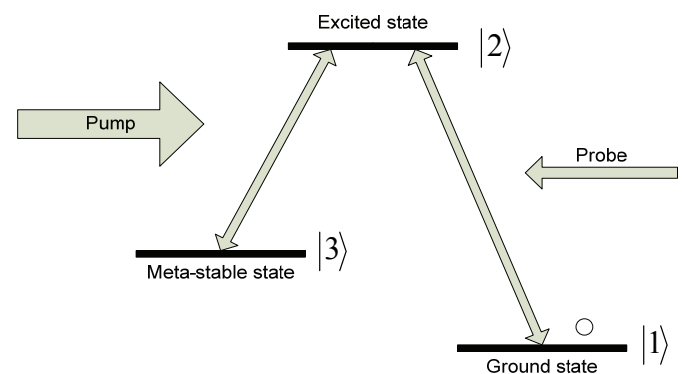


Fig. 1. Typical EIT configuration

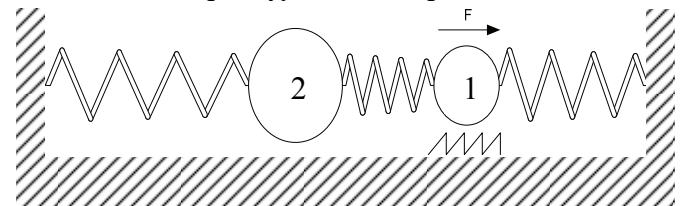


Fig. 2. Coupled mechanical oscillators

In Fig. 2 system of two coupled mechanical oscillators is shown, which we will use to explain the underlying mechanism of classical EIT. Suppose that the particles labelled as 1 and 2 have masses m_1 and m_2 , respectively. Both oscillators, when uncoupled (i.e. without the spring in the middle), have the same resonant frequency ω_0 , while the damping term associated with particle 2 is considerably smaller than that associated with particle 1, $\gamma_2 \ll \gamma_1$. Coupling coefficient is denoted as κ . Then, if external time-harmonic force is acting on the particle 1, $F = F_0 e^{j\omega t}$, we can write the following equations of motion ($x_{1,2}$ represent displacements of the respective particles from their equilibrium positions):

$$\frac{\partial^2 x_1}{\partial t^2} + \gamma_1 \frac{\partial x_1}{\partial t} + \omega_0^2 x_1 + \kappa x_2 = F = F_0 e^{j\omega t} \quad (1)$$

$$\frac{\partial^2 x_2}{\partial t^2} + \gamma_2 \frac{\partial x_2}{\partial t} + \omega_0^2 x_2 + \kappa x_1 = 0 \quad (2)$$

In this analogy, force F represents the incoming wave whose transmission is measured (i.e. probe beam), particle 1

represents the electrons, and particle 2 stands for the coupling to the pump beam. If there is movement of particle 1, there is some transfer of energy from the wave, which results in absorption. Therefore, the absorption will be absent in the case when particle 1 stands still.

By solving the system of equations (1), (2) in frequency domain, we obtain the following expression for the displacement of the first particle (as a function of frequency and amplitude of the external force):

$$x_1 = \frac{(\omega_0^2 - \omega^2 + j\omega\gamma_2)F_0}{\kappa^2 + (\omega_0^2 - \omega^2 + j\omega\gamma_1)(\omega_0^2 - \omega^2 + j\omega\gamma_2)} \quad (3)$$

It is apparent from (3) that at the frequency of the resonance ω_0 displacement of the first particle will be proportional to the damping term of the second oscillator, γ_2 , which is assumed to be very small, therefore the absorption will be very small too. In the limiting case, when $\gamma_2 \rightarrow 0$, it is obvious that x_2 also tends to zero, therefore the absorption of the system is fully removed.

III. REVIEW OF PUBLISHED PAPERS

One of the first attempts to explore the analogy between the EIT and resonators coupling in metamaterials was done by Tassin *et al.* in [2]. The geometry that was used is depicted in Fig. 3. In the first case (Fig. 3a), the excitation is by the electric field, and symmetrical gaps in the larger split ring have the purpose of preventing it from the coupling with incident field directly, therefore representing “dark” resonator, while the smaller one acts as “bright” resonator. In second case (Fig. 3b) excitation is by magnetic field, and orthogonal ring placement allows only one of them to couple with incident field directly. Dielectrics with different loss tangents have been inserted in the gaps to achieve different Q factors in order to obtain EIT like features.

The results for transmission, absorption and extracted effective permeability for the structure in Fig. 3b is shown in Fig. 4 (both cases from Fig. 3 have similar basic features and therefore we are showing only one). It can be seen that, for strong coupling (blue lines) two clearly separated resonances exist. However, for weaker coupling (red lines) there is narrow transmission window in which Lorentzian shaped absorption curve appears. This strong dispersion in transmission spectrum translates into dispersion in retrieved permeability in the case of electric coupling with external field (Fig. 3a), and in permeability in the case of magnetic coupling (Fig. 3b). The group index of refraction obtained is about 100, with the losses simultaneously being very small (which can be seen from the imaginary part of refractive index) [2].

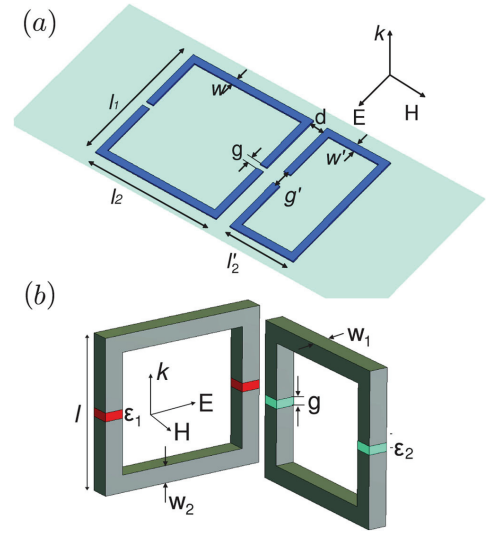


Fig. 3. EIT metamaterial (a) electrically (b) magnetically coupled to the external field [2]

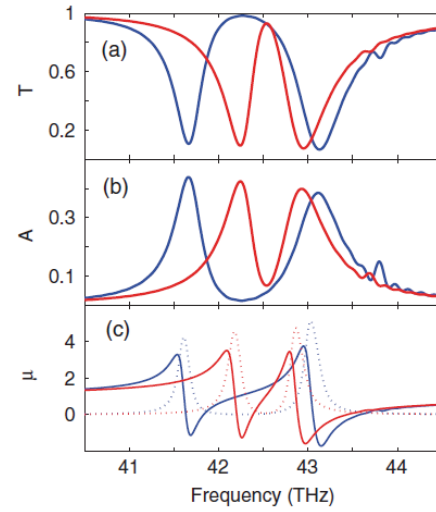


Fig. 4. Results for (a) transmission, (b) absorption and (c) extracted effective permeability for metamaterial in Fig. 3b [2]

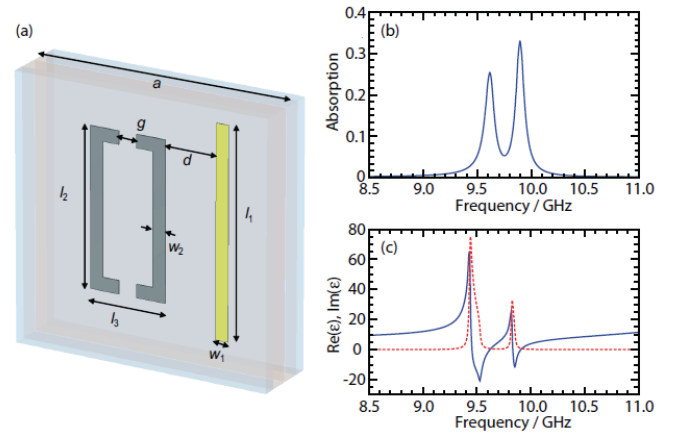


Fig. 5. (a) EIT metamaterial using wire and SRR; (b) absorption spectrum; (c) extracted effective permittivity [3]

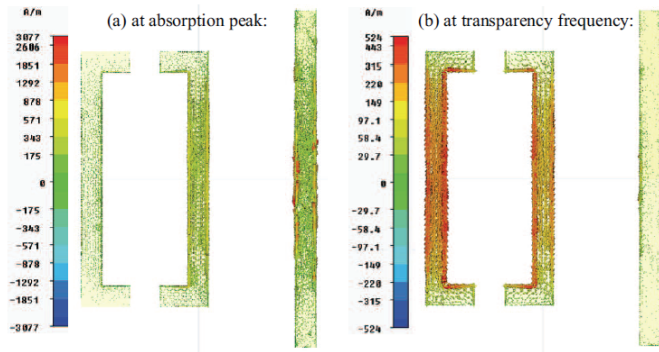


Fig. 6. Current distributions for metamaterial shown in Fig. 5a at (a) absorption peak; (b) transparency frequency [3]

In a subsequent paper from the same group [3] a slightly different approach is used to achieve the EIT-like effect: instead of using different dielectrics to achieve the needed loss contrast between the resonators, two different structures are used. Radiative or “bright” resonator is represented by cut-wire oriented in the direction of the external electric field, while the “dark” resonator is SRR with two symmetric gaps, which doesn’t couple to the external field. It was demonstrated experimentally that the SRR has significantly higher Q -factor than the wire, therefore enabling the EIT-like effect.

The absorption is calculated according to formula $A = 1 - |S_{11}|^2 - |S_{21}|^2$, and it is plotted in Fig. 5b, and the extracted effective permittivity is plotted in Fig. 5c. Again, transparency window is obtained within a wider absorption peak, accompanied by strong dispersion and low losses (imaginary part of permittivity).

The current distributions in resonators have also been calculated for two characteristic frequencies – of peak absorption and transparency, and they are shown in Fig. 6. We can see that at peak absorption, wire is strongly excited, while the current in SRR is small. In the other hand, at transparency frequency, SRR has strong current, while the wire is practically unexcited. This behavior is in a full agreement with that (?) what is expected in the case of EIT [3].

Similar structure is reported in [4], only this time two SRRs, symmetrically placed at both sides of the wire are used instead of one. The sample of this metamaterial was fabricated and measured using X-band waveguide [4].

The examples of classical EIT discussed above use resonators built from metals (e.g. copper), and therefore the difference in Q -factors between bright and dark resonators that can be achieved is about one order of magnitude. To fully pronounce EIT-like effects, Kurter *et al.* in [5] suggested a hybrid metal/superconductor metamaterial. It uses similar geometry as in [4] and [3], with cut wire made of gold, while two symmetrically placed SRRs made of superconductive Nb film. When cooled below its critical temperature, Nb film surface resistance in microwave range becomes very small, providing extremely high Q -factor for the rings.

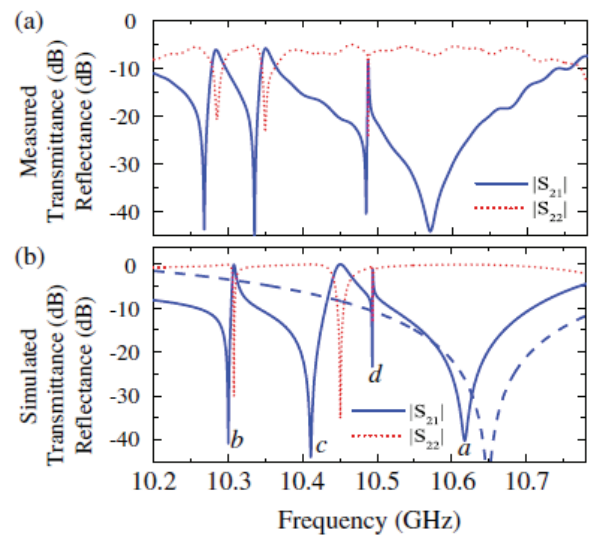


Fig. 7. (a) Measured and (b) simulated transmission and reflection spectrum for the hybrid metal/superconductor EIT metamaterial [5]

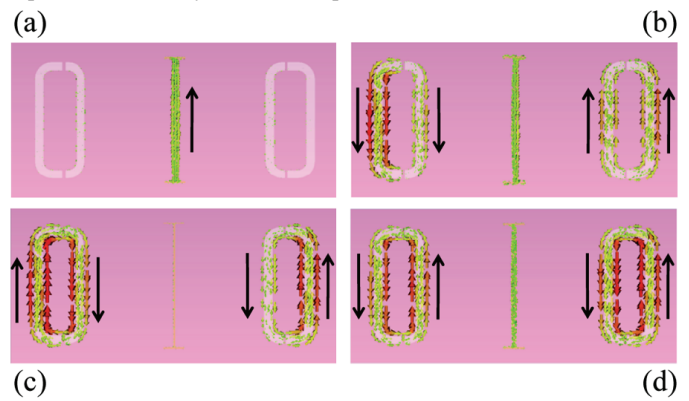


Fig. 8. Current distribution at the characteristic frequencies from Fig. 7a for hybrid metal/superconductor EIT metamaterial [5]

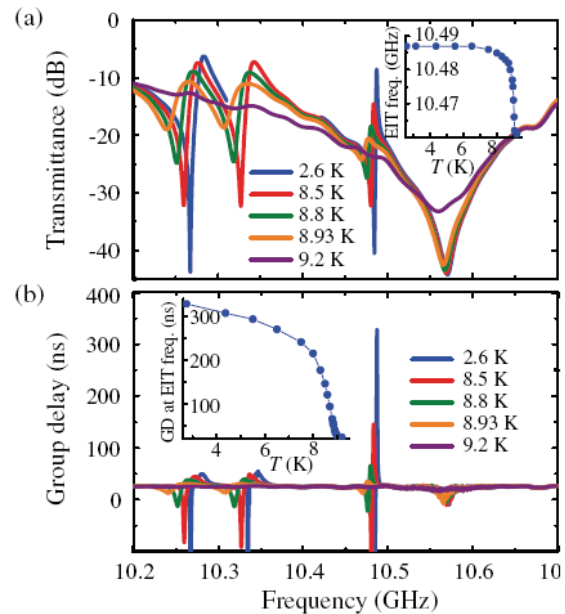


Fig. 9. Control of the group delay by temperature for hybrid metal/superconductor EIT metamaterial [5]

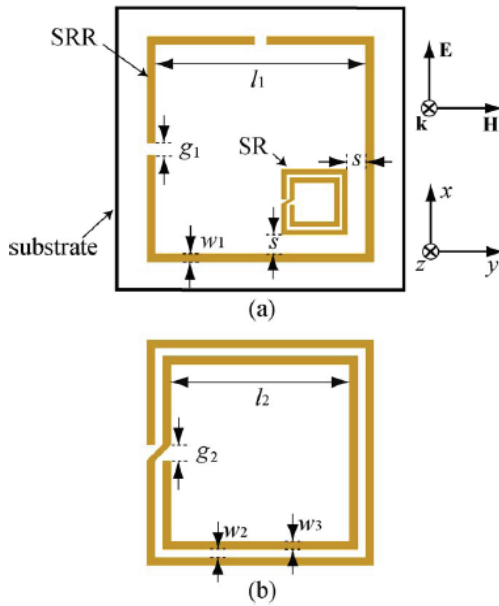


Fig. 10. Polarization independent EIT metamaterial unit cell [6]

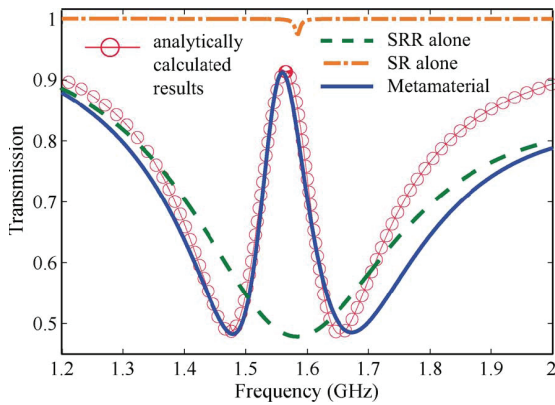


Fig. 11. Simulated transmission through metamaterial consisting only from SRRs, spirals, and both of them combined [6]

Measurement results for transmission in X-band waveguide with inserted unit cell of this metamaterial are shown in Fig. 7. A very interesting fact which can be noted on the plots is that transmission spectrum exhibits three EIT-like features (compared to one in all previous reports). Study of current distributions (see Fig. 8) provides insight into nature of these resonances. Fig 8a shows currents at the maximum absorption frequency, which coincides with dipole resonance of the wire. As it is expected, only the wire is excited, while the rings show? support current at all. Next, in Figs. 8b-d current distributions are shown at the frequencies that correspond to three EIT-like features in Fig. 7 (marked with corresponding letters on plot). It can be seen that the first feature (Fig. 8b) is related with electric dipole resonance of the rings, since both currents flow in the same direction. Other two features (Figs. 8c and d) correspond to symmetric and anti-symmetric normal modes of coupled magnetic resonances of the rings. In previous reports only one EIT-like feature appeared, probably because of the insufficiently high Q-factor of the dark resonator. The authors have also demonstrated the ability to tune EIT-like effect and consequent group delay by controlling the temperature (Fig 9).

All the metamaterials discussed so far exhibit EIT-like effects for a strictly defined linear polarization of incoming radiation, which can be a problem for a number of potential applications where polarization is not *a priori* defined. In an attempt to fix this issue, Meng *et al.* proposed metamaterial unit cell exhibiting EIT-like response for arbitrary (although linear) polarization, intended to be used as a refractive index based sensor [6].

The proposed geometry is shown in Fig. 10. It involves SRR as a bright element, with gaps at two orthogonal sides, therefore producing considerable dipole moment in both *x* and *y* directions. Because of this, it will couple to arbitrarily polarized electric field lying in the same plane. The dark element is spiral resonator, which produces negligible electric dipole moment and therefore is uncoupled with the external field. It can be excited, however, with the magnetic field perpendicular to its plane, which is produced by the currents flowing around the SRR, so the two resonators are coupled in this way. It was shown that, due to larger capacitance, the quality factor of the spiral resonator is much larger than that of the SRR (99.8 vs. 8.8).

Simulated transmission through metamaterial consisting only from SRRs, spirals, and both of them combined is plotted in Fig. 11. It can be seen that SRR produces wide Lorentzian-like absorption dip, while the spiral practically does not affect the transmission. When they are combined, though, a sharp transmission peak appears, again demonstrating the classical EIT effect. Current distribution analysis shows that the SRR is virtually unexcited at this frequency [6]. Authors analysed the change of the resonant wavelength with the change of refractive index of surrounding medium, and found it to be equal to 77.25mm per unit change of refractive index, thus making this material suitable for sensing applications.

IV. EIT EXCITED BY PLANAR TRANSMISSION LINE

In previously mentioned reports EIT metamaterials are excited either by plane waves or by a waveguide. The authors of this paper, however, proposed the transmission line EIT metamaterial, with the unit cell shown in Fig. 12b [7]. The difference in respect to the standardly used structure, shown in Fig. 12a, is that the SRRs in the middle layer are rotated by 90 degrees. Breaking the symmetry of the resonator in respect to the line result in a different coupling and consequently to considerable slowdown of the propagation field.

The simulated transmission is shown in Fig. 13 and it exhibits an EIT-like feature (shaded on the plot). To further establish this analogy, we extracted index of refraction for the standard transmission line metamaterial (SRRs with all gaps near the line) and for our EIT unit cell. Then we calculated group index according to the expression $n_g = n + \omega(\partial n / \partial \omega)$, and the obtained results are shown in Figs. 14-15 for the standard SRR arrangement and for the case with twisted SRRs, respectively.

It can be seen from the Figs. 14-15 that transmission line EIT metamaterial exhibits by the order of magnitude larger values of group index (222 vs. 25), which corroborates the aforementioned analogy.

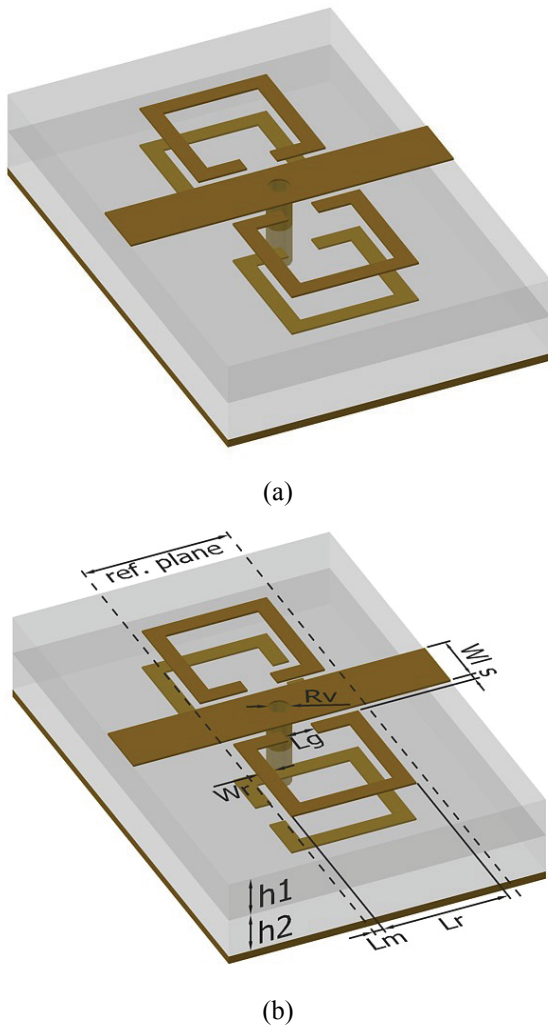


Fig. 12. (a) Standard transmission line metamaterial (b) the proposed transmission line EIT metamaterial with relevant dimensions $h_1=0.635\text{mm}$, $h_2=1.575\text{mm}$, $\epsilon_{r1}=10.2$, $\epsilon_{r2}=2.2$, $L_r=3.15\text{mm}$, $L_m=0.25\text{mm}$, $L_g=0.75\text{mm}$, $S=0.2\text{mm}$, $W_1=1.4\text{mm}$, $W_2=0.4\text{mm}$, $W_3=0.5\text{mm}$

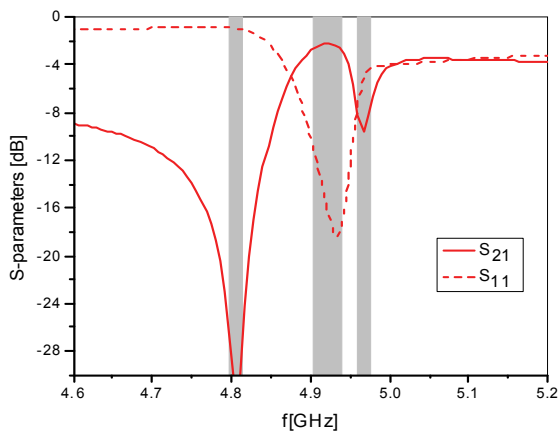


Fig. 13. Simulated S -parameters for metamaterial in Fig. 12. Rectangular bar denote characteristic frequencies in EIT response

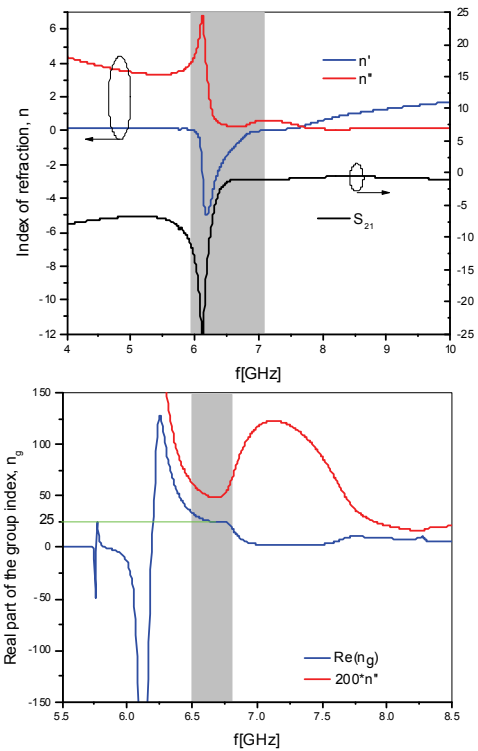


Fig. 14. Index of refraction (a) and group index (b) for the standard transmission line metamaterial with SRRs symmetrically coupled with transmission line

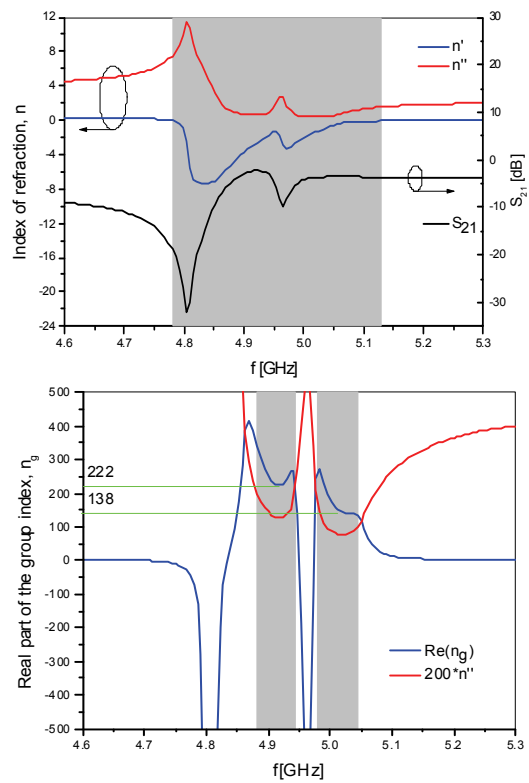
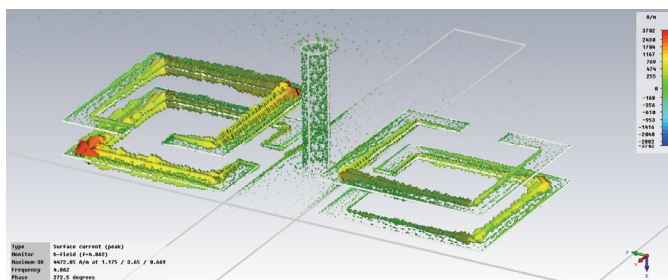
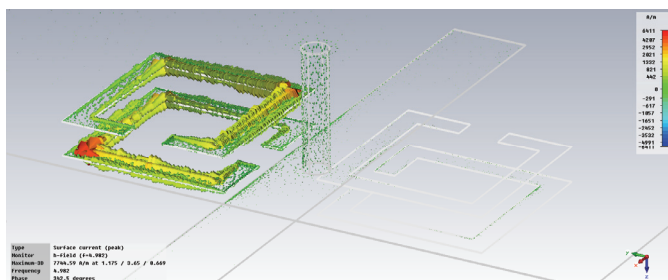


Fig. 15. Index of refraction (a) and group index (b) for the EIT-like transmission line metamaterial

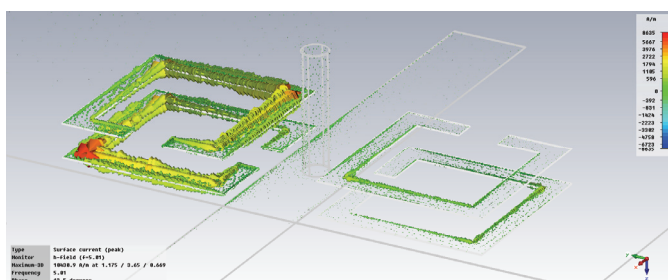
To provide additional insight, we calculated the current distribution at the EIT-like feature frequency, and the results are shown in Fig. 16. It can be seen that at the first characteristic frequency (Fig. 16a) all SRRs and via are excited simultaneously, while at the EIT frequency (Fig. 16b) two pairs of SRRs are excited out of phase and via is almost unexcited. It means that pair of SRRs acting as a “dark” element and since via is virtually unexcited it acts as a “bright” element. It should be noted that current in SRRs, at the different sides of the line, are in the same direction at the first characteristic frequency while there are opposite at the third characteristic frequency.



(a)



(b)



(c)

Fig. 16. Current distribution at EIT-like response at characteristic frequencies denoted in Fig. 13

V. CONCLUSION

In this paper EIT-like effects in metamaterials were presented, based on an analogy with laser physics. Model consisting of two coupled linear harmonic oscillators was studied in order to gain understanding of the underlying mechanism.

A review of the published literature on this topic was given, including our work on transmission line EIT metamaterials. Common features shared by all the examples discussed include: narrow transmission peak within wider absorption curve, low losses, strong dispersion accompanied by high values of group delay and group index of refraction. These properties make these materials suitable for various applications like slow light, delay lines and sensors.

ACKNOWLEDGEMENT

This work has been supported by Serbian Ministry of Education, Science and Technological Development through projects TR-32024 and III-45016.

REFERENCES

- [1] S. Harris, “Electromagnetically Induced Transparency”, *Physics Today*, vol. 50, no. 7, pp. 36-42, 1997.
- [2] P. Tassin, L. Zhang, Th. Koschny, E. N. Economou, and C. M. Soukoulis, “Low-Loss Metamaterials Based on Classical Electromagnetically Induced Transparency”, *Phys. Rev. Lett.*, vol. 102, pp. 053901, 2009
- [3] P. Tassin, L. Zhang, Th. Koschny, E. N. Economou, and C. M. Soukoulis, “Planar designs for electromagnetically induced transparency in metamaterials”, *Optics Express*, vol. 17, no. 7, pp. 5595-5605, 2009.
- [4] L. Zhang, P. Tassin, Th. Koschny, C. Kurter, S.M. Anlage, and C. M. Soukoulis, “Large group delay in a microwave metamaterial analog of electromagnetically induced transparency”, *Appl. Phys. Lett.*, vol. 97, pp. 241904, 2010.
- [5] C. Kurter, P. Tassin, L. Zhang, Th. Koschny, A.P. Zhuravel, A.V. Ustinov, S.M. Anlage, and C.M. Soukoulis, “Classical Analogue of Electromagnetically Induced Transparency with a Metal-Superconductor Hybrid Metamaterial”, *Phys. Rev. Lett.*, vol. 107, pp. 043901, 2011.
- [6] F.-Y. Meng, Q. Wu, D. Erni, K. Wu, and J.-C. Lee, “Polarization-Independent Metamaterial Analog of Electromagnetically Induced Transparency for a Refractive-Index-Based Sensor”, *IEEE Trans. Microw. Theory Tech.*, vol. 60, no. 10, pp. 3013-3022, 2012.
- [7] B. Jokanovic, V. Milosevic, R. Bojanic, and B. Jelenkovic, “Theoretical and Experimental Investigations of Reconfigurable Metamaterials Based on Split-Ring Resonators”, *3rd Mediterranean Conference on Nanophotonics MediNano-3 - Book of Abstracts*, pp. 26, Belgrade, Serbia, 18-19 October 2010.

Tx Leakage Cancellation Using Antenna Image Impedance for CW Radar Applications

Vojislav Milosevic, Milos Radovanovic, Branka Jokanovic
Institute of Physics
University of Belgrade
Pregrevica 118, 11080 Belgrade, Serbia
Email: vojislav@ipb.ac.rs, rmilos@ipb.ac.rs, brankaj@ipb.ac.rs

Olga Boric-Lubecke, Victor M. Lubecke
Department of Electrical Engineering
University of Hawaii at Manoa
2540 Dole St, Honolulu, HI 96822
E-mail: olgabl@hawaii.edu, lubecke@hawaii.edu

Abstract—In this paper we propose the Tx leakage cancellation method based on the antenna image impedance, i.e. the passive network synthesized to replicate the antenna impedance in the band of interest. The concept is verified for the patch antenna array operating in the Ku band, where the achieved isolation is measured to be better than 35 dB in the 17–17.4 GHz range. This method can provide great benefit for single antenna CW radar applications.

I. INTRODUCTION

Although the overwhelming majority of high-power long distance radar systems are pulsed, continuous wave (CW) systems have had their niche since the very beginning of radar development. The main reasons for this are their lower complexity and better suitability for certain applications, e.g. Doppler speed measurement, operation at small ranges, in the presence of a severe clutter, etc. More recently, with the possibility of on-chip integration leading to compactness and low cost [1], they are attracting attention for applications such as automotive collision-avoidance radars [2], wireless medical sensors (breathing, heart rate) [3], and many other.

Since in most radar systems the transmitter (Tx) signal is many orders of magnitude larger than the received one, it must be prevented, as much as possible, from leaking into the receiver (Rx). In pulse systems this is achieved by time gating, i.e. by switching off the receiver during the transmit cycle. In CW systems, the frequency of the received signal is usually shifted with respect to the frequency of the signal transmitted at the same time, so some degree of isolation can be achieved by filtering. However, there are two factors that limit the power of the leaked signal [4]:

- maximum power the Rx can handle without saturation or damage;
- sideband level, due to Tx noise or modulation, at the frequency of the received signal.

In practice, it is usually the second factor which is more limiting [4]. The most straightforward way to reduce the leakage is to use separate antennas, however this does not eliminate the leakage completely due to antenna coupling and echo from the static clutter. And since the antenna is usually the bulkiest part of the systems, there is the obvious disadvantage of doubling the size and increasing the cost of the system.

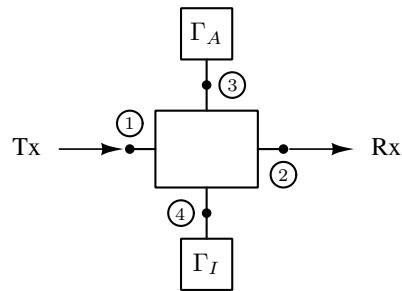


Fig. 1. Basic circuit of the proposed Tx leakage cancellation using the antenna image impedance.

If a single antenna is used, isolation can be achieved by using devices like a quadrature hybrid, directional coupler or circulator, with practically obtainable isolation of the order of 20–30 dB. A balanced topology can be used to suppress the direct leakage [5]. However, it is important to emphasize that if the antenna is not perfectly matched, its reflection adds to the total leakage. For instance, if we want the 30 dB isolation, an antenna with the VSWR better than 1.07 is required [4]. This is hard to achieve, since the typical broadband antenna is considered to be well matched if its VSWR is less than 2.

Antennas with quadrature feeding in conjunction with balanced topology can be used to reduce both the direct leakage and the antenna reflection [6]. This solution is very elegant, but relies on the circular polarization, which may be unsuitable for some applications (typical radar systems use linear polarization). There are also active methods of cancellation, which manipulate with the portion of the Tx signal so that it arrives to the Rx with the same magnitude and opposite phase to the leaked signal (this is also known as *feed-through nulling*). The drawback of this approach is that it requires a high-performance vector modulator, which can be complicated and costly to implement [7].

In this paper we present the method of suppressing the Tx leakage by using the antenna image impedance. The details of this method, along with theoretical considerations, are given in the paper and the practical implementation with measurements is demonstrated.

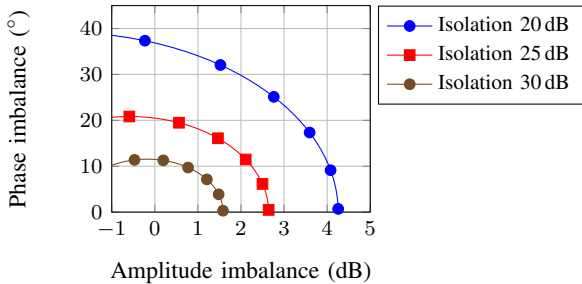


Fig. 2. Contours of the constant total isolation as function of amplitude and phase imbalance, for the antenna with reflection coefficient of -10 dB.

II. PROPOSED CONCEPT

Let us suppose that it is possible to synthesize a network that will have the same reflection coefficient as the antenna in the band of interest, but without actual radiating elements – using resistors, stubs, etc. We will refer to this network as the antenna image. Apart from it, we need a network which performs the separation of Tx and Rx channels in the actual cancellation process, which we will refer to as the canceller. In general case, we can represent the canceller as a four-port network with ports 1 and 2 attached to Tx and Rx, and the antenna and image (with reflection coefficients Γ_A and Γ_I) connected to the remaining ports 3 and 4 (Fig. 1).

The principle of operation can be described as follows: the transmitter signal is split between the antenna and the image, and the occurring reflection is combined in anti-phase before coming to the receiver, and therefore the leakage is cancelled out. In the receiving scenario, the signal comes to the antenna only, and not to the image, so it arrives to the receiver without cancellation. However there is an intrinsic 3 dB loss in both transmit and receive paths. While this may seem as much, it can be justified by considering that a single antenna has approximately twice the effective surface of two separate antennas of the same total size, and consequently a 3 dB higher gain, which equalizes the total loss; while adding the benefit of better spatial resolution.

We define the *total isolation* as the magnitude of the signal arriving from the transmitter to the receiver, $I_{Tx/Rx} = -|S_{21}^{eff}|$, where S_{21}^{eff} is the transmission from port 1 to port 2 when ports 3 and 4 are loaded with the antenna and its image impedance as it is shown in Fig. 1. Considering only the first-order reflections, it can easily be shown that the condition for proper canceller operation is:

$$S_{31}S_{23} = -S_{41}S_{24}. \quad (1)$$

In other words, the two paths from Tx to Rx have to be balanced in magnitude and with opposite phase. If the impedances of the antenna and the image are equal; if not it will produce an additional imbalance that can affect the isolation both constructively and destructively, depending on the phase, which is impossible to predict.

Therefore we will consider the antenna-image imbalance separately, assuming that (1) is fulfilled. In practice, we expect

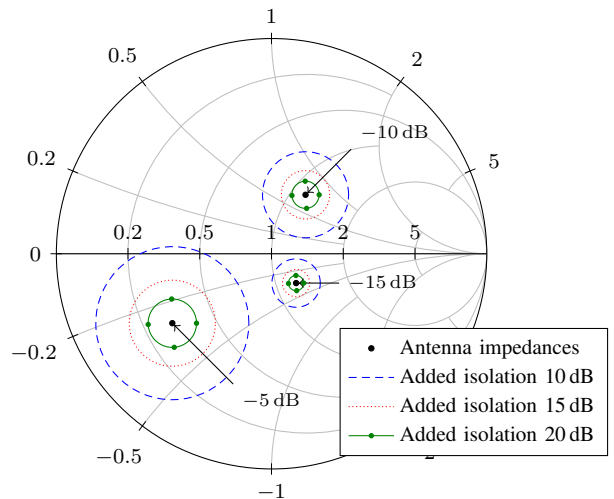


Fig. 3. Circles within which the image impedance must be to achieve certain level of added isolation, i.e. the isolation improvement, for the antenna reflection coefficients of -5 dB, -10 dB and -15 dB (indicated by arrows on the graph).

(1) to be reasonably well satisfied with conventional power dividers and couplers, so the bottleneck for the proposed method is the discrepancy between the antenna and its image impedance. In these conditions the total Tx/Rx isolation will be

$$I_{Tx/Rx} \approx \frac{1}{2} |\Gamma_A - \Gamma_I|. \quad (2)$$

To analyze the dependence of isolation on the antenna-image imbalance, we can put the image reflection coefficient in the following form

$$\Gamma_I = \alpha \Gamma_A e^{j\varphi}, \quad (3)$$

where α and φ are amplitude and phase imbalance, respectively. Then (2) becomes

$$\begin{aligned} I_{Tx/Rx} &\approx \left| \frac{1}{2} \Gamma_A (1 - \alpha e^{j\varphi}) \right| \\ &= \frac{1}{2} |\Gamma_A| |1 - \alpha \cos \varphi - j\alpha \sin \varphi| \\ &= \frac{1}{2} |\Gamma_A| \sqrt{1 + \alpha^2 - 2\alpha \cos \varphi}. \end{aligned} \quad (4)$$

Here it is convenient to separate the total isolation into two terms: the original antenna reflection Γ_A , and the *added isolation* $\frac{1}{2} |\Gamma_A| \sqrt{1 + \alpha^2 - 2\alpha \cos \varphi}$, which is used as a relative measure of image quality.

Based on (4), the contours with constant total isolation are plotted in Fig. 2 as function of amplitude and phase imbalance, for the antenna with reflection coefficient of -10 dB.

Another way to intuitively consider the antenna-image imbalance is using the Smith chart (Fig. 3). Assuming the antenna impedance is fixed, we may ask where the image impedance should be in order to obtain certain isolation. By examining (2) we can conclude that the geometric place of the image impedances is simply a circle around the antenna impedance in the Smith chart, whose radius depends on the desired total

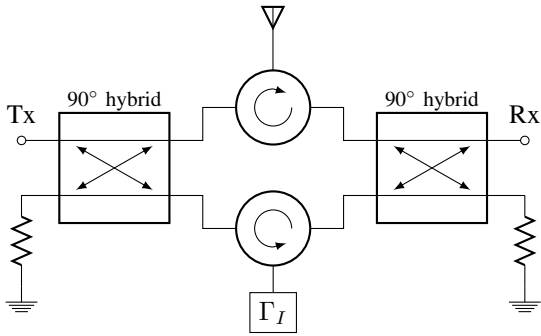


Fig. 4. Proposed canceller network.

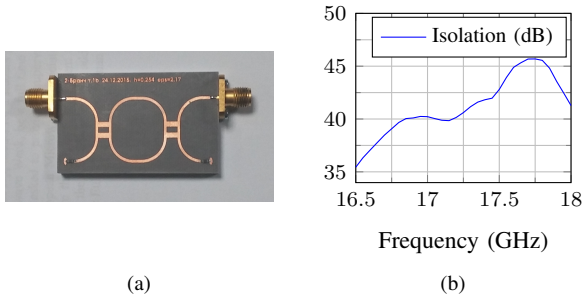


Fig. 5. Measured maximum achievable port isolation using two branch couplers.

$I_{Tx/Rx}$. If we consider the added isolation, then the circles will scale proportionally to Γ_A , as it is shown in Fig. 3 for several antenna impedances. However, the total isolation, according to (2), is a function of balance between the antenna and image only, regardless of the antenna reflection. This can be significant advantage of the proposed method for the antennas that are initially poorly matched.

III. IMPLEMENTATION AND RESULTS

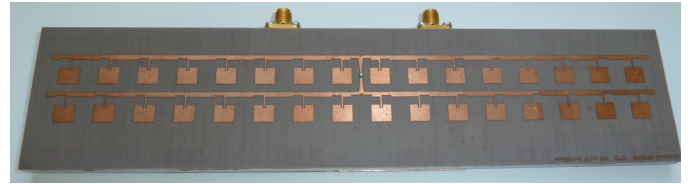
A. Canceller

The canceller from Fig. 1 can be implemented in practice in various ways. For example, the antenna and the image can be connected to through and coupled outputs of the quadrature hybrid, which will then perform the cancellation, and then a circulator can be used to separate the transmit and receive channels. However, there is leakage due to finite isolation of the circulator, which is about 20 dB, and also due to the mismatch at the input of the hybrid, which can be of the same order. Therefore, we propose the balanced network shown in Fig. 4, which has two important advantages:

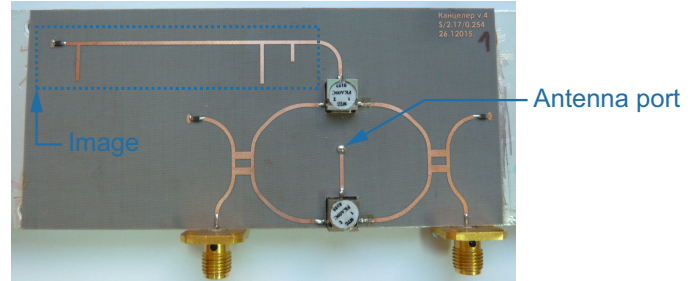
- direct leakage through the circulators is suppressed;
- reflections due to input mismatch of the hybrids do not contribute to the leakage.

Therefore, the only critical parameter of the hybrid is its balance, both in amplitude and in phase.

The target technology for implementation was chosen to be microstrip on PTFE fiberglass substrate with parameters $h = 0.254$ mm and $\epsilon = 2.17$. Hybrids were realized in branch-line form. In order to test the balance, we fabricated a circuit



(a)



(b)

Fig. 6. Fabricated antenna and canceller

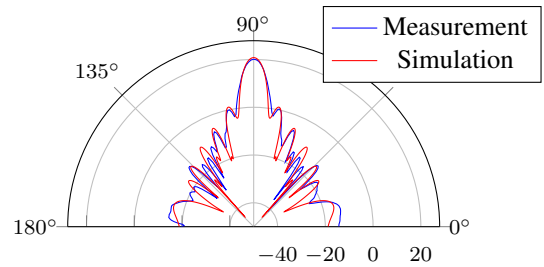


Fig. 7. Radiation pattern at 17.25 GHz

with two hybrids connected in series, as shown in Fig. 5a. If they are perfectly balanced, the transmitted signal should be cancelled out, so the residual transmission presents the bottom limit for the achievable isolation. It is measured to be around -40 dB in the range of interest (see Fig. 5b).

B. Antenna and image

The antenna which we used in this project is shown in Fig. 6a. It consists of 32 microstrip patches, with a single central feeding point, which is connected to the back side of the plate, where the canceller is intended to be. The measured radiation pattern of the antenna is shown in Fig. 7, from which it can be seen that the 3 dB beamwidth is about 5.4° in azimuth plane, with a gain of 20.7 dBi.

The antenna impedance is measured and deembedded at 8 mm from the feeding point at the back plate, and the result is shown at Fig. 8. The impedance is shifted from the Smith chart center probably due to difficulties with connection between two sides of the plate. The image is designed as a long 50Ω line which is terminated at the other end, with three radial stubs to replicate the antenna impedance as closely as possible in the whole frequency range. The design and optimization of the image are performed in two stages, first in a circuit solver, and then refined using 2.5D EM simulation. The fabricated circuit is

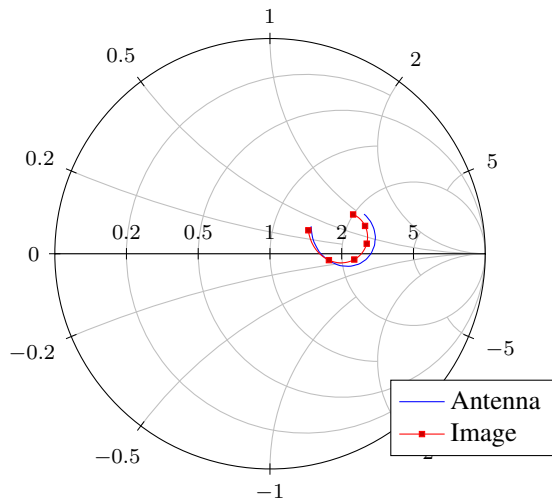


Fig. 8. Comparison of the measured antenna impedance and simulated image impedance in the range 17–17.5 GHz.

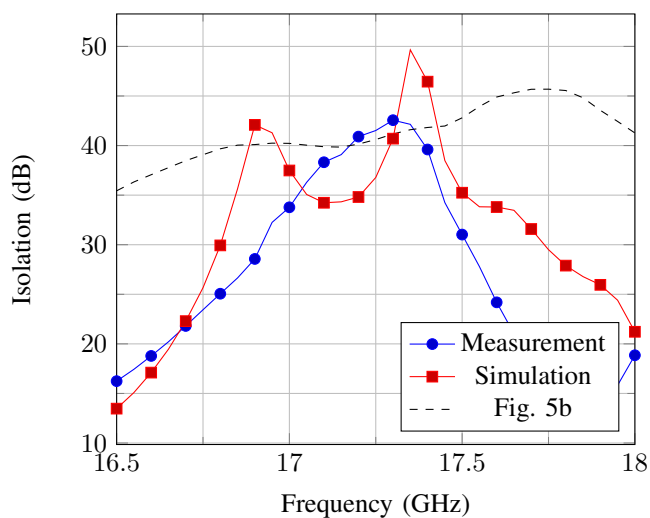


Fig. 9. Measurement and simulation for the total isolation, compared with the test with two branches from Fig. 5.

shown in Fig. 6b, while the simulated input impedance is shown in Fig. 8, where it can be seen to closely resemble the antenna impedance in the whole range of interest.

Final results for both measured and simulated isolation are shown in Fig. 9. It can be seen that the achieved value is better than 35 dB in the whole range of 17–17.4 GHz. These values are compared with the isolation obtained with the test with two branch-line couplers, and it can be seen that it is even exceeded at some frequencies, which demonstrates that the practical limit of the achievable isolation has been reached.

IV. CONCLUSION

The Tx leakage cancellation by using the antenna image impedance was studied theoretically and confirmed in practice. The design of the actual canceller along with synthesizing of the antenna image impedance was presented. The proposed

concept was verified by measurements, which showed isolation better than 35 dB in the frequency range 17–17.4 GHz. We believe that this approach can greatly improve the performance of the single antenna CW radar systems, which makes it interesting for numerous practical applications.

ACKNOWLEDGMENT

This work was supported by the Serbian Ministry of Education, Science and Technological Development through Projects TR-32024 and III-45016.

REFERENCES

- [1] P. Abele, A. Trasser, E. Sonmez, K.-B. Schad, A. Munding, and H. Schumacher, "A compact low-cost doppler sensor MMIC in SiGe technology for the ISM band at 24 GHz," in *Microwave Conference, 2004. 34th European*, vol. 2, Oct. 2004, pp. 1037–1040.
- [2] *Short range radar equipment operating in the 24 ghz range*, ETSI, 2006.
- [3] A. Droitcour, O. Boric-Lubecke, V. Lubecke, J. Lin, and G. Kovacs, "Range correlation and I/Q performance benefits in single-chip silicon Doppler radars for noncontact cardiopulmonary monitoring," *Microwave Theory and Techniques, IEEE Transactions on*, vol. 52, no. 3, pp. 838–848, Mar. 2004, ISSN: 0018-9480. DOI: 10.1109/TMTT.2004.823552.
- [4] M. Skolnik, *Introduction to Radar Systems*, ser. Electrical Engineering Series. McGraw-Hill, 1980, ISBN: 9780070579095.
- [5] J.-G. Kim, S. Ko, S. Jeon, J.-W. Park, and S. Hong, "Balanced topology to cancel Tx leakage in CW radar," *Microwave and Wireless Components Letters, IEEE*, vol. 14, no. 9, pp. 443–445, Sep. 2004, ISSN: 1531-1309. DOI: 10.1109/LMWC.2004.832080.
- [6] W.-G. Lim and J.-W. Yu, "Balanced circulator structure with enhanced isolation characteristics," *Microwave and Optical Technology Letters*, vol. 50, no. 9, pp. 2389–2391, 2008, ISSN: 1098-2760. DOI: 10.1002/mop.23696. [Online]. Available: <http://dx.doi.org/10.1002/mop.23696>.
- [7] P. Beasley, A. Stove, B. Reits, and B. As, "Solving the problems of a single antenna frequency modulated CW radar," in *Radar Conference, 1990., Record of the IEEE 1990 International*, May 1990, pp. 391–395. DOI: 10.1109/RADAR.1990.201197.

Преглед постигнутих научних резултата

Кандидат Војислав Милошевић је од 2010. године ангажован у Лабораторији за метаматеријале, у оквиру Центра за фотонику на Институту за физику у Београду. У свом истраживачком раду бавио се електромагнетним метаматеријалима у микроталасној техници, као и другим иновативним приступима за побољшање класичних микроталасних уређаја.

Најпре је овладао техникама нумеричке симулације електромагнетних структура, посебно у софтверском пакету Wipl-D. Претежно су испитиване структуре које се састоје од микроталасног вода (микрострип и друге врсте тракастих водова) спрегнутих са једним или више резонатора, које чине јединичну ћелију једнодимензионалних метаматеријала (у литератури су познати као „мета-линије“ или CRLH водови). Овакве структуре су занимљиве са аспекта примене у микроталасним филтрима, линијама за кашњење и фазним шифтерима, где могу пружити знатно боље перформансе у односу на класичне методе пројектовања. За карактеризацију је имплементиран код за екстракцију ефективних параметара у Matlab-у, на основу Nicolson-Ross-Weir (NRW) процедуре. Како ова процедура није примењива на асиметричне јединичне ћелије, теоријски је развијена нова метода, у складу са сличним приступом за 2Д и 3Д метаматеријале, која може да укључи и овај случај. Метода је базирана на коришћењу бианизотропних параметара, и имплементирана је у Matlab-у. Валидност методе је потврђена „инверзним“ симулацијама хомогеног материјала са одговарајућим параметрима, и поређењем резултирајућих параметара расејања са оригиналном структуром.

- В. Милошевић, Б. Јокановић, Р. Бојанић, "Effective Electromagnetic Parameters of Metamaterial Transmission Line Loaded with Asymmetric Unit Cells", *IEEE Trans. Microw. Theor. Tech.*, vol. 61, br. 8, pp. 2761-2772, doi: 10.1109/TMTT.2013.2268056, 2013.
- В. Милошевић, Б. Јокановић, Р. Бојанић, "Retrieval and validation of the effective constitutive parameters of bianisotropic metamaterials", *Phys. Scr.*, vol. T162, br. , pp. 014046, doi: 10.1088/0031-8949/2014/T162/014046, 2014.

Моделовање микроталасних кола типично се врши помоћу еквивалентних електричних шема, при чему се елементи са дистрибуираним параметрима (као што су секције водова упоредиве по димензијама са таласном дужином) апроксимирају елементима са концентрисаним параметрима (као што су калемови и кондензатори). На овај начин се омогућава драстично лакша анализа, пројектовање и оптимизација, као и боље разумевање физичких процеса који се одвијају. Иако су еквивалентне шеме за вод спрегнут са сплит-ринг резонатором биле познате у литератури, кандидат је предложио нову топологију која може драстично да прошири опсег њиховог важења. Такође је детаљно успостављена веза између физичких параметара структуре, њеног одзива и параметара еквивалентне шеме, и показано је како она може да се примени на велики број случајева, од којих неки раније нису били познати – нпр. када постоји комбинација електричне и магнетне спреге.

- Р. Бојанић, Б. Јокановић, В. Милошевић, F. Medina, F. Mesa, "Enhanced Modelling of Split-Ring Resonators Couplings in Printed Circuits", *IEEE Trans. Microw. Theor. Tech.*, vol. 62, br. 8, pp. 1605 - 1615, doi: 10.1109/TMTT.2014.2332302, 2014.
- Р. Бојанић, Б. Јокановић, В. Милошевић, "Enhanced Modelling of Asymmetric Split-Ring-Resonators in Printed Circuits", *Metamaterials 2014*.

Кандидат је проучавао класичну аналогију електромагнетно индуковане транспаренције (ЕИТ) у метаматеријалима. Ово је ефекат код кога се оштар трансмисиони максимум јавља у иначе непропусном опсегу учестаности, и последица је спреге између резонатора. Вршено је моделовање овог ефекта помоћу теорије спрегнутих модова.

- В. Милошевић, Б. Јокановић, Г. Исић, "Coupled-mode Theory Approach for Analysis of Resonant Transmission Line", *Metamaterials* 2015.
- В. Милошевић, Б. Јокановић, Р. Бојанић, Б. Јеленковић, "Classical Electromagnetically Induced Transparency in Metamaterials", *Microw. Rev.*, vol. 19, br. 2, pp. 76-81, 2013.

Кандидат је такође учествовао у развоју радарске антене на 17 ГХц, конкретно пројектовао је микроталасно коло за потискивање преслушавња из предајника у пријемник. Када се иста антена користи за пријем и предају сигнала, потребан је додатни склоп које ће обезбедити међусобну изолацију, као што је циркулатор који на том опсегу има има коначну изолацију од око 20дБ, што није довољно за далекодометне радаре код којих је пријемни сигнал за много редова величине слабији од предајног. Због тога се користе два решења: импулсни радари (који емитују у кратким интервалима са великом снагом, за време којих је пријемник искључен, али цена се плаћа повећаном сложености кола) или одвојене антене за пријем и предају, што повећава димензије и цену уређаја. Развијено је иновативно решење које користи тзв. „имиџ“ импедансу која служи за поништавање рефлексије од антене као и два циркулатора тако да се потисне директно преслушавање предајног сигнала у пријемник. . Остварена је изолација од преко 30 дБ у жељеном опсегу 17-17,5 ГХц.

- V. Milosevic, M. Radovanovic, B. Jokanovic, O. Boric-Lubecke, V.M. Lubecke, "Tx Leakage Cancellation Using Antenna Image Impedance for CW Radar Applications," *European Microwave Conference (EuMC) 2016*.



Универзитет у Београду
Физички факултет
Д.Бр.2012/8022
Датум: 10.06.2016. године

На основу члана 161 Закона о општем управном поступку и службене евиденције издаје се

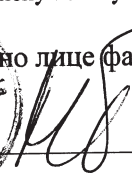
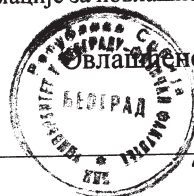
УВЕРЕЊЕ

Милошевић (Урош) Војислав, бр. индекса 2012/8022, рођен 05.04.1986. године, Београд, Београд-Савски Венац, Република Србија, уписан школске 2015/2016. године, у статусу: самофинансирање; тип студија: докторске академске студије; студијски програм: Физика.

Према Статуту факултета студије трају (број година): три.
Рок за завршетак студија: у двоструком трајању студија.

Ово се уверење може употребити за регулисање војне обавезе, издавање визе, права на дечији додаток, породичне пензије, инвалидског додатка, добијања здравствене књижице, легитимације за повлашћену возњу и стипендије.

Овлашћено лице факултета



Република Србија
Универзитет у Београду
Физички факултет
Д.Бр.2012/8022
Датум: 10.06.2016. године

На основу члана 161 Закона о општем управном поступку и службене евиденције издаје се

УВЕРЕЊЕ

Милошевић (Урош) Војислав, бр. индекса 2012/8022, рођен 05.04.1986. године, Београд, Београд-Савски Венац, Република Србија, уписан школске 2015/2016. године, у статусу: самофинансирање; тип студија: докторске академске студије; студијски програм: Физика.

Према Статуту факултета студије трају (број година): три.
Рок за завршетак студија: у двоструком трајању студија.

Ово се уверење може употребити за регулисање војне обавезе, издавање визе, права на дечији додаток, породичне пензије, инвалидског додатка, добијања здравствене књижице, легитимације за повлашћену возњу и стипендије.

Овлашћено лице факултета





Универзитет у Београду
Електротехнички факултет
Број индекса: 2009/3269
Број: М20110169
Датум: 06.04.2012.

На основу члана 161 Закона о општем управном поступку ("Службени лист СРЈ", бр. 33/97, 31/2001 и "Службени гласник РС", бр. 30/2010), дозволе за рад број 612-00-588/2008-04 од 17.11.2008. године коју је издало Министарство просвете Републике Србије и службене евиденције, Универзитет у Београду - Електротехнички факултет, издаје

У В Е Р Е Њ Е

Војислав Милошевић

име једног родитеља Урош, ЈМБГ 0504986710130, рођен 05.04.1986. године, Београд, општина Савски Венац, Република Србија, уписан школске 2009/10. године, дана 30.03.2012. године завршио је мастер академске студије на студијском програму Електротехника и рачунарство, модул Микроталасна техника, у трајању од једне године, обима 60 (шездесет) ЕСПБ бодова, са просечном оценом 9,57 (девет и 57/100).

На основу наведеног издаје му се ово уверење о стеченом високом образовању и академском називу **мастер инжењер електротехнике и рачунарства.**



Проф. др Миодраг Поповић



Универзитет у Београду
Електротехнички факултет
Број: 17698
Датум: 30.10.2009.

На молбу коју је поднео **Војислав (Урош) Милошевић**, а на основу члана 161 Закона о општем управном поступку (Службени лист СРЈ бр. 33/97, 31/01), Електротехнички факултет Универзитета у Београду издаје

У В Е Р Е Њ Е

Војислав (Урош) Милошевић, рођен 05.04.1986. године, Београд, општина Савски венац, уписан школске 2005/06 у 1. годину, дипломирао је 30.10.2009. (општи успех 9.09, на дипломском испиту 10) Одсек за телекомуникације и информационе технологије - смер Микроталасна техника Електротехничког факултета и стекао звање дипломираног инжењера електротехнике.

Диплома ће носити број овог уверења.

Уверење се издаје без наплате таксе на основу члана 19 тачка 7 Закона о административним таксама (Службени гласник РС бр. 43/03, 51/03).

Декан
Електротехничког факултета


Проф. др Миодраг Поповић



На основу члана 82. Закона о научноистраживачкој делатности ("Службени гласник Републике Србије", број 110/2005, 50/2006 - испр. и 18/2010), члана 33. тачка 5. Статута Института за физику и захтева који је поднео

ВОЈИСЛАВ МИЛОШЕВИЋ
на седници Научног већа Института за физику одржаној 24.09.2013. године,
донета је

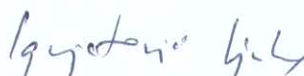
ОДЛУКА О СТИЦАЊУ ИСТРАЖИВАЧКОГ ЗВАЊА

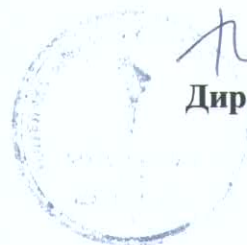
ВОЈИСЛАВ МИЛОШЕВИЋ
стиче истраживачко звање
Истраживач сарадник

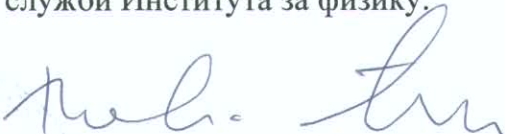
ОБРАЗЛОЖЕЊЕ

Војислав Милошевић је 08.07.2013. године поднео захтев за стицање истраживачког звања истраживач сарадник. Научно веће Института за физику је на седници одржаној 12.07.2013. године образовало Комисију за спровођење поступка у саставу др Бранка Јокановић, научни саветник у Институту за физику, др Брана Јеленковић, научни саветник у Институту за физику, и Проф. др Слободан Вуковић, научни саветник, ИХТМ у Београду. Научно веће је на седници од 24.09.2013. године утврдило да именовани испуњава услове из члана 70. став 3. Закона о научноистраживачкој делатности за стицање истраживачког звања **истраживач сарадник**, па је одлучило као у изреци ове одлуке.

Одлуку доставити подносиоцу, архиви Института за физику, кадровској служби Института за физику и рачуноводственој служби Института за физику.


Председник Научног већа
др Љубинко Игњатовић




Директор Института за физику
др Александар Белић